

DISSERTATION

PHYSICAL MODELING OF JOINTED BEDROCK EROSION
BY BLOCK QUARRYING

Submitted by
Ian Michael Dubinski
Department of Geosciences

In partial fulfillment of the requirements
For the Degree of Doctor of Philosophy
Colorado State University
Fort Collins, Colorado
Summer 2009

UMI Number: 3385138

All rights reserved

INFORMATION TO ALL USERS

The quality of this reproduction is dependent upon the quality of the copy submitted.

In the unlikely event that the author did not send a complete manuscript and there are missing pages, these will be noted. Also, if material had to be removed, a note will indicate the deletion.



UMI 3385138

Copyright 2009 by ProQuest LLC.

All rights reserved. This edition of the work is protected against unauthorized copying under Title 17, United States Code.



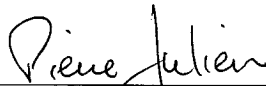
ProQuest LLC
789 East Eisenhower Parkway
P.O. Box 1346
Ann Arbor, MI 48106-1346

COLORADO STATE UNIVERSITY

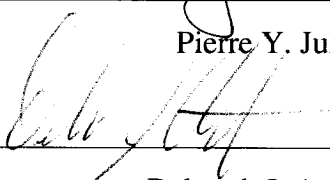
May 19, 2008

WE HEREBY RECOMMEND THAT THE DISSERTATION PREPARED UNDER OUR SUPERVISION BY IAN MICHAEL DUBINSKI ENTITLED PHYSICAL MODELING OF JOINTED BEDROCK EROSION BY BLOCK QUARRYING BE ACCEPTED AS FULFILLING IN PART REQUIREMENTS FOR THE DEGREE OF DOCTOR OF PHILOSOPHY.

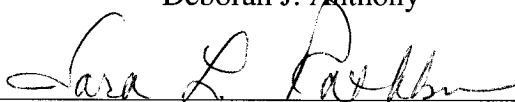
Committee on Graduate Work



Pierre Y. Julien



Deborah J. Anthony

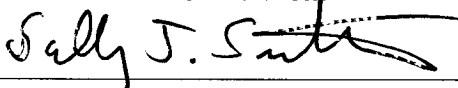


Sara L. Rathburn



Adviser

Ellen E. Wohl



Department Head/Director

Sally J. Sutton

ABSTRACT OF DISSERTATION
PHYSICAL MODELING OF JOINTED BEDROCK EROSION
BY BLOCK QUARRYING

The primary objective of this dissertation is to provide insight in erosional processes, types of channel geometry, and relative rates of incision and knickpoint retreat of channels formed on jointed, resistant rock in a controlled experimental flume setting. Jointed, resistant rock occurs primarily in crystalline lithologies such as granite, gneiss, quartzite, and basalt. These lithologies can be found in a wide range of climatic and tectonic settings. Channels in jointed bedrock may have distinctive erosional processes and geometry relative to channels formed in unjointed bedrock. Joints, fractures, and other discontinuities such as bedding planes in the bedrock are locally weakly resistant zones in contrast to the resistance of unjointed bedrock. These areas may be preferentially weathered to form weakly or completely detached blocks that may be mobilized by flows in the channel. Channels in jointed bedrock commonly have abrupt lateral or downstream discontinuities in bed elevation including steps and knickpoints. A physical model of jointed bedrock using concrete divided into discrete blocks was constructed in a flume and allowed to erode over time by primarily block quarrying. Experimental controls examined in the flume included discharge, channel width, and joint spacing. Observed changes in planform geometry were retreat of the downstream knickpoint with no development of anabranching channels. Erosion by block quarrying occurred with variation between runs of differing control variables. A force analysis of block quarrying combined with a statistical analysis of the erosion results in conjunction

with the control variables, including joint spacing and stream power, provided insight into the process of block quarrying. Wider vertical joint spacing produced more easily eroded blocks than a narrower joint spacing with equal block height in each case when friction forces along the side of the blocks are considered. As blocks loosen over time, the side forces diminish. Without side forces resisting motion, blocks formed by the wider vertical joint spacing are less easily mobilized than the smaller blocks. The other important element in defining block erosion is the key block concept. Erosion of blocks occurred as either a few blocks at one time or a mass movement of blocks at roughly the same time. Mass movements sometimes occurred after removal of a few blocks. These movements of a few blocks were termed key block movements and formed a bimodal population in terms of event magnitude with the mass movements as the other sub-population. Comparison with joint spacing field data from observed anabranching, inner channel, and transitional reaches along the Orange River in South Africa generally concurred with the conclusions drawn from analysis of the model results. Block quarrying is controlled by the balance between block mobility and hydraulic conditions that change over time with periods of little block movement punctuated by mass movements.

Ian Michael Dubinski
Geosciences Department
Colorado State University
Fort Collins, CO 80523
Summer 2009

ACKNOWLEDGMENTS

I would like to acknowledge and thank several individuals and groups who providing invaluable assistance during this project. First, I thank the National Science Foundation for funding this study. I especially thank all the staff at the Colorado State University Engineering Research Center whom without their help this project could never have been completed. I give especially great appreciation to Ellen Wohl, advisor and graduate committee member, for providing me with the opportunity to do this project and her invaluable guidance and insight. I would also like to thank Joe Dartt for his excellent assistance in setting up and running the physical model. For their wisdom and instructive critique concerning this project, I give thanks to graduate committee members Brian Bledsoe, Sara Rathburn, Deb Anthony, Pierre Julien, Greg Springer, and Stephen Tooth. For my wife Hannah, I owe the most thanks for her loving support and guidance that were priceless in helping me complete this dissertation.

TABLE OF CONTENTS

1. Introduction.....	1
1.1 Channels Formed on Jointed Bedrock.....	5
1.2 Statement of Purpose	9
2. Description of Setup, Operation, and Monitoring of Flume Experiment	11
2.1 Flow Regime.....	19
2.2 Operational Time Periods.....	28
2.3 Block Dimensions and Mass	29
2.4 Block Mass Density.....	31
3. Analysis.....	33
3.1 Erosion Record	33
3.2 Changes in Channel Geometry	37
3.3 Planform Geometry	41
3.3.1 Linear Face.....	48
3.3.3 Quasi-Parabolic Curve Opening Downstream.....	50
3.3.4 Irregular Form	50
3.3.5 Quasi-Potholes	51
3.4 Force Analysis for Ideal Block at Knickpoint.....	53
3.4.1 Resisting Forces along Sides of Block.....	63
3.4.2 Forces Acting over Time and Space	68
3.5 Statistical Analysis	70
3.5.1 Probability of Event Occurrence.....	73
3.5.2 Probability of Event Magnitude	78
3.5.3 Modeling Erosion.....	81

4. Conclusions.....	94
5. Application to Anabranching Bedrock Channels	99
6. Further Research in Bedrock Erosion	104
7. References.....	105
Appendix A Flume Data	109
Appendix B Block Coefficient of Friction Test.....	146
Appendix C Statistical Analysis	149
C.1 Further Description of Probabilities of Event Occurrence and Magnitude	150
C.2 Correlation between Event Magnitude and Time Lapse Between Events.....	151
C.3 Correlation between Event Magnitude and Energy Expenditure per Event	154
C.4 Probability of Event Occurrence Supplement.....	154
C.5 Probability of Event Magnitude Supplement.....	172
C.6 Modeling Erosion Supplement	186
Appendix D Orange River Joint Spacing Data	194

LIST OF TABLES

Table 2.1 Characteristics of Flume Runs	11
Table 2.2 Identifying Color of Layers by Run	18
Table 2.3 Discharge and Unit Discharge by Run	20
Table 2.4 Measured Flow Depth (h) and Velocity (u) by Run and Discharge	21
Table 2.5 Hydraulic Parameters by Run and Discharge	23
Table 2.6 Dimensionless Parameters by Run and Discharge	24
Table 2.7 Mean ω and Ω by Run and Discharge	26
Table 2.8 Total Run Time and Cumulative Energy Expenditure by Run	28
Table 2.9 Total Run Time and Cumulative Energy Expenditure by Run and Discharge	28
Table 2.10 Operational Time Periods by Run	28
Table 2.11 Operational Time Periods by Run and Discharge	29
Table 2.12 Characteristic Block Dimensions	30
Table 3.1 Cumulative Erosion by Volume and Block Count by Run	35
Table 3.2 Overall Erosion Rate by Volume and Block Count by Run	35
Table 3.3 Time Lapse Between Events By Run	36
Table 3.4 Time Interval Between Events by Run and Discharge	36
Table 3.5 <i>CUSP</i> per Block by Run	36
Table 3.6 Notation for Figure 3.24	53
Table 3.7 Ranking of Runs by $\ln(\text{Event Volume})$	79
Table 3.8 Event Block Count by Run	80
Table 5.1 Descriptive Statistics for Joint Spacing by Channel Type - Orange River, South Africa	101
Table A.1 Event Data for Run A	110
Table A.2 Event Data for Run B	112
Table A.3 Event Data for Run C	113
Table A.4 Event Data for Run D	116
Table A.5 Event Data for Run E	119
Table A.6 Event Data for Run G	120

Table A.7 Discharge Data for Run A	121
Table A.8 Discharge Data for Run B	125
Table A.9 Discharge Data for Run C	128
Table A.10 Discharge Data for Run D	132
Table A.11 Discharge Data for Run E	138
Table A.12 Discharge Data for Run F	141
Table A.13 Discharge Data for Run G	143
Table B.1 Coefficient of Friction for Block on Baseboard	147
Table B.2 Coefficient of Friction for Block on Block.....	148
Table C.1 Correlation between Time Lapse Between Events and Event Magnitude.....	152
Table C.2 Correlation between <i>CUSP</i> per Event and Event Magnitude	154
Table C.3 KS GOF for Fitted CDF to <i>CUSP</i> per Event by Run	155
Table C.4 <i>CUSP</i> per Event by Run	156
Table C.5 Levene’s Test of Homogeneity of Variances for \ln (<i>CUSP</i> per Event).....	157
Table C.6 Welch’s Robust Test of Equality of Means for \ln (<i>CUSP</i> per Event)	157
Table C.7 Multiple Comparisons by Run of \ln (<i>CUSP</i> per Event) using Dunnett’s C	157
Table C.8 KS GOF Comparison of Fitted CDFs of <i>CUSP</i> per Event by Run.....	157
Table C.9 <i>CUSP</i> per Event by Channel Width Groups.....	158
Table C.10 <i>CTSP</i> per Event by Run.....	159
Table C.11 <i>CTSP</i> per Event by Channel Width Groups	159
Table C.12 Time Lapse Between Events by Channel Width Groups.....	160
Table C.13 Hydraulic Radius (R_h) by Channel Width Groups.....	161
Table C.14 Cumulative Discharge per Event ($Q\Delta t$) by Channel Width Groups	162
Table C.15 Discharge (Q) Between Events by Channel Width Groups.....	162
Table C.16 AOV of Full Model of <i>CTSP</i> per Event	163
Table C.17 AOV of Reduced Model of <i>CTSP</i> per Event.....	164
Table C.18 Descriptive Statistics of Time Lapse Between Events by Run.....	166
Table C.19 Levene’s Test of Homogeneity of Variances for \ln (Time Lapse Between Events) by Run	166

Table C.20 Welch Robust Test of Equality of Means for $\ln(\text{Time Lapse Between Events})$ by Run	166
Table C.21 ANOVA for $\ln(\text{Time Lapse Between Events})$ by Run	166
Table C.22 Multiple Comparisons by Run of $\ln(\text{Time Lapse Between Events})$ using Dunnett's C	167
Table C.23 Comparison of Discharge Between Events by Run	167
Table C.24 Comparison of Time Lapse Between Events by Width and Joint Groupings.....	169
Table C.25 Ranking of Width and Joint Spacing Groups by Time Lapse Between Events.....	169
Table C.26 Robust ANOVA for Full Model of Time Lapse Between Events	170
Table C.27 Robust ANOVA for Reduced Model of Time Lapse Between Events.....	171
Table C.28 KS GOF for Fitted CDF of Event Volume by Run	174
Table C.29 Descriptive Statistics for Event Volume by Run	175
Table C.30 Levene's Test of Homogeneity of Variances for $\ln(\text{Event Volume})$ by Run	176
Table C.31 ANOVA for $\ln(\text{Event Volume})$	176
Table C.32 Welch Robust Test of Equality of Means for $\ln(\text{Event Volume})$ by Run	176
Table C.33 KS GOF Comparison of $\ln(\text{Event Volume})$ by Run	176
Table C.34 Multiple Comparisons by Run of $\ln(\text{Event Volume})$ using Tukey and Dunnett's C.....	177
Table C.35 Descriptive Statistics for Full Model of Event Volume	178
Table C.36 AOV for Full Model of Event Volume.....	179
Table C.37 Levene's Test of Equality of Error Variances for Full Model of Event Volume	180
Table C.38 Event Block Count by Run.....	181
Table C.39 Levene's Test of Homogeneity of Variances for $\ln(\text{Event Block Count})$ by Run	181
Table C.40 ANOVA for $\ln(\text{Event Block Count})$ by Run	181
Table C.41 Welch robust test of equality of means for $\ln(\text{Event Block Count})$ by Run	182
Table C.42 Multiple Comparisons by Run of $\ln(\text{Event Block Count})$ using Tukey and Dunnett's C	182
Table C.43 Descriptive Statistics for Full Model of Event Block Count.....	183
Table C.44 Levene's Test for Equality of Error Variances for $\ln(\text{Event Block Count})$	183
Table C.45 AOV for Full Model of Event Block Count	184
Table C.46 AOV for Reduced Model of Event Block Count.....	185
Table C.47 Levene's Test for Equality of Error Variances for Reduced Model of Event Block Count.....	185

Table C.48 Descriptive Statistics for Reduced Model of Event Block Count.....	185
Table C.49 AOV of Final Model of Event Volume	186
Table C.50 AOV for Full Revised Model of Event Volume.....	188
Table C.51 AOV for Reduced Revised Model of Event Volume	189
Table D.1 Summary of Joint Spacing Data from Sampling Sites - Orange River, South Africa	195

LIST OF FIGURES

Figure 2.1 Step in Entrance Reach Forcing Critical Flow Condition.....	13
Figure 2.2 Example of Simulated Jointed Bedrock in Flume.....	15
Figure 2.3 Discharge Record by Run	19
Figure 2.4 Block Length and Height Measurements.....	30
Figure 2.5 Estimation of Block Density from Block Volume and Mass.....	32
Figure 3.1 Time Series of Erosion by Run.....	34
Figure 3.2 Cumulative Volume Eroded by Run.....	34
Figure 3.3 Knickpoint Slope Measurement.....	37
Figure 3.4 Knickpoint Slopes by Run	37
Figure 3.5 Downstream Position of Knickpoint Layers - Run A	38
Figure 3.6 Downstream Position of Knickpoint Layers - Run B	38
Figure 3.7 Downstream Position of Knickpoint Layers - Run C	39
Figure 3.8 Downstream Position of Knickpoint Layers - Run D	39
Figure 3.9 Downstream Position of Knickpoint Layers - Run E.....	40
Figure 3.10 Downstream Position of Knickpoint Layers - Run G	40
Figure 3.11 Run A – Plan View of Knickpoint Edge Outline over Time	42
Figure 3.12 Run B – Plan View of Knickpoint Edge Outline over Time.....	43
Figure 3.13 Run C – Plan View of Knickpoint Edge Outline over Time.....	44
Figure 3.14 Run D – Plan View of Knickpoint Edge Outline over Time	45
Figure 3.15 Run E – Plan View of Knickpoint Edge Outline over Time	46
Figure 3.16 Run G – Plan View of Knickpoint Edge Outline over Time	47
Figure 3.17 Linear Face of Initial Knickpoint Edge - Run B.....	48
Figure 3.18 Quasi-Parabolic Curve Opening Upstream on Knickpoint Edge - Top Layer in Run B.....	49
Figure 3.19 Another Example of Arch from Photographic Surveys	49
Figure 3.20 Quasi -Parabolic Curve Opening Downstream at Knickpoint Edge -Top Layer in Run B.....	50
Figure 3.21 Irregular Form at Knickpoint Edge - Top and Middle Layers in Run B.....	51
Figure 3.22 Quasi-Potholes Formed by Hydraulic Removal of Blocks	51

Figure 3.23 Removal of Top of Block	52
Figure 3.24 Force Diagram for Ideal Block at Knickpoint	53
Figure 3.25 Distance from Water Surface to Centroid of Side Area, $\bar{\zeta}$	55
Figure 3.26 Diagram of Spring Gage Setup for Measuring F_f	56
Figure 3.27 Spring Gage Attached to Standard Block via Hook.....	57
Figure 3.28 Spring Gage Results for C_f	58
Figure 3.29 Estimated Critical Dimensionless Shear Stress of 1 to 3 Block Events by G_a for $C_f = 0.43$	62
Figure 3.30 Estimated Critical Dimensionless Shear Stress of 1 to 3 Block Events by G_a for $C_f = 0.73$	62
Figure 3.31 Side View of Typical Large Block	63
Figure 3.32 Top View of Typical Large Block.....	63
Figure 3.33 Interlocking Joints between Blocks	64
Figure 3.34 Grains between Blocks	64
Figure 3.35 Example of Arching Created by Mallet	65
Figure 3.36 Example of Arching Created by Mallet	65
Figure 3.37 Empirical CDF and Fitted (Hypothesized) Lognormal CDF - Run A	74
Figure 3.38 Comparison of Mean $\ln(\text{CUSP per Event})$ by Run.....	74
Figure 3.39 Event Volume and $CTSP$ by Run.....	83
Figure 3.40 Event Volume and $CUSP$ by Run.....	83
Figure 3.41 Normal QQ Plot of Residuals of Final Model of Event Volume	85
Figure 3.42 Frequency Plot for Event Magnitude	86
Figure 3.43 Standardized Residuals for Reduced Revised Model of Event Volume	88
Figure 3.44 Density Plot of Residual for Reduced Revised Model of Event Volume	88
Figure 3.45 Normal QQ Plot of Residuals for Reduced Revised Model of Event Volume	89
Figure 3.46 Plot of Response versus Fitted Values for Reduced Revised Model of Event Volume.....	89
Figure C.1 Correlations between Time Lapse Between Events and Block Count - Run A	153
Figure C.2 Correlations between Time Lapse Between Events and Block Count - Run G	153
Figure C.3 Empirical CDF and Fitted (Hypothesized) Lognormal CDF - Run A.....	155
Figure C.4 Standardized Residuals for Reduced Model of $CTSP$ per Event.....	164

Figure C.5 Comparison of Mean $\ln(\text{Time Lapse Between Events})$ by Run	165
Figure C.6 Comparison of Mean $\ln(\text{Discharge Between Events})$ by Run.....	168
Figure C.7 Empirical Normal and Lognormal CDFs for Event Volume - Run A.....	173
Figure C.8 Empirical Normal and Lognormal CDFs for Event Volume - Run D.....	174
Figure C.9 Comparison of Mean $\ln(\text{Event Volume})$ by Run	175
Figure C.10 Estimated Marginal Means of $\ln(\text{Event Volume})$ by Channel Width and Joint Spacing	180
Figure C.11 Comparison of Mean $\ln(\text{Event Block Count})$ by Run	181
Figure C.12 Estimated Marginal Means for $\ln(\text{Block Count})$ by Channel Width and Joint Spacing.....	184
Figure C.13 Normal QQ Plot of Residuals of Final Model of Event Volume	187
Figure C.14 Standardized Residuals for Reduced Revised Model of Event Volume	190
Figure C.15 Density Plot of Residual for Reduced Revised Model of Event Volume.....	190
Figure C.16 Normal QQ Plot of Residuals for Reduced Revised Model of Event Volume.....	191
Figure C.17 Plot of Response versus Fitted Values for Reduced Revised Model of Event Volume	191

NOTATION

A	Anabranching channel type
a	Length of block
AOV	Analysis of variance
AS	Transitional channel type between A and S .
B	Random variable denoting event magnitude
b	Width of block
BC	Discrete random variable denoting number of blocks removed in event.
c	Height of block
CDF	Cumulative distribution function
C_f	Coefficient of friction for a block on a surface
$CTSP$	Cumulative total stream power expended
$CUSP$	Cumulative unit stream power expended
$E[N]$	Expected value of a random variable N
E_e	Continuous random variable denoting $CUSP$ between events
f_s	Side friction force per unit area
F_b	Buoyancy force acting on the block.
F_{bx}	x component of F_b
F_{bz}	z component of F_b
F_f	Force due to friction along the base of the block.
F_f	Force necessary to initially mobilize the block.
F_{fs}	Friction force between blocks acting along the sides of the block.
F_{fsx}	x component of F_{fs}

F_{fsz} ,	z component of F_{fs}
$F_{P_{ds}}$	Force from hydrostatic pressure along the downstream block side (P_{ds}).
$F_{P_{us}}$	Force from hydrostatic pressure along the upstream block side (P_{us}).
Fr	Froude number
F_w	Block weight (not submerged)
F_{wx}	x component of F_w
F_{wz}	z component of F_w
F_{τ}	Force due to τ_b applied to the top surface of the block.
g	Gravitational acceleration (9.81 m/s ²)
G_a	Specific gravity of aerated volume immediately downstream of the block at the knickpoint.
G_s	Specific gravity of the block
h	Flow depth
h/d_s	Ratio of flow depth to block height
J	Dummy variable denoting joint spacing
KS GOF	Kolmogorov-Smirnov goodness of fit test
M	Dummy variable denoting event type (key block or mass events)
M_{block}	Mass of block
N	Normal force at base of the block
P	Wetted perimeter
$P(B)$	Probability of event magnitude
$P(E_e)$	Probability of event after <i>CUSP</i>
P_{ds}	Hydrostatic pressure distribution along the downstream block side.

P_{us}	Hydrostatic pressure distribution along the upstream block side.
$Q \Delta t$	Expended discharge in time span Δt
Q	Discharge
q	Unit discharge
Re	Reynolds number
R_h	Hydraulic radius
S	Inner channel with an outer bedrock strath
S_b	Bed slope
S_f	Friction slope
SP	Stream power (ω or Ω)
T_e	Continuous random variable denoting <i>CTSP</i>
T_t	Continuous random variable denoting time lapse between events
u	Flow velocity
u_∞	Approach flow velocity
u_t	Threshold velocity for block mobilization
V	Continuous random variable denoting event volume
V_{block}	Volume of block
W	Channel width of flume and dummy variable for channel width of flume.
W/h	Ratio of channel width to flow depth
γ_s	Specific weight of block
γ_w	Specific weight of water
γ_{wa}	Specific weight of the aerated nappe flow below the knickpoint edge
Δt	Time lapse between events

ν	Kinematic viscosity (assumed constant at $10^{-6} \text{ m}^2/\text{s}$)
ρ_s	Bedrock mass density
ρ_w	Mass density of water ($1,000 \text{ kg}/\text{m}^3$ at 4°C)
ρ_{wa}	Mass density of the aerated nappe flow below the knickpoint edge
ω	Unit stream power
ω_{narrow}	ω for narrow flume width
ω_{wide}	ω for wide flume width
Ω	Total stream power
Ω_{narrow}	Ω for narrow flume width
Ω_{wide}	Ω for wide flume width
θ	Bed slope angle
τ_b	Bed shear stress
$\bar{\zeta}$	Distance from the water surface to the centroid of the upstream side area.

1. Introduction

The number and scope of studies of the geomorphology of bedrock streams and the processes involved have increased in the late 20th century and into the 21st century. The qualitative concepts and mathematical models of previous studies in alluvial rivers, especially large sand-bed rivers, do not fully describe the processes and forms found in bedrock channels (Tinkler and Wohl, 1998). The channel forms in alluvial rivers reflect competing forces of water and sediment conditions such as those expressed in downstream geometry relationships. Channel morphology in an alluvial river can change dramatically on an annual basis. For example, lateral migration of the Jamuna River, a large sand-bed braided river in Bangladesh, has been estimated to exceed 500 m/yr (Klassen et al., 1993). In comparison, bedrock streams change morphologically at much lower rates. The rock forming the channel in bedrock streams is far more resistant to the erosive forces of sediment-laden flows through the channel than in alluvial channels. The maximum estimated incision rate in the actively incising Indus River in northern Pakistan was 0.012 m/yr (12 mm/yr) based on strath terraces (Burbank et al., 1996). This is orders of magnitude less than the alluvial river example. This comparison of an alluvial river to a bedrock river illustrates that adjustment in bedrock channels towards equilibrium between resistance and erosive forces operates over long time spans and may be difficult to observe quantitatively.

Bedrock erosional fluvial processes include plucking (quarrying), abrasion, cavitation, and dissolution (chemical weathering) (Wohl, 1998). Plucking or quarrying is the removal of bedrock blocks by hydraulic forces. Abrasion is the removal of bedrock material by the impact force of grains transported by the flow. Cavitation is the removal

of bedrock material by high instantaneous pressure forces resulting from the collapse of air bubbles generated in turbulent flow under a high pressure gradient (Annandale, 2006). Dissolution of bedrock such as limestone can also occur through chemical interactions between water and bedrock along the bedrock-water interface. These processes are not mutually exclusive in a given system and can provide feedback to one another. For example, plucking or quarrying of a given block may require loosening of that block by abrasion, cavitation, and dissolution along joints (Wohl, 1998).

Bedrock channels can exhibit heterogeneity associated with joint spacing, rock type, and degree of weathering over a range of spatial scales. Such variables are factors in the total resistance of bedrock to erosion and may give rise to longitudinal variation in bedrock channels that does not produce regular hydraulic geometry relationships (Wohl, 1998). Flows through highly irregular resistant boundary channels can become highly turbulent such that the assumption of a logarithmic velocity profile may not accurately describe the distribution of velocities in the flow and resultant forces acting on the limited sediment supply and bedrock. The behavior of alluvial channels can be modeled over time by using the concepts of equilibrium between known local water conditions (discharge, etc.) and sediment conditions (sediment inputs, grain size of bed sediment). Bedrock channels are very different in that local conditions may be highly variable in terms of resistance to erosion. Instead of sediment aggradation and degradation as the primary means of channel adjustment in alluvial rivers, bedrock rivers adjust by the erosional mechanisms of quarrying, abrasion, and corrosion. Quarrying (i.e., detachment of bedrock blocks) has been shown to depend on available gravitational energy and dominates in zones of macroturbulence and steep energy slopes (Hancock et al., 1998).

Abrasion is principally influenced by flow velocity and sediment characteristics.

Corrosion is driven primarily by chemically corrosive agents such as acidic fluids chemically reacting with limestone, and is relatively independent of mechanical energy.

The magnitude and frequency of each of these processes are linked with changes in the channel gradient and bedrock characteristics. Typically, channel gradients tend to adjust so that gravitational energy expenditures are localized atop resistant strata and minimized on less resistant substrates such that the longitudinal profile of the channel is not smooth given local variability in bedrock resistance (Wohl, 1998).

Correlations among channel geometry, hydraulics, and incision processes along bedrock rivers in a headwater catchment and a base level river have recently been seen using multiple comparisons of hydraulic variables among many stream reaches (Springer, 2002). Unit stream power and shear stress varied by up to three orders of magnitude in small and large catchments as the channel bed material changed from clastic sedimentary rocks to carbonates. High values of stream power per unit area and boundary shear stress were correlated with quarrying of the streambed, whereas corrosion was correlated with extremely low values of stream power per unit area and boundary shear stress.

Sklar and Dietrich (2001) experimentally measured the abrasive erosion rates of different lithologies under different grain sizes and supply rates. They found that the erosion rate decreased with increasing rock tensile strength. They also found that sediment supply at very low levels results in low erosion rates, increasing with increased supply to a peak, and then decreasing as the sediment covers and protects the bedrock surface.

Montgomery and Gran (2001) suggest that the geometry of the channel reflects a tendency towards a balance between hydraulic driving forces and substrate resistance that may be predicted if the balance of forces is quantified. Wohl and Merritt (2001) used a discriminant criterion to correctly classify 70% of the reaches in a dataset of bedrock streams into one of five morphologic types. The discriminant criterion utilized reach-averaged channel gradient, substrate heterogeneity, and Selby rock-mass strength.

Recent studies have attempted to quantify erosional processes and channel geometry in relation to long-term landscape evolution, primarily incision rates. Stock and Montgomery (1999) proposed that abrupt fall of base level will produce channel incision primarily through knickpoint retreat, where the incision rate is weakly dependent on drainage area. The rate of channel incision under stable base level conditions, however, depends strongly on drainage area. Hayakawa and Matsukura (2003) developed a predictive equation for waterfall recession rates by modeling the recession rates using a dimensional analysis of the ratio of erosive forces to bedrock compressive strength. The discharge was approximated using drainage area multiplied by mean precipitation, an approximation that utilizes landscape characteristics to estimate the rate of erosion occurring at the reach scale of the waterfall. Their predictive equation fit the measured mean erosion rate data with an R-squared value of 0.9 on the logarithmic scale.

Channel reaches where incision is driven by knickpoint retreat have a different incision rate than areas where incision is driven by other channel-lowering processes (Seidl and Dietrich, 1992; Stock and Montgomery, 1999). Whipple et al. (2000a) observed that channel erosion was more efficient in areas along Alaska's Ukak River

where the substrate is densely jointed, allowing for more effective quarrying of jointed blocks, rather than a massive substrate.

1.1 Channels Formed on Jointed Bedrock

The primary objective of the research proposed here is to focus on erosional processes, types of channel geometry, and relative rates of incision and knickpoint retreat of channels formed on jointed, resistant rock in a controlled experimental flume setting. Jointed, resistant rock occurs primarily in crystalline lithologies such as granite, gneiss, quartzite, and basalt. These lithologies can be found in a wide range of climatic and tectonic settings. Channels that form in jointed bedrock may have distinctive erosional processes and geometry relative to channels formed on unjointed bedrock. The joints or other discontinuities such as bedding planes in the bedrock are locally weakly resistant zones, in contrast to the resistance of unjointed bedrock, and may be preferentially weathered to form weakly or completely detached blocks that may be mobilized by flows in the channel (Hancock et al., 1998; Tinkler and Wohl, 1998). Channels that form on jointed bedrock commonly have abrupt lateral or downstream discontinuities in bed elevation, including steps and knickpoints (Miller, 1991; Wohl, 1998, 2000; Wende, 1999), and longitudinal grooves (Wohl, 1993).

Bretz hypothesized that The Dalles of the Columbia were formed by large discharges flowing in a high gradient channel “over closely and vertically jointed rock” which is eroded by plucking of blocks rather than abrasion (Bretz, 1924). He described multiple irregularly anabranching channels combined with large scale potholes hypothesized to result from plucking and noted little evidence of large-scale smoothing of

the basalt bedrock by abrasion. The hypothesized conditions necessary for anabranching bedrock channels were high discharge, high gradient, and close and vertical joint spacing. Note that the product of discharge and gradient is stream power. Bretz notes that similar anabranching bedrock channels in the Columbia Basin only occur in large streams with relatively high discharges and hypothesizes that they represent the early stages of stream evolution towards a single equilibrium inner channel. Bretz states that the lack of any of the three conditions of discharge, gradient or joint spacing results in no formation of anabranching bedrock channels. He also suggests that such anabranching channels require a wide area across which flow can spread and develop multiple channels. For Bretz (1924), discharge, gradient, joint spacing, and width were major factors in both the effectiveness of plucking as an erosional process and the formation of anabranching bedrock channels.

More recent descriptive studies have also inferred that jointed and resistant bedrock may facilitate formation of knickpoints and anabranching channels (Baker, 1973; Holland and Pickup, 1976; Baker and Pickup, 1987; Kale and Shingade, 1987; Miller, 1991; Wohl et al., 1994; Van Niekerk et al., 1995, 1999; Kale et al., 1996; Gupta et al., 1999; Heritage et al., 1999). An anabranching bedrock channel has multiple flow paths that branch and rejoin downstream incised into bedrock. Previous terms in the literature used for these types of channels include anabranching, anastomosing, scablands, braided, and erosional braids. Anabranching bedrock channels have been described in North America, South America, India, Africa, and Australia (Tooth and McCarthy, 2004). Short anabranching bedrock channels are commonly observed upstream from major waterfalls (Ahnert, 1994). Under such circumstances, anabranching may be a short-

duration morphology that migrates upstream with the retreating knickpoint. However, more persistent anabranching bedrock channels have been observed far from any active knickpoint, implying that such morphology may arise during channel evolution (Tooth and McCarthy, 2004). Explanations of the occurrence of anabranching bedrock channels include insufficient channel capacity during extreme floods (Baker, 1973, 1978); localized uplift along the channel (Kale et al., 1996; Gupta et al., 1999); and joint-controlled weathering (Van Niekerk et al., 1999). Despite these few case studies, there has been little experimental examination of how different combinations of potential control variables such as available energy and jointing characteristics might influence the onset of anabranching bedrock channel morphology and rates of erosion. The goal of the proposed flume study is to attempt such an experimental examination within the wider context of fluvial erosion of jointed bedrock through primarily block removal.

A first-order consideration of the possible influence of joint spacing and bedrock erosion suggests that larger blocks, being of greater mass, will require greater driving forces to remove. A higher joint density, i.e., narrower joint spacing, divides the bedrock into smaller blocks of less mass that require less net force to mobilize. The force balance of a block shows that a greater block mass will require greater net force to mobilize:

Net Force = Mass of Block x Net Acceleration = Sum of Driving and Resisting Forces
where motion occurs when net force is greater than zero. However, the difficulty lies in determining the nature of the driving and resisting forces acting on the block. Hancock et al. (1998) derived a force balance for a sliding block where the dominant driving force is bed shear stress. The derivation was essentially one dimensional and neglected any friction or driving forces on the sides of the block. An updated derivation was developed

in Whipple et al. (2000a), which included a frictional force for each side of the block. This simple derivation has some important implications for assessing the influence of joint spacing on net force and fluvial force required to remove the block, i.e., erodibility of bedrock by plucking. Under equal bed shear stress and horizontal joint spacing, a wider vertical joint spacing produces a lower critical force required to mobilize the block as it varies with the inverse of width and length. The potential magnitude of the frictional forces depends on the nature of these forces. Whipple et al. (2000b) include within the friction force the effects of rotation of the block and crushing or displacement of material between blocks. In the force balance by Hancock et al. (1998), these sidewall frictional forces were assumed to be negligible.

It is important to consider changes in the frictional forces over time through block loosening (Whipple et al., 2000b). Loosening of the block may be expressed as the lowering of the side and bottom frictional forces and mechanical attachments occurring over time. Physical weathering of bedrock at surface temperature and pressure conditions is by brittle deformation rather than ductile deformation (e.g., tectonic folding), which occurs under higher temperature and pressure conditions (Davis and Reynolds, 1996). Brittle deformation such as by physical weathering occurs in a discontinuous fashion over time. This may rapidly lower the threshold force necessary to mobilize the block and possibly lead to discontinuous erosion of the blocks. Alternatively, loosening may be sufficiently slow to produce a more continuous decline in the erosional threshold for a region of bedrock to yield a more continuous erosion rate.

Returning to Bretz's statement about the geomorphic evolution of The Dalles of the Columbia, joint spacing does play a major role in determining the threshold force

necessary to remove a block and hence the erodibility of bedrock. But the shape of the block, especially the ratio of vertical to horizontal dimensions, and loosening rates are important factors in assessing the erodibility of bedrock and erosion rates, which likely vary over time (Whipple et al., 2000a). Considering the possible importance of block shape, the simple correlation of lower block mass (via narrower joint spacing) to higher erosion might not always accurately portray the erosional conditions and possible relative importance of different erosional processes and the morphology developed in a jointed bedrock channel.

1.2 Statement of Purpose

The basic research question is:

What are the characteristics of channel morphology development on jointed, resistant bedrock as a function of joint spacing, sediment discharge, and channel width?

The study will consider how the morphology develops over time with the goal of developing some insight into the role of joint spacing, discharge, and channel width.

With this basic research question in mind, three specific hypotheses were considered concerning jointed bedrock channels:

H1: The erosional threshold for bedrock with more widely spaced joints is higher than for more narrowly spaced joints.

H2: Erosion is discontinuous over time.

H3: A relationship exists between stream power expenditure over time and event magnitudes.

The hypothesis *H1* considers that more closely spaced joints will produce smaller blocks which may be more readily quarried and transported by the flow due to smaller

mass. More widely spaced joints produce larger blocks which may be more difficult to quarry and transport due to larger mass. This hypothesis focuses on testing the role of block geometry on block mobility.

Considering *H2*, when flow parameters are set just above the erosional threshold for mobilizing an ideal block so that erosion may occur, the hypothesis suggests there will be periods of no motion in between periods of rapid erosion. This reflects block loosening interrupted by block motion as suggested by Whipple et al. (2000a).

Stream power is a variable describing the energy per unit time provided by the stream. Stream power expenditure expresses the expenditure of energy over a given period. Blocks removed from the bed are the results of work done on the bed. Hypothesis *H3* surmises that the work done (i.e., expenditure of energy) to observably remove material may be expressed as some portion of the expenditure of stream power over time. Thus work done on the blocks resulting in observable block removal ought to be a function of stream power expenditure. As blocks loosen over time as described by Whipple et al. (2000a), event magnitudes may possibly increase with increased expended stream power loosening more blocks, assuming uniform block characteristics. However, there may be key blocks in the system which must be removed before surrounding blocks can move. This may complicate the relationship between stream power expenditure and event magnitudes and is investigated, but does not preclude a relationship between stream power expenditure and event magnitude.

This dissertation is part of a larger study funded under a grant from the National Science Foundation that includes a field study of bedrock channels in South Africa. The field data from this study are briefly compared with the findings of our flume experiment.

2. Description of Setup, Operation, and Monitoring of Flume Experiment

The flume experiment was conducted in a flume located at Colorado State University's Engineering Research Center in Fort Collins, Colorado. The flume is 10 m long with available widths of 0.6 m and 1.2 m. Discharges up to 0.28 m³/s (10 ft³/s) can be supplied to the flume consistently with monitoring via a pressure gauge on the supply line. The flume is supported on a metal structure to allow incremental change in slope. A constant slope of 0.029 was used for all experimental setups. A valve at the flume and a bypass valve at the pump site are manually operated to regulate the discharge magnitude. The six flume runs conducted (A through G) are characterized in Table 2.1.

Table 2.1 Characteristics of Flume Runs

Run	Jointing Pattern	Discharge Conditions	Flume Width	Total Run Time (hrs)
A	Even, closely spaced joints (~3cm)	0.20 m ³ /s	0.6 m	99.15
B	Even, widely spaced joints (~6cm)	0.11 and 0.20 m ³ /s	0.6 m	92.93
C	Closely and widely spaced joints at longitudinal intervals	0.11 and 0.20 m ³ /s	0.6 m	119.76
D	Even, closely spaced joints (~3cm)	0.11 and 0.20 m ³ /s	1.2 m	100.00
E	Even, widely spaced joints (~6cm)	0.11 and 0.20 m ³ /s	1.2 m	45.07
F	Closely and widely spaced joints at lateral intervals	0.20 m ³ /s	1.2 m	22.50
G	Even, closely spaced joints (~3cm)	0.20 m ³ /s	1.2 m	50.00

This flume experiment is an idealized analog model of jointed bedrock channel boundaries in natural channels and associated hydraulics. Longer time scales and greater spatial scales are required for more accurate scaling of quarrying in bedrock channels with block scales on the order of meters and much greater discharge and hydraulic variables. These conditions cannot be reproduced within the available space and capacity of this flume experiment. However, a degree of scaling to natural bedrock channels may

be achieved in the flume runs based on the Froude number, Fr (Thompson and Wohl, 1998).

Equation 2.1

$$Fr = \frac{u}{(g h)^{0.5}}$$

where u is velocity, g is gravitational acceleration, and h is flow depth. This is based on the assumption that bedrock channels are primarily eroded during high discharges with Fr near 1 (critical flow) (Grant, 1997; Tinkler, 1997a,b).

After emplacing the unbroken blocks in Run A, channel conditions were adjusted for slope, initial channel dimensions and roughness to produce Fr along the bed that are at or close to 1. During this period, no bedrock erosion occurred and no blocks were disjointed by the supplied flows. An entrance reach of the flume immediately below the discharge input pipe was constructed to bring the flow to $Fr \sim 1$ at the beginning of the simulated jointed bedrock by using a diffusive wire mesh with rocks placed at the lower third of the vertical mesh followed by a step that is 1 m in length covered with a roughness formed by pebbles glued to plywood (Figure 2.1). In addition to the entrance reach, wooden blocks measuring 25 cm height by 4 cm wide by 9 cm long in the downstream direction were placed regularly at 1 m intervals beginning at the exit of the entrance section (Figure 2.1). The wooden blocks act as roughness elements that restrain the flow to maintain near-critical flow along the bedrock sections after the flow exits the entrance section with $Fr \sim 1$. During the beginning operation of the flume, the discharge was increased over a period of at least 5 minutes to the pre-determined experimental discharge in order to mitigate the flood wave effect on the rate of block quarrying.

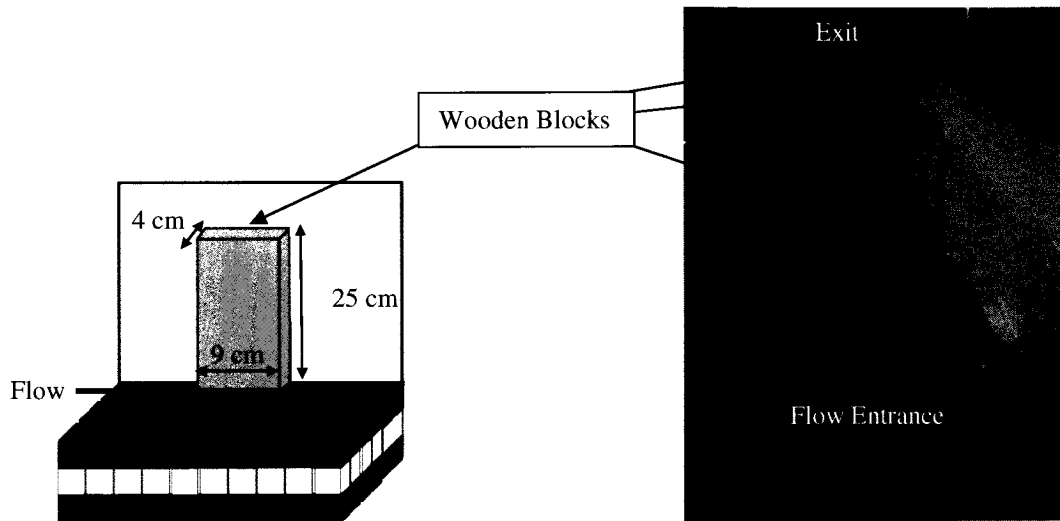


Figure 2.1 Step in Entrance Reach Forcing Critical Flow Condition. Note the roughness elements (wooden blocks along wall and pebbles glued to plywood in the approach section) along edge of flume used to keep flow near critical ($Fr = 1$). Flow is from bottom to top of figure.

In addition to flow with $Fr \sim 1$, the other important scaling factor relating flow conditions to joint spacing and resultant block size was the estimated critical flow conditions necessary for erosion of blocks of a given size where the blocks have been disjointed in place. Joint spacing and resulting block dimensions were chosen with consideration for model limits imposed by the dimensions of the flume and limits in possible discharge that can be provided to the flume to erode the blocks of a given size. Previous flume and field studies suggest that incipient motion of large boulders on bedrock surfaces occurs when Froude numbers are near unity with flow depth of similar order to boulder height (Carling and Tinkler, 1998). Hancock et al. (1998) showed that the block thickness that a river is theoretically capable of quarrying through sliding is proportional to the square of the local flow velocity:

Equation 2.2

$$u_t = \left[\left(2 g c \frac{\rho_s}{\rho} \right) - 1 \right]^{0.5}$$

where u_t is threshold velocity for block mobilization, c is vertical block dimension, ρ is the mass density of water, and ρ_s is bedrock mass density.

Two different block sizes formed by two different joint spacings were selected. A block size of 3 cm depth and 3 cm width and length was chosen for the narrow joint spacing (i.e., small blocks type A), and 3 cm depth with 6 cm width and length for the wide joint spacing (i.e., large blocks type B). With respect to hydraulic conditions, the Hancock et al. (1998) equation for critical velocity for block height of 3 cm, assuming block mass density of 2,650 kg/m³ and water mass density of 1,000 kg/m³, yields a critical flow velocity of 0.75 m/s. For Fr of 1 to 2.0, the flow depth is 0.06 m, twice the block height, to 0.12 m, four times the block height. Given a narrow flume width of 0.6 m, the minimum critical discharge was estimated to be 0.027 m³/s (0.95 ft³/s) for Fr of 1 and 0.054 m³/s (1.9 ft³/s) for Fr of 2. This minimum discharge range was easily achieved in the flume and used as a minimum starting discharge that was increased to provide measurable and manageable erosion rates for Run A, as discussed later. The block dimensions allow for several blocks to span the width of flume, geometrically allowing for possible multiple channels to develop from blocks being quarried.

These block dimensions were easily constructed in frames of manageable sizes. The bedrock consists of concrete with regularly spaced horizontal and vertical joints. The concrete is a 4:1 mixture of fine, masonry grade sand to Portland cement. The concrete was poured into 0.6 m by 1 m forms to a uniform depth of 3 cm (height of one layer) monitored by point measurements of cement depth in the form. A thin metal sheet was then forced into the drying concrete at regular intervals to form a grid pattern of regularly spaced vertical joints. This process produces one horizontal layer from one

form. The horizontal layers are placed on top of each other to simulate horizontal jointing. There is a 6 cm border on the longitudinal sides of the form that abuts the flume walls to aid in the layering of the concrete layers and act as a buffer zone between the jointed section and the flume wall. The finished forms are placed inside the flume with the concrete layer and a form base creating the bottom, and the next layer is slid from the form base onto the layer already in the flume. The final product is a channel bed consisting of regularly horizontally and vertically jointed concrete where quarrying of blocks of consistent size can occur (Figure 2.2). Any cohesive bond between blocks is removed by physically breaking the blocks apart along the joints using hammers and wedges. The lack of sediment in the flow for abrasion and use of sufficiently strong concrete to resist abrasion by water alone was maintained such that quarrying and not abrasion is the dominant erosive process on jointed channel substrates where joint spacing is sufficiently close to produce blocks that can be transported by flow (Hancock et al., 1998; Whipple et al., 2000a,b).

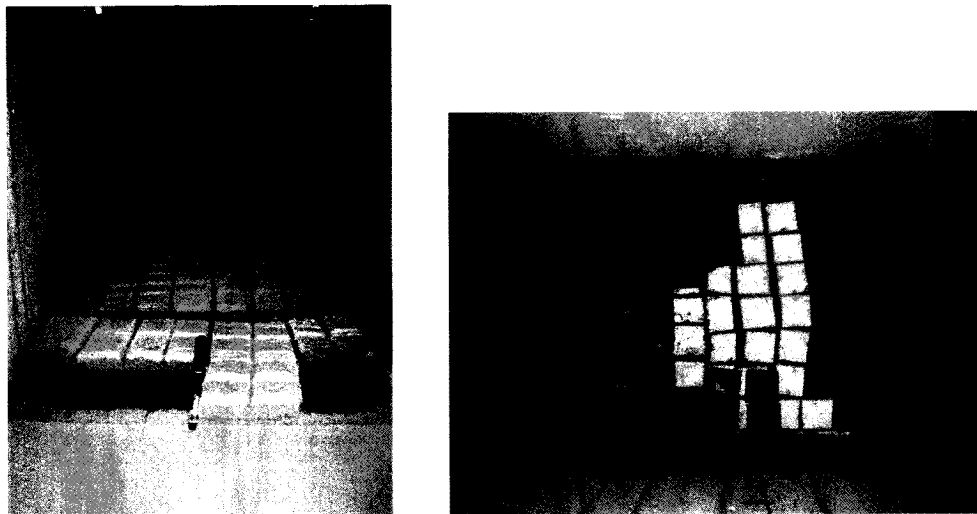


Figure 2.2 Example of Simulated Jointed Bedrock in Flume. The vertical joint spacing is 6 cm and the horizontal joint spacing is 3 cm. Both photos taken after quarrying occurred.

During the initial design stages for Run A setup, the estimated minimum critical discharge of $0.05 \text{ m}^3/\text{s}$ ($2 \text{ ft}^3/\text{s}$) for Fr of 2 was initially used, then increased to $0.085 \text{ m}^3/\text{s}$ ($3 \text{ ft}^3/\text{s}$), $0.11 \text{ m}^3/\text{s}$ ($4 \text{ ft}^3/\text{s}$), $0.11 \text{ m}^3/\text{s}$ ($5 \text{ ft}^3/\text{s}$), $0.17 \text{ m}^3/\text{s}$ ($6 \text{ ft}^3/\text{s}$), and $0.20 \text{ m}^3/\text{s}$ ($7 \text{ ft}^3/\text{s}$). During these discharges, velocity and flow depth measurements were taken to assess and refine Froude numbers and flow conditions for conducting runs. Note that the blocks were not disjointed during this initial design stage. If quarrying occurs at too high a rate, significant backwater develops and the water must be turned off to allow removal of the blocks. Thus the discharge is limited to a flow at which the rate of quarrying is manageable. This is an issue because if one setup is quarrying at too high a rate at the discharge of the previous runs, then in order to practically run the experiment, the discharge must be lowered to a manageable rate. After disjointing the blocks for Run A setup, the discharge was gradually increased from $0.05 \text{ m}^3/\text{s}$ ($2 \text{ ft}^3/\text{s}$), when a few end blocks moved out of place, to $0.11 \text{ m}^3/\text{s}$ ($4 \text{ ft}^3/\text{s}$), during which a few additional blocks moved, and then to $0.17 \text{ m}^3/\text{s}$ ($6 \text{ ft}^3/\text{s}$), which moved a few more blocks. A discharge of $0.17 \text{ m}^3/\text{s}$ ($6 \text{ ft}^3/\text{s}$) was used for the first 7.5 hours of Run A. Discharge was then increased to $0.20 \text{ m}^3/\text{s}$ ($7 \text{ ft}^3/\text{s}$), which in the narrow flume setup was determined to be the highest manageable discharge without risk of flow overtopping the flume entrance section or walls. This was increased to the highest manageable discharge to maximize erosion so that measurable erosion might occur in a reasonable time span to allow for other runs to be conducted in the time available for use of the flume. For consistency between runs, the same set of discharges was used in both the wide and narrow flume setups. A discharge of $0.20 \text{ m}^3/\text{s}$ ($7 \text{ ft}^3/\text{s}$) was the maximum discharge used, whereas a lower discharge of $0.11 \text{ m}^3/\text{s}$ ($4 \text{ ft}^3/\text{s}$) was used to examine the effects of hydraulics on the

erosion rate. A high discharge of $0.255 \text{ m}^3/\text{s}$ ($9 \text{ ft}^3/\text{s}$) was achieved in the wide flume, but at this discharge the water depth at the entrance section nearly reaches the top of the containing walls in the narrow flume setup. At such a high discharge the flow in the narrower flume setup with width of 0.6 m was at risk of overtopping the flume walls. The lower discharge of $0.20 \text{ m}^3/\text{s}$ ($7 \text{ ft}^3/\text{s}$) was successfully contained within the flume in both narrow and wide flume width setups. The measured flow velocity and depth and calculated flow parameters are summarized later for all runs, following the description of measurement techniques.

While the flume experiment was running, digital photography was used to document the changes in bed topography over time by photographing from above the full length and width of the bedrock channel between each operation of the flume during all runs. Video was also utilized to monitor quarrying and morphological change over time and space.

Both the discharge and local hydraulic conditions in the flume were regularly monitored during all runs. Discharge was set and regularly monitored manually during each operation of the flume using the digital pressure gage located on the line feeding into the flume. The digital pressure gage readout on the 40 hp pump line gave pressure in feet of water which was converted into cubic feet of water using the provided calibration equation. The 40 hp pump line was the primary discharge provider during all runs. The 75 hp pump line was used on a few occasions when the 40 hp pump line was unavailable. The digital pressure gage readout on the 75 hp pump line was discharge in cubic feet per second. Local hydraulic conditions in the flume were monitored. Repeat measurements of water-surface topography and bed elevation using a point gage mounted above the

flume were coupled with measurements of local downstream flow velocity using a one-dimensional Marsh-McBirney flow meter, except for Run G during which no flow velocity measurements were taken. Flow depth and flow velocity measurements were taken once at the beginning of each operation of the flume after the desired discharge was established. These measurements were made along the longitudinal center of the channel at regular intervals located at the sidewall roughness elements, half-way between elements, at the top of the entrance section step, at the top of the knickpoint, and below the knickpoint where the flow returns from jetting over the knickpoint edge.

Regular measurements of flow depth with the point gage were taken in a regular grid fashion covering the entire width and length of the bedrock channel. These were sometimes accompanied with point velocity measurements using the Marsh-McBirney flow meter. The longitudinal and lateral position of each measurement was recorded. The block layers were painted different colors to aid in visual identification (Table 2.2).

Table 2.2 Identifying Color of Layers by Run

Run	Top Layer	Middle Layer	Bottom Layer
A	Green	Yellow	White
B	Red	White	Green
C	Red	White	Gold
D	Red	White	Gold
E	Red	White	Gold
F	Red	N/A	Gold
G	Red	White	Gold

Quarried blocks were caught at the end of the flume by the grating at the flume exit where the flow freefalls into the facility's reservoir. These blocks were removed by hand. The end section was checked for any blocks at regular intervals of at least 30 minutes. Blocks were removed immediately after mobility was directly observed. The

removed blocks were recorded by count for each type (3 cm or 6 cm), color, and possibly multiple blocks still attached to each other such as 2 by 1 for two blocks still attached to each other. For Run A only, the color of each block was not recorded.

2.1 Flow Regime

The record of discharge (Q) for all runs is provided in Figure 2.3. The mean, median, and standard deviation of Q and q were calculated by run and discharge condition (0.20 m³/s and 0.11 m³/s) (Table 2.3). Unit discharge (q) was also calculated for each discharge record entry as:

Equation 2.3

$$q = \frac{Q}{W}$$

where W is channel width of flume.

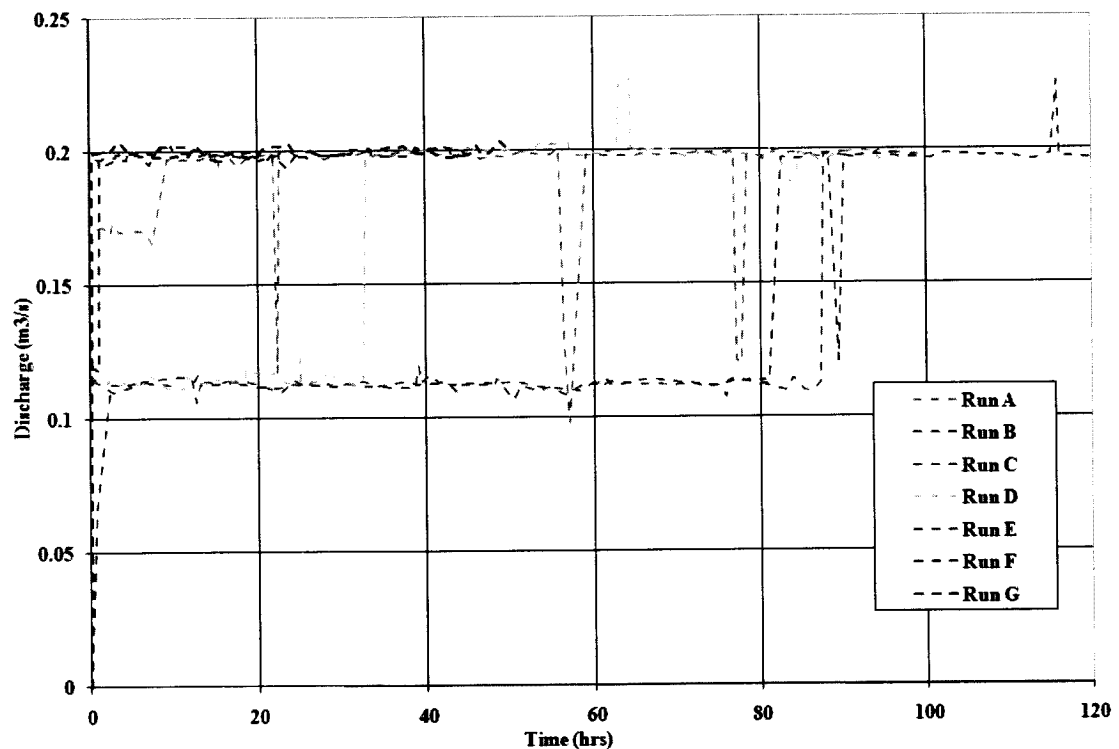


Figure 2.3 Discharge Record by Run

Table 2.3 Discharge and Unit Discharge by Run

Run A at 0.20 m³/s			Run B at 0.11 m³/s		
	Q (m³/s)	q (m²/s)	Q (m³/s)	q (m²/s)	
Mean:	0.19	0.31	0.11	0.18	
Median:	0.20	0.33	0.11	0.19	
Std Dev:	0.0197	0.0322	0.0059	0.0096	
Total N:	96	96	64	64	
Run B at 0.20 m³/s			Run C at 0.11 m³/s		
	Q (m³/s)	q (m²/s)	Q (m³/s)	q (m²/s)	
Mean:	0.19	0.31	0.11	0.18	
Median:	0.20	0.32	0.11	0.18	
Std Dev:	0.0288	0.0472	0.0023	0.0038	
Total N:	7	7	69	69	
Run C at 0.20 m³/s			Run D at 0.11 m³/s		
	Q (m³/s)	q (m²/s)	Q (m³/s)	q (m²/s)	
Mean:	0.20	0.33	0.11	0.10	
Median:	0.20	0.32	0.11	0.10	
Std Dev:	0.0053	0.0087	0.0021	0.0018	
Total N:	29	29	50	50	
Run D at 0.20 m³/s			Run E at 0.11 m³/s		
	Q (m³/s)	q (m²/s)	Q (m³/s)	q (m²/s)	
Mean:	0.20	0.17	0.12	0.10	
Median:	0.20	0.17	0.12	0.10	
Std Dev:	0.0052	0.0045	0.0013	0.0011	
Total N:	97	97	2	2	
Run E at 0.20 m³/s			Run F at 0.20 m³/s		
	Q (m³/s)	q (m²/s)	Q (m³/s)	q (m²/s)	
Mean:	0.20	0.17	0.19	0.17	
Median:	0.20	0.17	0.20	0.17	
Std Dev:	0.0016	0.0014	0.0359	0.0307	
Total N:	66	66	31	31	
Run F at 0.20 m³/s			Run G at 0.20 m³/s		
	Q (m³/s)	q (m²/s)	Q (m³/s)	q (m²/s)	
Mean:	0.19	0.17	0.20	0.17	
Median:	0.20	0.17	0.20	0.17	
Std Dev:	0.0359	0.0307	0.0016	0.0014	
Total N:	31	31	63	63	

Within flume-scale conditions, local hydraulic conditions at the knickpoint are of primary importance because this is the location of most if not all erosional activity. The flow depth (h) and velocity (u) along the centerline of the channel were regularly measured during all runs. Measurements of h and u are summarized in Table 2.4.

Table 2.4 Measured Flow Depth (*h*) and Velocity (*u*) by Run and Discharge

Run A at 0.20 m³/s

	<i>h</i> (m)	<i>u</i> (m/s)
Mean:	0.17	1.73
Median:	0.16	1.73
Std Dev:	0.04	0.16
Total N:	17	17

Run B at 0.20 m³/s

	<i>h</i> (m)	<i>u</i> (m/s)
Mean:	0.17	1.75
Median:	0.17	1.75
Std Dev:	0.05	0.07
Total N:	2	2

Run C at 0.20 m³/s

	<i>h</i> (m)	<i>u</i> (m/s)
Mean:	0.16	1.93
Median:	0.15	1.93
Std Dev:	0.03	0.11
Total N:	5	5

Run D at 0.20 m³/s

	<i>h</i> (m)	<i>u</i> (m/s)
Mean:	0.08	1.82
Median:	0.08	1.82
Std Dev:	0.01	0.05
Total N:	18	18

Run E at 0.20 m³/s

	<i>h</i> (m)	<i>u</i> (m/s)
Mean:	0.09	1.80
Median:	0.09	1.81
Std Dev:	0.01	0.07
Total N:	12	12

Run F at 0.20 m³/s

	<i>h</i> (m)	<i>u</i> (m/s)
Mean:	0.09	1.81
Median:	0.09	1.83
Std Dev:	0.01	0.04
Total N:	6	6

Run B at 0.11 m³/s

<i>h</i> (m)	<i>u</i> (m/s)
0.11	1.43
0.10	1.48
0.02	0.18
25	25

Run C at 0.11 m³/s

<i>h</i> (m)	<i>u</i> (m/s)
0.12	1.40
0.12	1.37
0.01	0.15
15	15

Run D at 0.11 m³/s

<i>h</i> (m)	<i>u</i> (m/s)
0.05	1.52
0.05	1.56
0.00	0.08
9	9

Run E at 0.11 m³/s

<i>h</i> (m)	<i>u</i> (m/s)
0.05	NA
0.05	NA
NA	NA
1	1

Run G at 0.20 m³/s

<i>h</i> (m)	<i>u</i> (m/s)
0.08	1.68
0.08	1.71
0.01	0.08
10	10

Measurements of flow depth and velocity were used to calculate the difference between flow velocity and the critical flow velocity of 0.75 m/s calculated earlier from the Hancock et al. (1998) equation, hydraulic radius R_h , and bed shear stress τ_b . Assuming steady uniform flow, τ_b may be simplified to:

Equation 2.4

$$\tau_b = \rho g R_h S_f$$

Assuming $S_f \sim S_b$, where S_f is the friction slope and S_b is the bed slope, and a rectangular cross section of the channel, then bed shear stress and hydraulic radius are:

Equation 2.5

$$\tau_b = \rho g R_h S_b$$

Equation 2.6

$$R_h = \frac{W h}{W + 2h}$$

Flow depth measurements were used to estimate τ_b using Equation 2.5 and Equation 2.6. The mean, median, and standard deviation of these local hydraulic parameters were calculated by run and discharge condition (Table 2.5).

A number of dimensionless parameters were also calculated including the ratio of flume width to flow depth (W/h); ratio of flow depth to block height (h/c); the Reynolds number (Re), and the Froude number (Fr). The Reynolds number (Re) is a measurement of flow turbulence intensity and may be written as:

Equation 2.7

$$\text{Re} = \frac{u h}{\nu}$$

where ν is kinematic viscosity, assumed constant at $10^{-6} \text{ m}^2/\text{s}$. The mean, median, and standard deviation of these dimensionless parameters were calculated by run and discharge condition ($0.20 \text{ m}^3/\text{s}$ and $0.11 \text{ m}^3/\text{s}$, if applicable) (Table 2.6).

Table 2.5 Hydraulic Parameters by Run and Discharge

Run A at 0.20 m³/s			
	$u - u_t$ (m/s)	R_h (m)	τ_b (N/m ²)
Mean:	1.04	0.106	30.3
Median:	1.04	0.105	29.9
Std Dev:	0.16	0.015	4.2
Total N:	17	17	17

Run B at 0.20 m³/s			
	$u - u_t$ (m/s)	R_h (m)	τ_b (N/m ²)
Mean:	1.06	0.110	31.2
Median:	1.06	0.110	31.2
Std Dev:	0.07	0.022	6.3
Total N:	2	2	2

Run B at 0.11 m³/s			
	$u - u_t$ (m/s)	R_h (m)	τ_b (N/m ²)
	0.73	0.078	22.2
	0.78	0.075	21.4
	0.18	0.012	3.4
	25	25	25

Run C at 0.20 m³/s			
	$u - u_t$ (m/s)	R_h (m)	τ_b (N/m ²)
Mean:	1.24	0.103	29.2
Median:	1.24	0.098	28.0
Std Dev:	0.11	0.014	4.0
Total N:	5	5	5

Run C at 0.11 m³/s			
	$u - u_t$ (m/s)	R_h (m)	τ_b (N/m ²)
	0.71	0.084	24.0
	0.67	0.086	24.4
	0.15	0.008	2.2
	15	15	15

Run D at 0.20 m³/s			
	$u - u_t$ (m/s)	R_h (m)	τ_b (N/m ²)
Mean:	1.13	0.061	17.5
Median:	1.13	0.061	17.4
Std Dev:	0.05	0.003	1.0
Total N:	18	18	18

Run D at 0.11 m³/s			
	$u - u_t$ (m/s)	R_h (m)	τ_b (N/m ²)
	0.83	0.041	11.7
	0.86	0.040	11.4
	0.08	0.003	1.0
	9	9	9

Run E at 0.20 m³/s			
	$u - u_t$ (m/s)	R_h (m)	τ_b (N/m ²)
Mean:	1.10	0.070	20.0
Median:	1.12	0.069	19.6
Std Dev:	0.07	0.005	1.5
Total N:	12	12	12

Run E at 0.11 m³/s			
	$u - u_t$ (m/s)	R_h (m)	τ_b (N/m ²)
	NA	0.042	12.0
	NA	0.042	12.0
	NA	NA	NA
	1	1	1

Run F at 0.20 m³/s			
	$u - u_t$ (m/s)	R_h (m)	τ_b (N/m ²)
Mean:	1.12	1.963	24.8
Median:	1.13	1.974	24.6
Std Dev:	0.04	0.080	1.6
Total N:	6	6	6

Run G at 0.20 m³/s			
	$u - u_t$ (m/s)	R_h (m)	τ_b (N/m ²)
	0.99	0.066	18.7
	1.02	0.064	18.2
	0.08	0.004	1.1
	10	10	10

Table 2.6 Dimensionless Parameters by Run and Discharge

Run A at 0.20 m³/s				
	W/h	h/c	Re	Fr
Mean:	3.82	5.54	283235	1.39
Median:	3.81	5.33	267960	1.40
Std Dev:	0.73	1.27	40212	0.25
Total N:	17	17	17	17

Run B at 0.20 m³/s				
	W/h	h/c	Re	Fr
Mean:	3.67	5.82	303382	1.37
Median:	3.67	5.82	303382	1.37
Std Dev:	1.15	1.82	83040	0.27
Total N:	2	2	2	2

Run B at 0.11 m³/s				
	W/h	h/c	Re	Fr
	5.97	3.54	148751	1.43
	6.10	3.33	145030	1.50
	1.19	0.75	27483	0.27
	25	25	25	25

Run C at 0.20 m³/s				
	W/h	h/c	Re	Fr
Mean:	4.01	5.22	300026	1.58
Median:	4.21	4.83	278400	1.65
Std Dev:	0.70	1.17	49022	0.22
Total N:	5	5	5	5

Run C at 0.11 m³/s				
	W/h	h/c	Re	Fr
	5.30	3.90	162384	1.33
	5.13	3.97	162150	1.26
	0.72	0.47	9727	0.23
	15	15	15	15

Run D at 0.20 m³/s				
	W/h	h/c	Re	Fr
Mean:	15.29	2.56	140265	2.10
Median:	15.30	2.55	138825	2.11
Std Dev:	1.08	0.18	9732	0.11
Total N:	18	18	18	18

Run D at 0.11 m³/s				
	W/h	h/c	Re	Fr
	24.87	1.58	72243	2.24
	25.43	1.53	67620	2.19
	2.39	0.15	8877	0.14
	9	9	9	9

Run E at 0.20 m³/s				
	W/h	h/c	Re	Fr
Mean:	12.90	3.05	166133	1.89
Median:	13.15	2.97	161558	1.93
Std Dev:	1.10	0.32	20339	0.11
Total N:	12	12	12	12

Run E at 0.11 m³/s				
	W/h	h/c	Re	Fr
	23.88	1.63	NA	NA
	23.88	1.63	NA	NA
	NA	NA	NA	NA
	1	1	1	1

Run F at 0.20 m³/s				
	W/h	h/c	Re	Fr
Mean:	13.50	2.90	157547	1.96
Median:	13.53	2.89	159471	1.97
Std Dev:	0.86	0.19	10422	0.08
Total N:	6	6	6	6

Run G at 0.20 m³/s				
	W/h	h/c	Re	Fr
	14.06	2.79	140297	1.87
	14.45	2.70	138895	1.92
	0.99	0.21	3407	0.15
	10	10	10	10

Although expressions for stream power are relatively consistent, the nomenclature is not always well-defined (Graf, 1983; Rhoads, 1987). Unit stream power (ω) will be defined as stream power per unit area of the wetted perimeter and total stream power (Ω) is stream power per unit length along the channel based on nomenclature and corresponding definitions used in Graf (1983) and Rhoads (1987). Both ω and Ω were calculated for each discharge record entry using:

Equation 2.8

$$\omega = \rho g u R_h S_f$$

Equation 2.9

$$\Omega = \omega P$$

where P is the wetted perimeter (Bagnold, 1960, 1966; Graf, 1983; Rhoads, 1987). The calculated R_h was used instead of approximating it as equal to flow depth because the width to depth ratios in the flume are as low as ~ 3 . After assuming $S_f \sim S_b$, substituting in expression for R_h from Equation 2.6, and substituting $Q = u W h$ (continuity equation), the expressions for stream power are further simplified to:

Equation 2.10

$$\omega = \frac{\rho g Q S_b}{W + 2 h}$$

Equation 2.11

$$\Omega = \rho g Q S_b$$

These simplified expressions were used to estimate ω and Ω . For stream power values, SI units will be used where ω is W/m^2 and Ω is W/m . Because the location of primary erosion is at the knickpoint, mean flow depth measurements at the knickpoint will be used in stream power calculations. The mean ω and Ω were calculated by run and discharge condition ($0.20 \text{ m}^3/\text{s}$ and $0.11 \text{ m}^3/\text{s}$, if applicable) (Table 2.7).

Table 2.7 Mean ω and Ω by Run and Discharge

Run	Mean ω (W/m²)	Mean Ω (W/m)
A7	58	0.26
B4	36	0.24
B7	59	0.27
C4	37	0.24
C7	61	0.26
D4	25	0.36
D7	43	0.37
E4	26	0.36
E7	42	0.38
F7	43	0.37
G7	42	0.37

The flow applies a load on the jointed concrete bed over a period of time. Eventually some blocks are dislodged and mobilized. This action is a brittle fracture process where the load applied to the material degrades the material until catastrophic failure, in this case erosion of material through the removal of blocks (Annandale, 2006). Not only is the magnitude of the load important, but also the length of time that load is applied. If a load is applied for only a short period of time, then little degradation of the material will occur. The longer the load is applied, the more degradation will occur. This action is analogous to breaking rocks with a hammer as the load applicator. A few strikes of the hammer will not break the rock, but will perhaps create only superficial fractures. Over time, as the hammer repeatedly applies a load to the rock, the density of fractures and magnitude of individual fractures grows without major change to the shape of the rock until the rock suddenly breaks apart in a catastrophic failure. The total energy expended leading to catastrophic failure of the rock is the integration of the load applied by the hammer over time. The loading mechanism in the flume is the flow. Stream power provides a measure of the rate of energy (i.e., force over a length) expenditure of

the flow. The total energy expended over time may then be represented as the integration of stream power over time.

Although stream power is a continuous function, the discharge and hence stream power were kept at a nearly constant rate during operation of the flume with manual regular monitoring and measurement of the actual discharge, the integral is replaced by a summation over time of intervals corresponding to discharge measurements:

Equation 2.12

$$\text{Total Energy Expenditure} = \sum \text{Stream Power } (Q_x) \Delta t_{xx}$$

For example, flow starts at time t_{Start} . Discharge measurements Q_1 , Q_2 and Q_3 are taken at time t_1 , t_2 , and t_3 and the flow ends at time t_{End} . The corresponding period where Q_2 is the discharge used for calculating stream power and the time period is from $(t_2 - t_1) / 2$ to $(t_3 - t_2) / 2 = \Delta t_{13}$. *Total Energy Expenditure* corresponding to Q_2 is then $\Omega (Q_2) \Delta t_{13}$. For the starting and ending periods, the time period is from t_{Start} to $(t_2 - t_1) / 2 = \Delta t_{Start2}$ and $(t_3 - t_2) / 2$ to $t_{End} = \Delta t_{3End}$. *Total Energy Expenditure* for the entire run is then:

Equation 2.13

$$\text{Total Energy Expenditure} = SP (Q_1) \Delta t_{Start2} + SP (Q_2) \Delta t_{13} + SP (Q_3) \Delta t_{2End}$$

where *SP* is the selected stream power value (e.g. ω or Ω). The summation of unit stream power is the same as for total stream power. For total stream power, Ω the function only depends on the discharge value. As discussed earlier, the mean flow depth at the knickpoint is used to calculate the hydraulic radius for calculating ω . The cumulative ω (*CUSP*) and cumulative Ω (*CTSP*) were calculated for each run and by run and discharge pair (Table 2.8 and Table 2.9).

Table 2.8 Total Run Time and Cumulative Energy Expenditure by Run

Run	Total Run Time (hrs)	Cumulative ω (kJ/m ²)	Cumulative Ω (kJ/m)
A	99.15	20844.30	19642.61
B	92.93	13034.20	11647.50
C	119.76	18748.44	16644.07
D	100.00	13349.00	17627.50
E	45.07	6729.35	9099.32
F	22.50	3487.05	4603.95
G	50.00	7630.50	10203.50

Table 2.9 Total Run Time and Cumulative Energy Expenditure by Run and Discharge

Run	Total Run Time (hrs)	Cumulative ω (kJ/m ²)	Cumulative Ω (kJ/m)
A7	99.15	20844	19643
B4	81.93	10702	9415
B7	11.00	2332	2233
C4	87.34	11631	10067
C7	32.42	7117	6577
D4	32.50	2898	3792
D7	67.50	10451	13836
E4	1.00	93	122
E7	44.07	6636	8978
F7	22.50	3487	4604
G7	50.00	7631	10204

2.2 Operational Time Periods

It may be the case that the length of time run during each individual period of operation has an impact on the erosion of the jointed concrete bed. Of particular concern are the startup and shutdown intervals during a given period of operation. The distributions of the length of operational periods during each run were calculated for comparison (Table 2.10 and Table 2.11).

Table 2.10 Operational Time Periods by Run

Run:	A	B	C	D	E	F	G
Mean Time (hrs):	3.00	3.20	5.99	3.57	3.47	3.21	5.00
Median Time (hrs):	2.00	2.83	6.59	4.00	3.50	3.33	5.00
Std Dev:	2.18	1.63	1.34	1.13	1.41	1.71	0.37
Maximum:	7.00	7.50	7.25	5.50	5.00	5.08	5.67
Minimum:	0.10	0.50	3.00	0.33	1.00	0.17	4.50
Total Time:	99.15	92.93	119.76	100.00	45.07	22.50	50.00
N:	33	29	20	28	13	7	10

Table 2.11 Operational Time Periods by Run and Discharge

Run:	A7	B4	C4	D4	E4	F7	G7
Mean Time (hrs):	3.00	3.03	5.82	3.61	1.00	3.21	5.00
Median Time (hrs):	2.00	2.75	6.50	3.50	1.00	3.33	5.00
Std Dev:	2.18	1.50	1.45	1.05	NA	1.71	0.37
Maximum:	7.00	7.50	7.25	5.00	1.00	5.08	5.67
Minimum:	0.10	0.50	3.00	2.00	1.00	0.17	4.50
Total Time:	99.15	81.93	87.34	32.50	1.00	22.50	50.00
N:	33	27	15	9	1	7	10

Run:	B7	C7	D7	E7
Mean Time (hrs):	5.50	6.48	3.55	3.67
Median Time (hrs):	5.50	6.67	4.00	3.75
Std Dev:	2.12	0.85	1.20	1.25
Maximum:	7.00	7.08	5.50	5.00
Minimum:	4.00	5.00	0.33	1.67
Total Time:	11.00	32.42	67.50	44.07
N:	2	5	19	12

Longer and similar periods of continuous operation were desired, but the available operating time periods were not always the same length of time because of constraints caused by a water supply shared with adjacent flumes. In the interest of conducting the maximum length and number of runs, unequal (usually shorter) time periods were used instead of delaying until a longer time period was available. A more detailed discussion of the possible influence of different time periods is in the discussion section following analysis of erosion observed.

2.3 Block Dimensions and Mass

A sample of 120 type A blocks and 100 type B blocks were taken from those used in the flume runs. Because block construction methods did not vary between runs, it is assumed that the samples accurately represent the range of blocks produced in each run. Each block was recorded by an identifying number written on the block, color, and type (A or B). The length of two horizontal sides that intersect at the same corner and the

height taken as the block lies in the flume was measured to the nearest mm using a standard metric ruler (Figure 2.4).

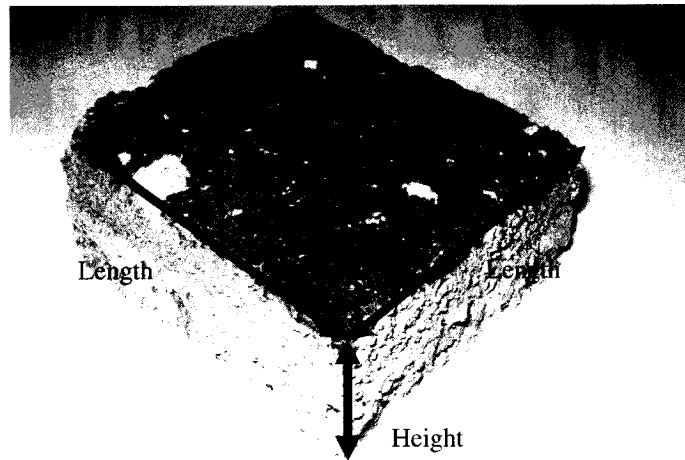


Figure 2.4 Block Length and Height Measurements

The ratio between the two length measurements made on sides that are perpendicular to each other for each block was calculated. Each block was then weighed on a digital scale accurate to the nearest 0.01 kg to determine the block mass. Measurements of side length, height, side length ratio, and mass are summarized by block type (Table 2.12).

Table 2.12 Characteristic Block Dimensions

Block Type A				
	Side Length (cm)	Height (cm)	Side Length Ratio	Mass (kg)
Mean:	3.09	2.70	1.03	0.05
Median:	3.00	2.70	0.99	0.04
Std Dev:	0.41	0.41	0.18	0.01
Total N:	240	120	120	120
Block Type B				
	Side Length (cm)	Height (cm)	Side Length Ratio	Mass (kg)
Mean:	6.41	2.97	0.99	0.22
Median:	6.20	3.00	1.00	0.22
Std Dev:	0.74	0.21	0.15	0.04
Total N:	200	100	100	100

The ratio of the mean length of block type B to block type A is 2.07, which is very close to the ratio of 2 for ideal model block dimensions. The height of block type A

is very similar to block type B, approximating the equal height of the ideal model block dimensions.

A ratio of one would indicate that on average the two sides are of equal length, the idealized model shape for each block, and form a square assuming that the sides are perpendicular to each other. The mean ratio for block type A is 1.03, standard deviation of 0.18. The mean ratio for block type B is 0.99, standard deviation of 0.15. Both ratios are approximately 1, indicating that the sides are approximately equal length on average and match the ideal model block shape.

The ratio of the mass of block type B to the mass of block type A is 4.4, nearly matching the ideal model block ratio of 4. The lengths and height of the block were used to estimate the volume of the block.

2.4 Block Mass Density

A linear regression of mass (M_{block}) on volume (V_{block}) was used to determine the mass density of the block material where the slope of the linear regression represents M_{block} / V_{block} equal to p_s , mass density of the block material (Figure 2.5). Note the assumption that the mass density is the same for all the concrete used in the flume experiment. This assumption is based on the use of the same standard containers to measure out the sand and cement for mixing the concrete for all blocks for all runs. The mass density of the block material, p_s was estimated to be $1,814 \text{ kg/m}^3$. This value will be used for the mass density of a block in later calculations.

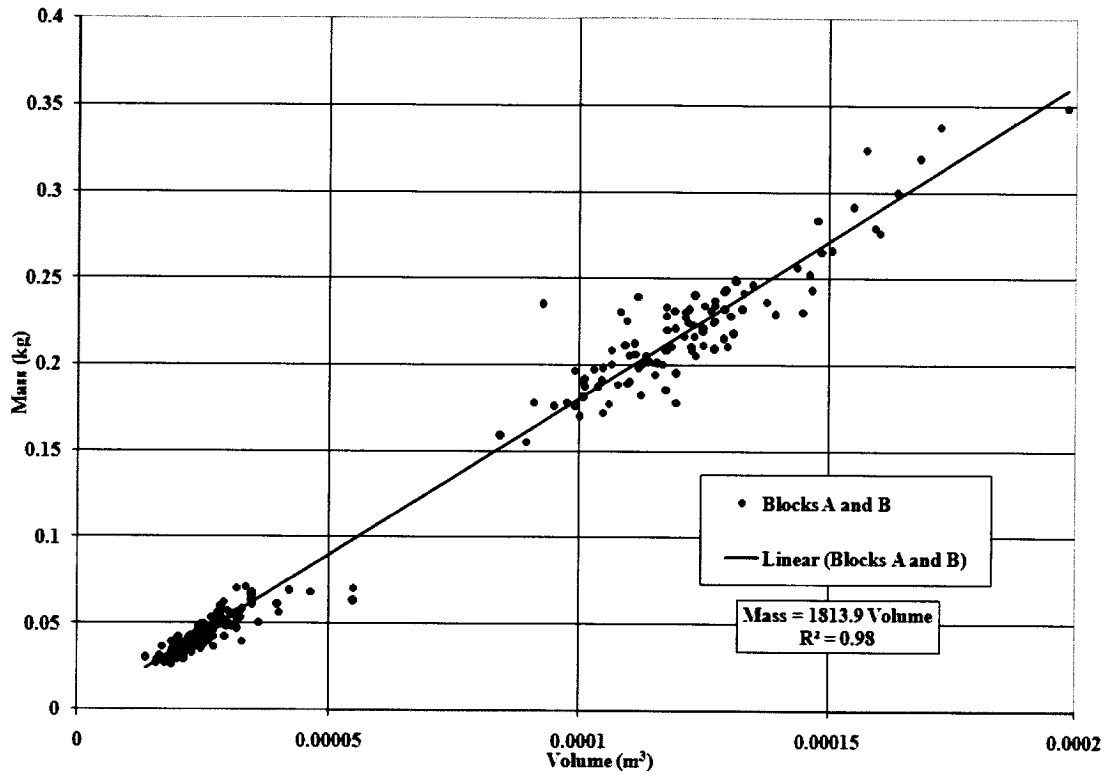


Figure 2.5 Estimation of Block Density from Block Volume and Mass

3. Analysis

Analysis will focus on evaluating qualitatively and quantitatively the following:

- Channel morphology
- Rate and nature of changes in channel morphology over time
- Magnitude and variability of the erosion rate over time
- Relationship between channel morphology and erosion rates with hydraulics and joint spacing

The discussion of analysis will focus on the basic research question and the three hypotheses presented addressing erosion of jointed bedrock.

3.1 Erosion Record

The combination of regular inspections of the channel and block catchment area at the end of the flume and video surveillance were used as previously described to monitor erosion of the channel over time. Erosion of the channel occurred episodically over time with differing magnitudes during constant flow conditions (Figure 3.). Total erosion during Run F equaled only a few blocks, so it is not included in Figure 3..

Examination of the cumulative erosion over time during all runs clearly exhibits a step pattern, the result of the episodic nature of the erosional events (Figure 3.2). Runs C and E have similar cumulative volume curves, suggesting similar erosional process rates.

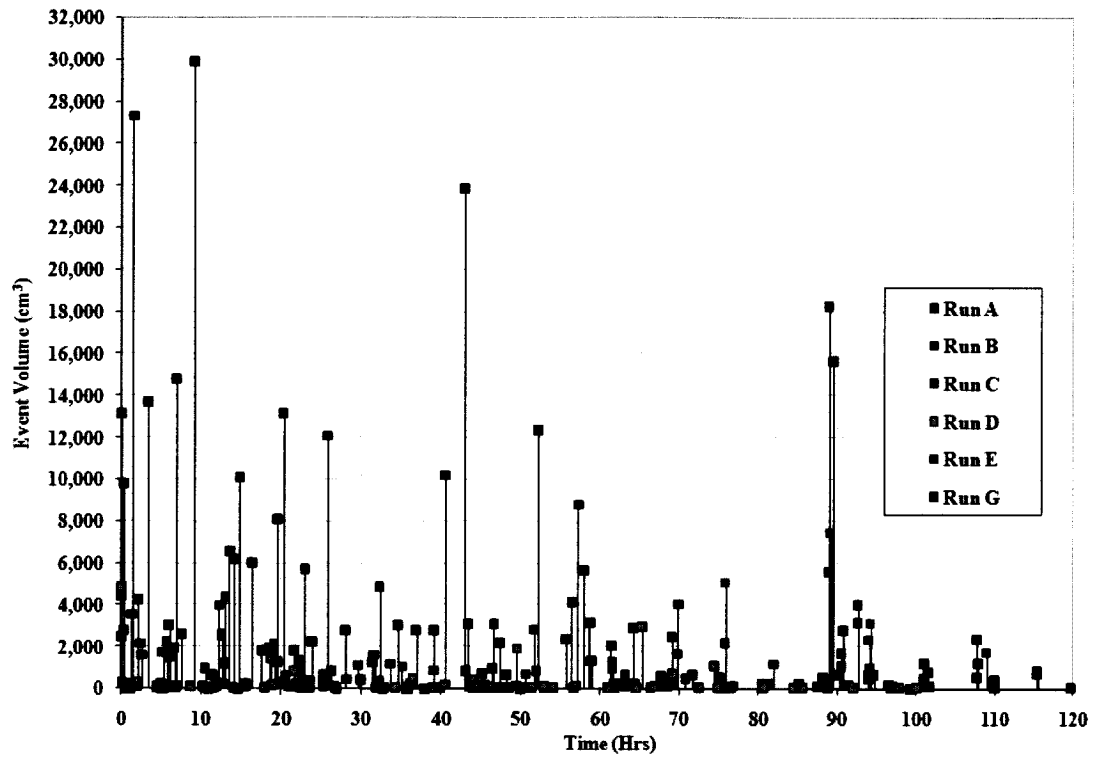


Figure 3.1 Time Series of Erosion by Run

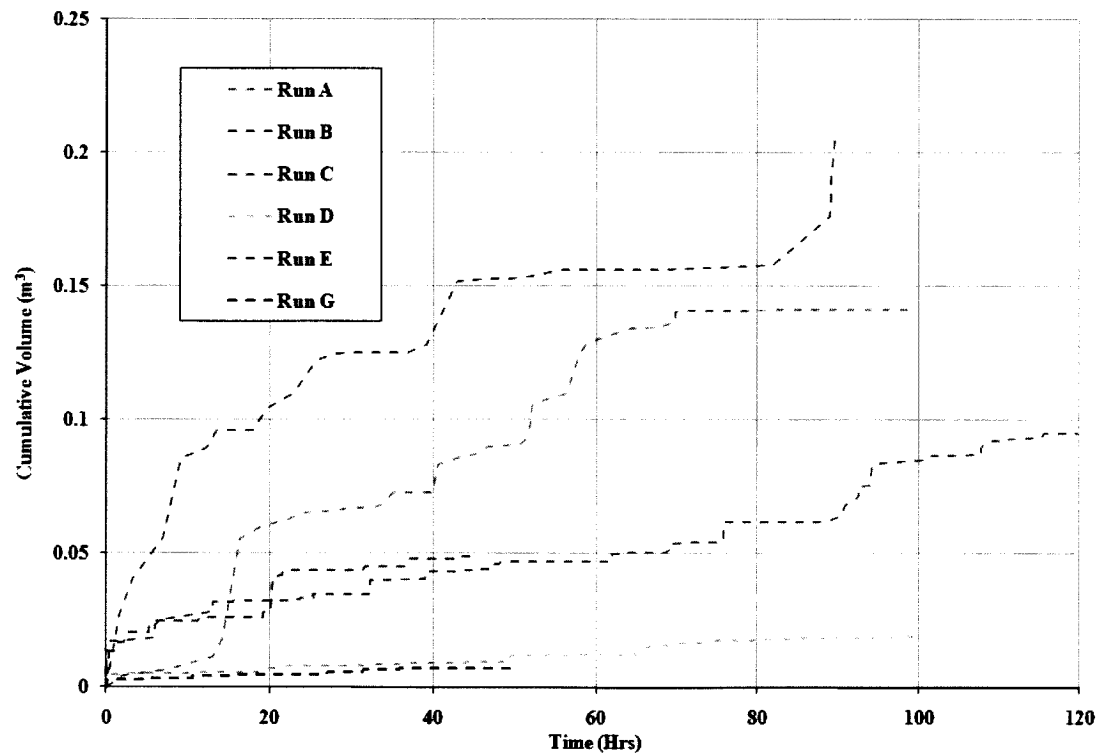


Figure 3.2 Cumulative Volume Eroded by Run

Total erosion by volume for the first three runs (A, B and C), which were in the narrow flume, are higher than Runs D and G in the wide flume setup with narrow joint spacing, which had the lowest totals (excluding Run F) (Table 3.1). Taking time into consideration by comparing total erosion per unit time, the differences between runs remain the same (Table 3.2).

Table 3.1 Cumulative Erosion by Volume and Block Count by Run

Run	Total Run Time (hrs)	Total Block Count	Total Volume (m ³)
A	99.15	5245	0.142
B	92.93	1906	0.206
C	119.76	1758	0.095
D	100.00	709	0.019
E	45.07	456	0.049
F	22.50	36	0.001
G	50.00	260	0.007

Table 3.2 Overall Erosion Rate by Volume and Block Count by Run

Run	Erosion Rate (m ³ /hr)	Erosion Rate (Blocks/hr)
A	0.00143	52.9
B	0.00222	20.5
C	0.00080	14.7
D	0.00019	0.0
E	0.00109	10.1
F	0.00004	1.6
G	0.00014	5.2

In addition to event magnitude, the timing of an event is also of interest in understanding the erosional kinematics and dynamics. The time intervals between events during each run were measured using the video record and estimated from the run log when a video record was not available (e.g., Run A and most of Run B) (Table 3.3 and Table 3.4).

The ratio of total energy input or expenditure as expressed by cumulative stream power expended to the total erosion provides a comparison of the effectiveness of the flow regime to erode the jointed concrete channel configuration between runs with

different configurations. The ratio of ω to total eroded volume and block count expresses the ratio of total energy expended to total erosion (Table 3.5).

Table 3.3 Time Lapse Between Events By Run

	Run A	Run B	Run D	Run E	Run G
Time Lapse Between Events (hrs.)					
Mean:	1.89	3.76	1.64	1.80	1.98
Median:	1.50	3.26	1.10	0.80	0.43
Std Dev:	1.48	3.03	1.86	2.25	3.00
Max:	6.00	12.00	10.15	7.22	10.77
Min:	0.10	0.08	0.02	0.03	0.02
Total N:	43	24	61	24	23

Table 3.4 Time Interval Between Events by Run and Discharge

	Run A at 0.20 m ³ /s	Run B at 0.20 m ³ /s	Run D at 0.20 m ³ /s	Run E at 0.20 m ³ /s	Run G at 0.20 m ³ /s
Time Lapse Between Events (hrs.)					
Mean:	2.17	1.65	1.57	1.83	1.98
Median:	1.50	0.38	1.10	0.78	0.43
Std Dev:	2.37	3.00	1.57	2.28	3.00
Max:	14.00	7.00	5.78	7.22	10.75
Min:	0.10	0.08	0.00	0.07	0.00
Total N:	43	5	43	23	23

	Run B at 0.11 m ³ /s	Run D at 0.11 m ³ /s	Run E at 0.11 m ³ /s
Time Lapse Between Events (hrs.)			
Mean:	4.31	1.81	0.03
Median:	3.50	1.16	0.03
Std Dev:	2.86	2.45	NA
Max:	12.00	10.15	0.03
Min:	1.33	0.00	0.03
Total N:	19	18	1

Table 3.5 CUSP per Block by Run

Run	Total Run Time (hrs)	CUSP per Block (kWh/(m ² m ³))
A	99.15	4.0
B	92.93	6.8
C	119.76	10.7
D	100.00	18.8
E	45.07	14.8
F	22.50	96.9
G	50.00	29.3

3.2 Changes in Channel Geometry

Repeated point gage and photographic surveys of the bed over time during each flume run were used to estimate the downstream end position of the three layers composing the knickpoint. The slope of the knickpoint was estimated using the survey data (Figure 3.3). The knickpoint slope varied through time during all runs but differences were more pronounced during runs A, B, C, and E (Figure 3.4). Non-uniform erosion of the layers over time led to observed changes in slope. This is clearly shown in a comparison of layer positions and slopes for each run (Figure 3.5 to Figure 3.10).

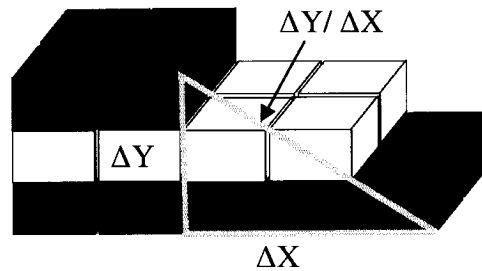


Figure 3.3 Knickpoint Slope Measurement

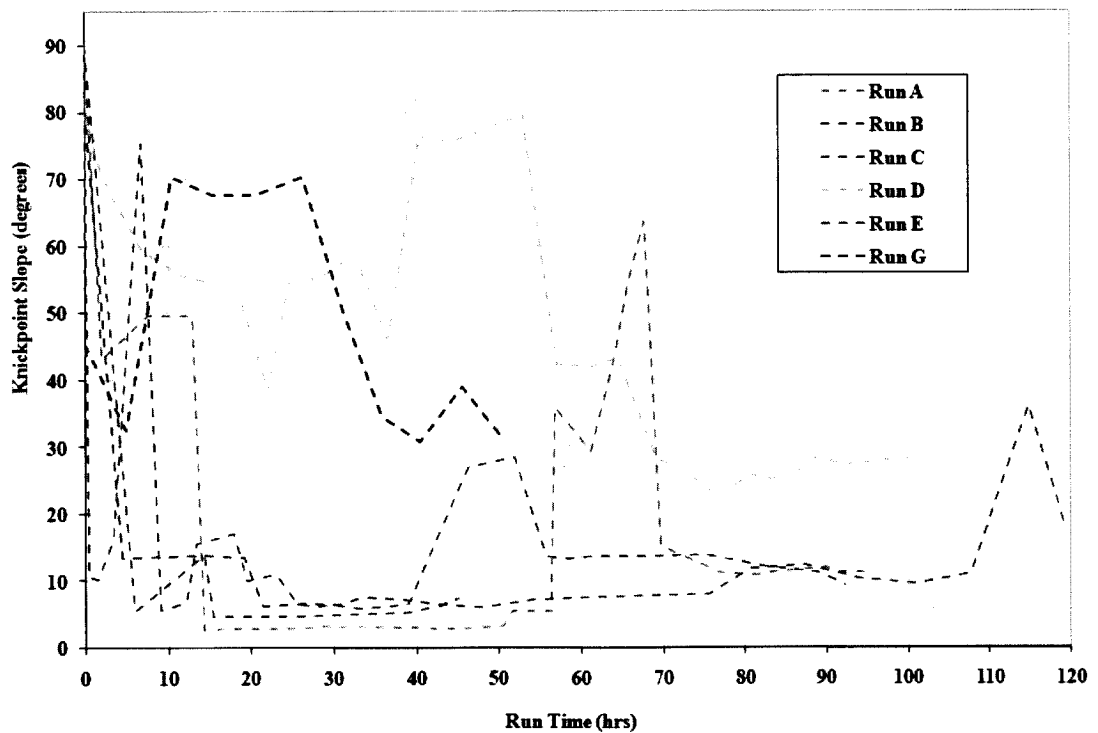


Figure 3.4 Knickpoint Slopes by Run

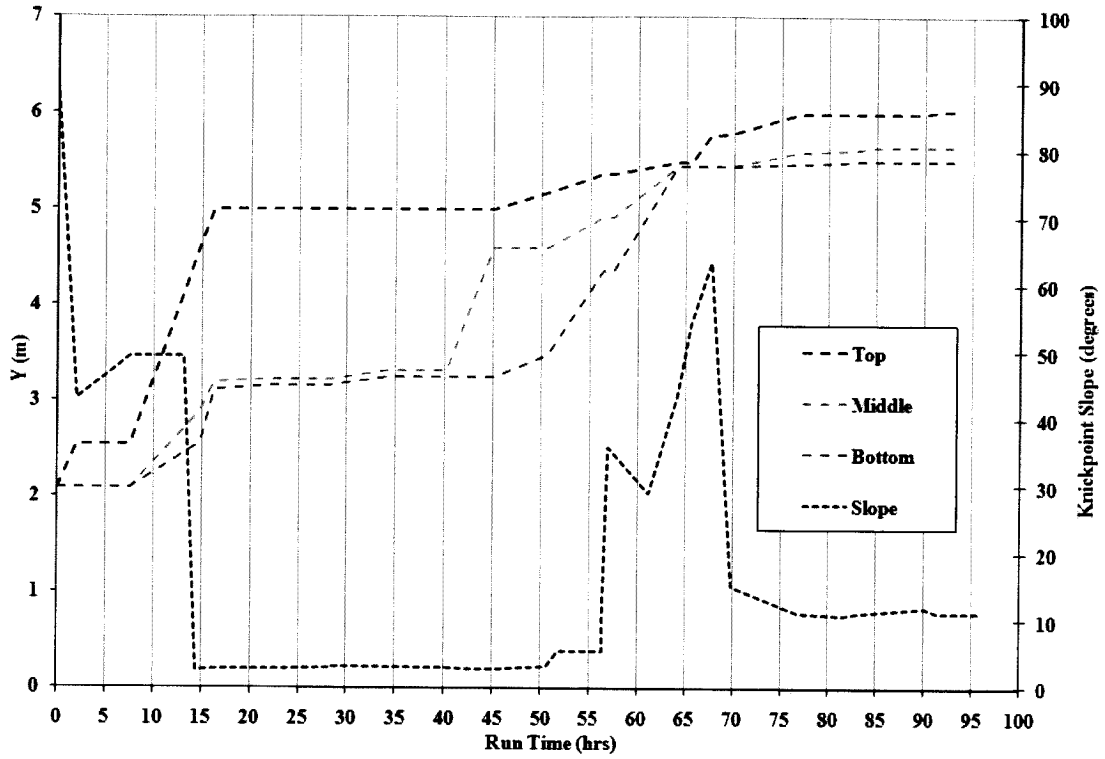


Figure 3.5 Downstream Position of Knickpoint Layers - Run A

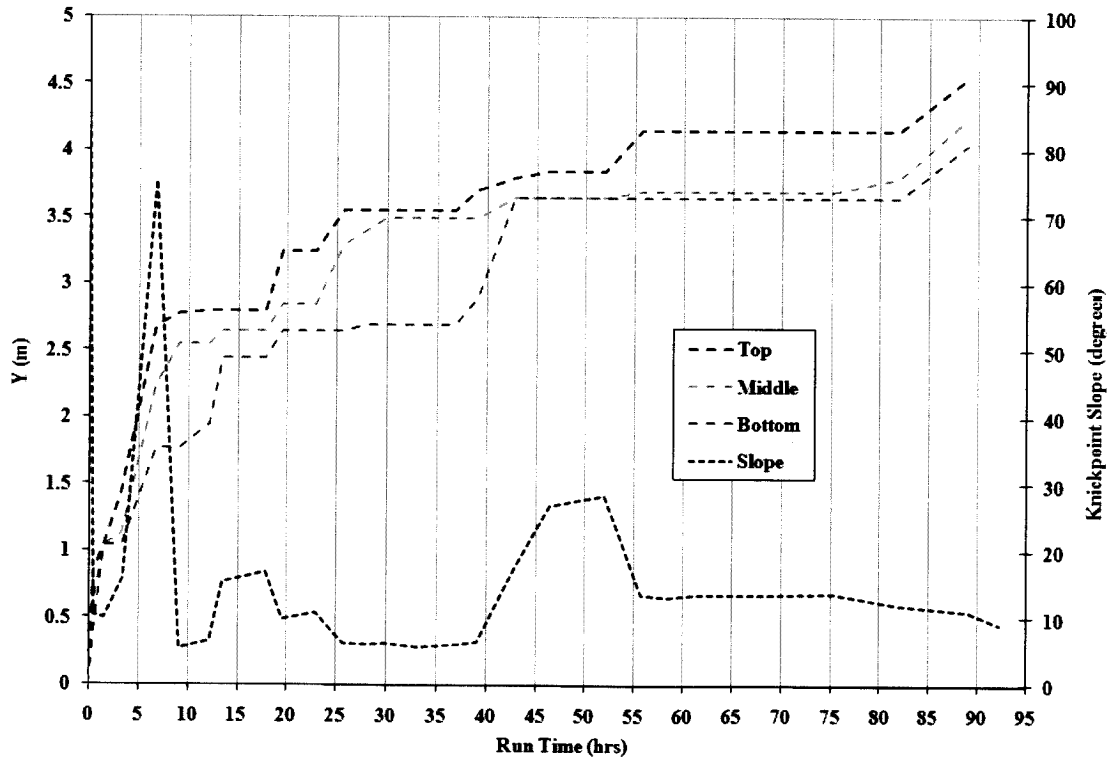


Figure 3.6 Downstream Position of Knickpoint Layers - Run B

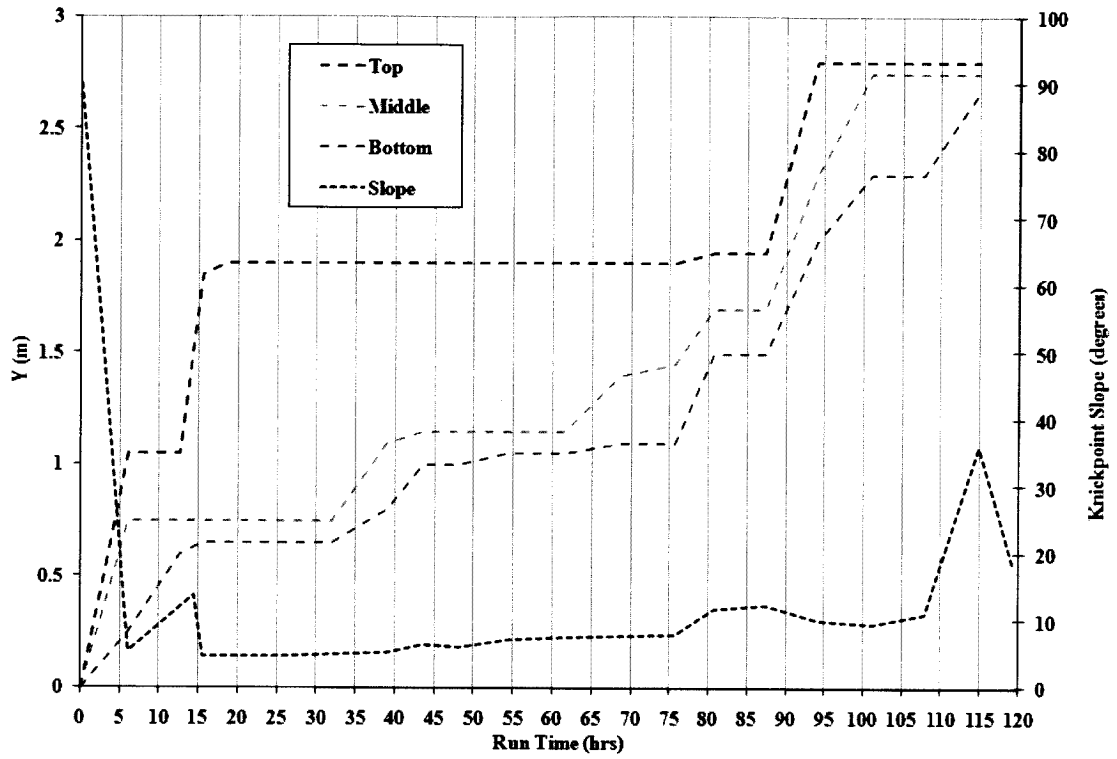


Figure 3.7 Downstream Position of Knickpoint Layers - Run C

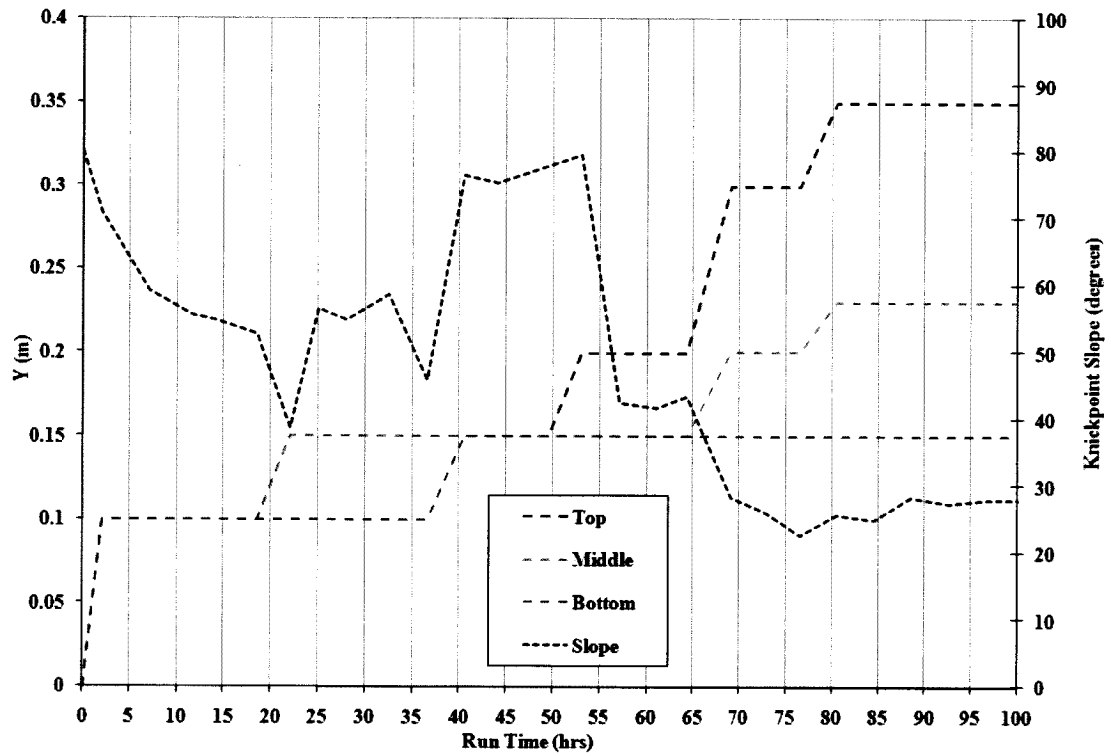


Figure 3.8 Downstream Position of Knickpoint Layers - Run D

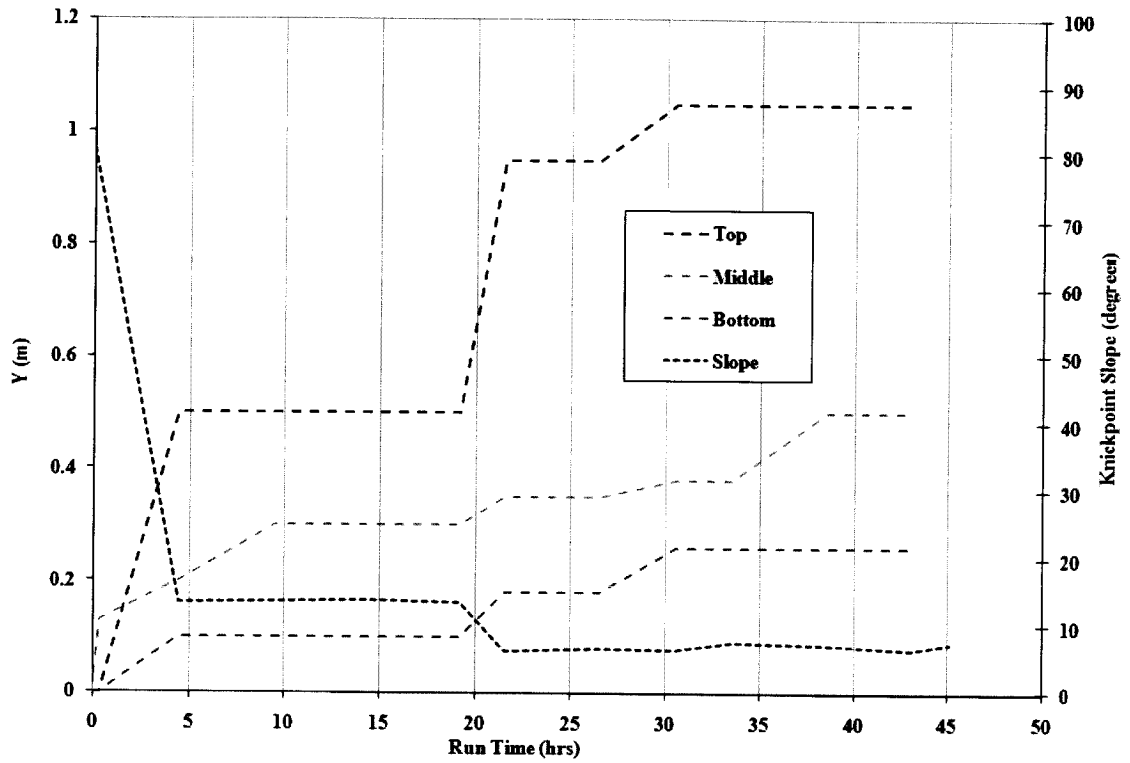


Figure 3.9 Downstream Position of Knickpoint Layers - Run E

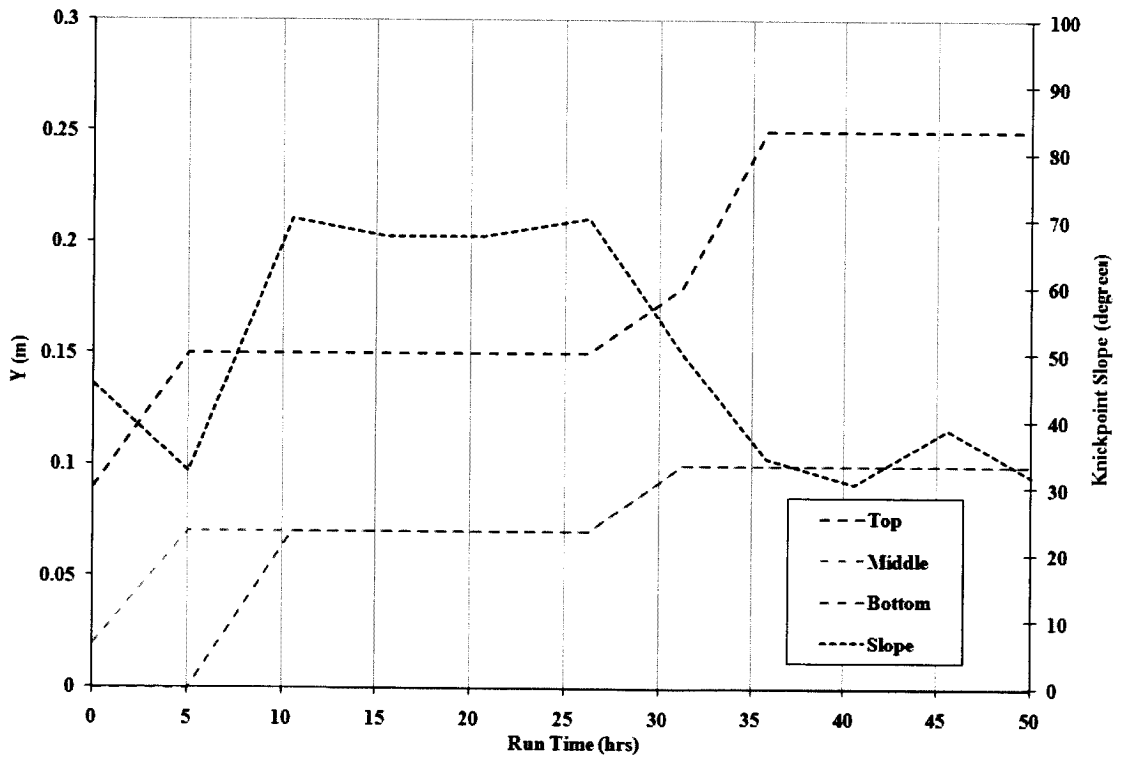


Figure 3.10 Downstream Position of Knickpoint Layers - Run G

A definitive equilibrium slope was not easily detected during any of the runs, but higher slopes occurred during runs D and G under lower calculated τ and measured flow depth compared to A, B, and C. There is also a noticeable difference in slopes encountered in Run E (10 to 20 degrees) with wider joint spacing than in runs D and G (20 to 70 degrees), although both were under similar hydraulic conditions in the wide flume setup. Joint spacing and associated erodibility by the flow may be a factor in determining the slope of the knickpoint. Some control is fixed by the longitudinal length of the block, which fixes the possible slopes obtainable in our run, but other factors such as net erosional force may play a role when differences are seen between runs with the same joint spacing (e.g., Runs A and D).

3.3 Planform Geometry

The planar geometry was dominated by the knickpoint and took on four forms: a linear face perpendicular to the sidewall, a quasi-parabolic curve opening upstream, a quasi-parabolic curve opening downstream, and irregular form. The outline of the knickpoint face for each layer at different time intervals throughout each run was developed from the photographic surveys of the bed (Figure 3.11 to Figure 3.16).

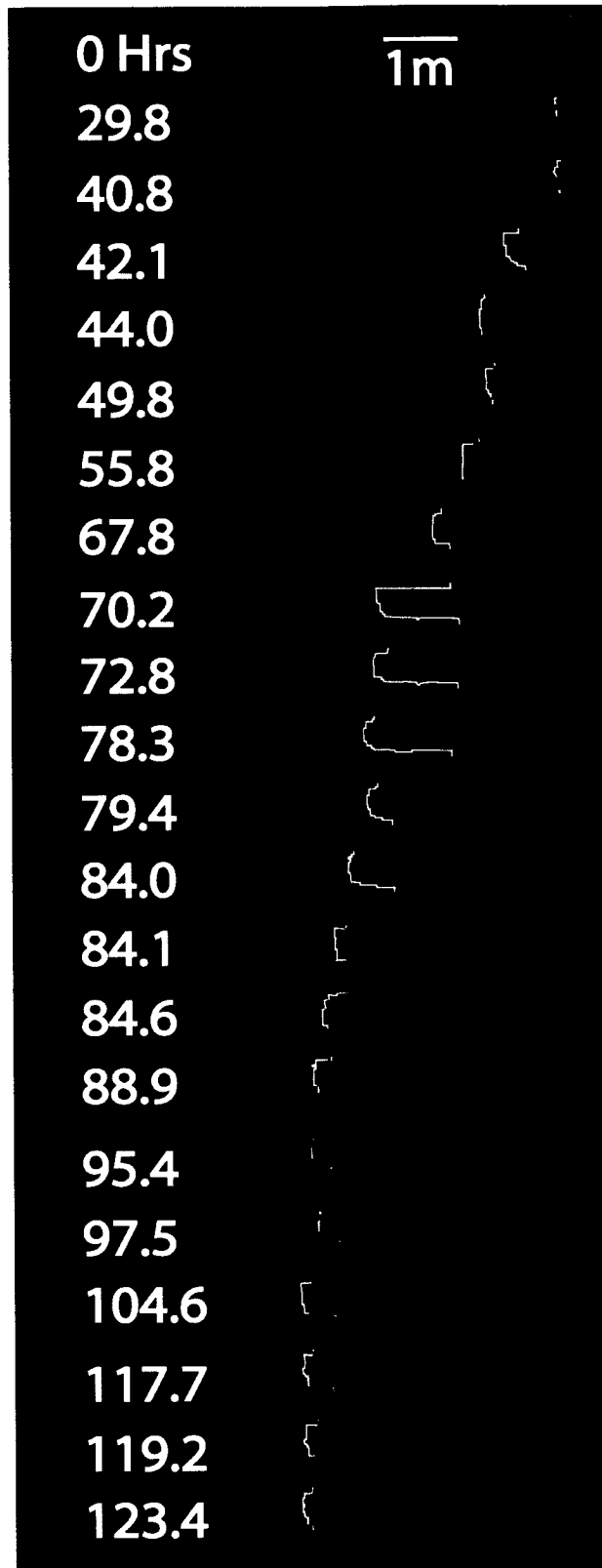


Figure 3.11 Run A – Plan View of Knickpoint Edge Outline over Time. Top layer is in red, middle layer is yellow, bottom layer is blue. Flow is from left to right. Corresponding run time is given in hours to left of outlines.

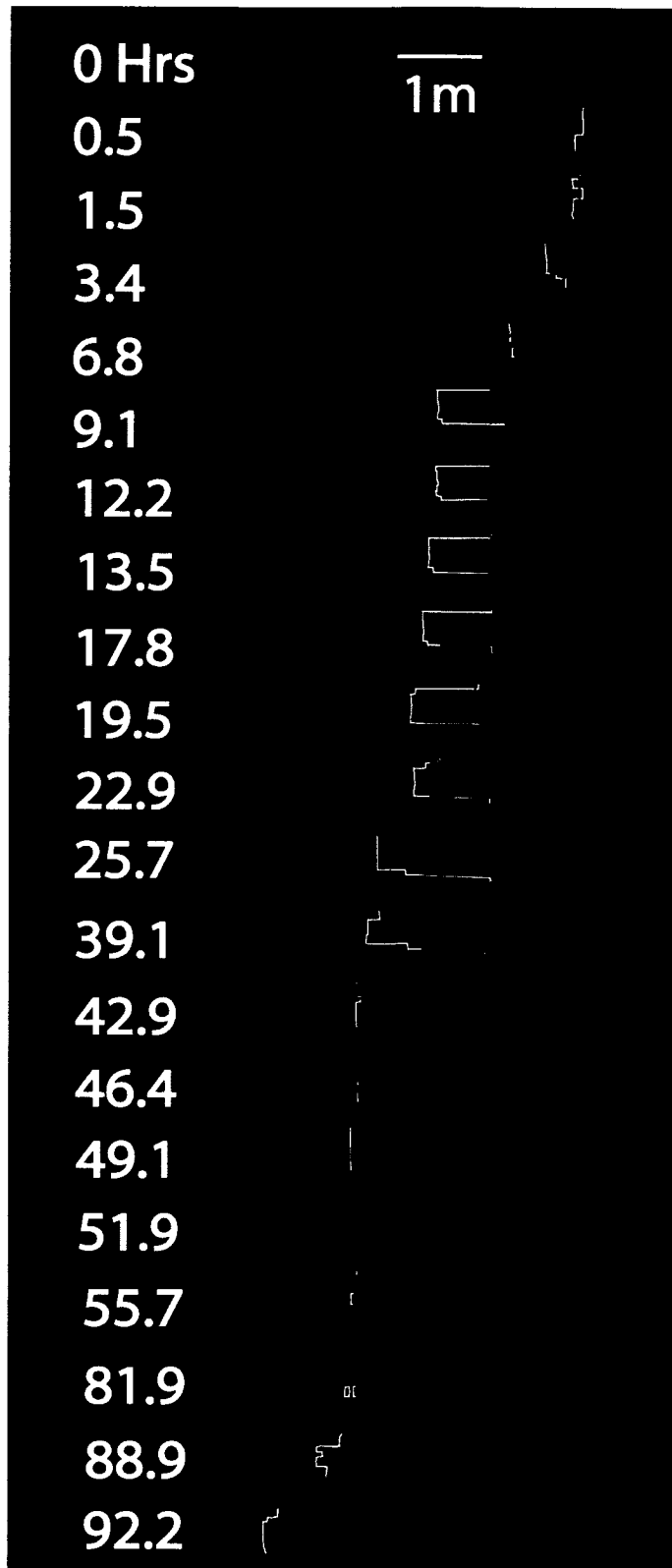


Figure 3.12 Run B – Plan View of Knickpoint Edge Outline over Time. Top layer is in red, middle layer is yellow, bottom layer is blue. Flow is from left to right. Corresponding run time is given in hours to left of outlines.

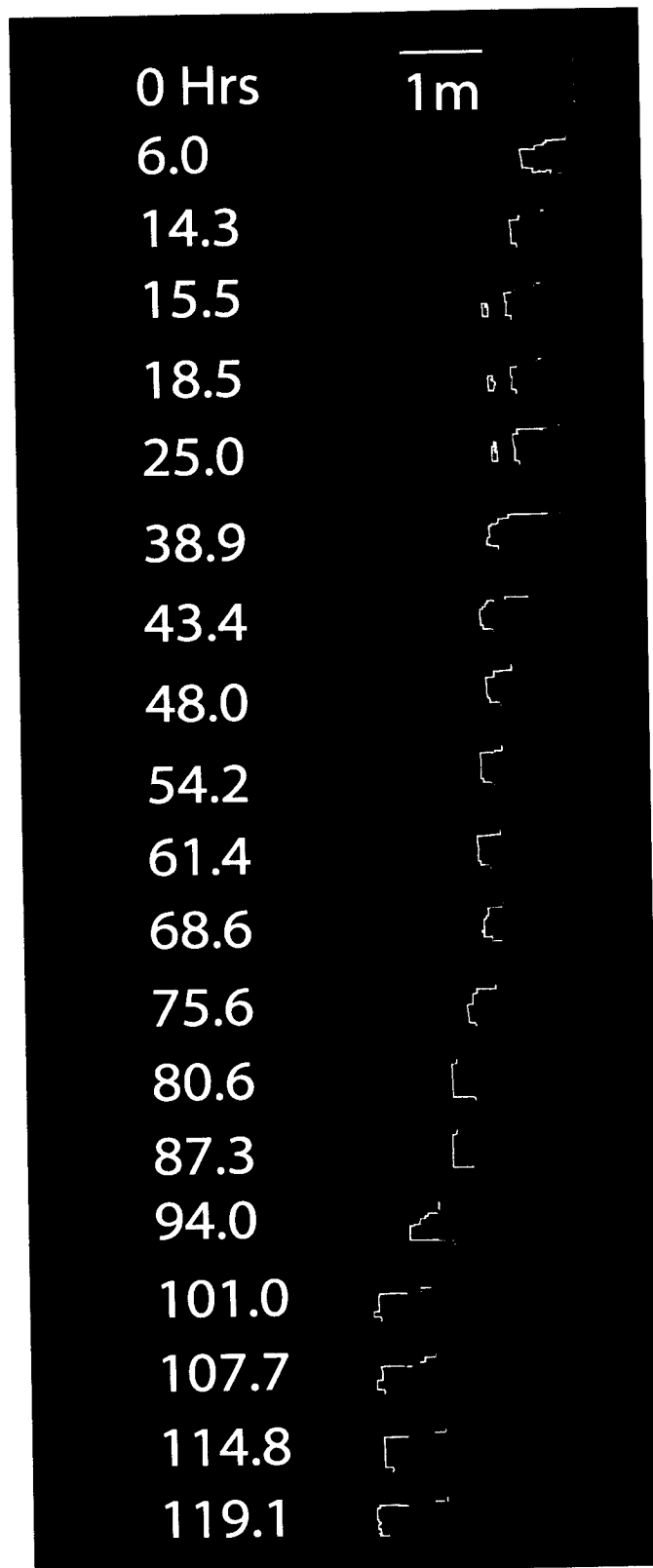


Figure 3.13 Run C – Plan View of Knickpoint Edge Outline over Time. Top layer is in red, middle layer is yellow, bottom layer is blue. Flow is from left to right. Corresponding run time is given in hours to left of outlines.

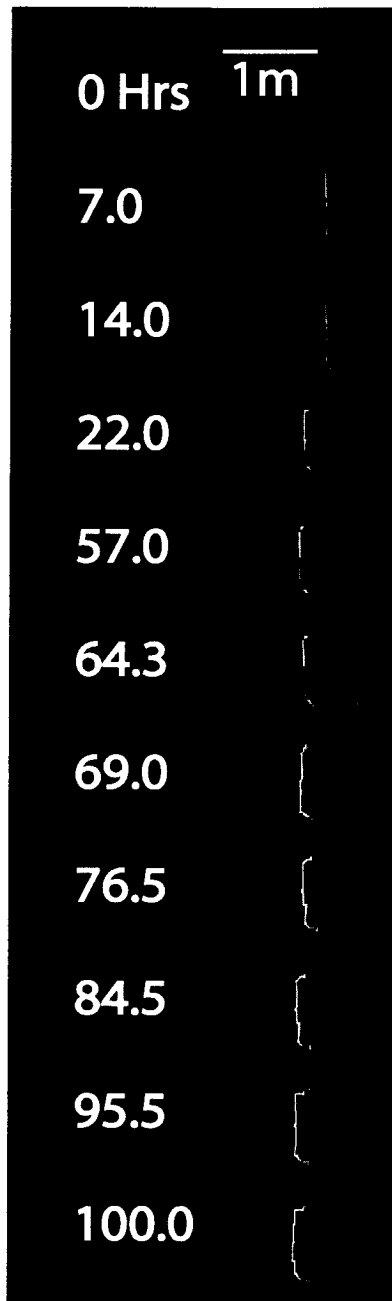


Figure 3.14 Run D – Plan View of Knickpoint Edge Outline over Time. Top layer is in red, middle layer is yellow, bottom layer is blue. Flow is from left to right. Corresponding run time is given in hours to left of outlines.

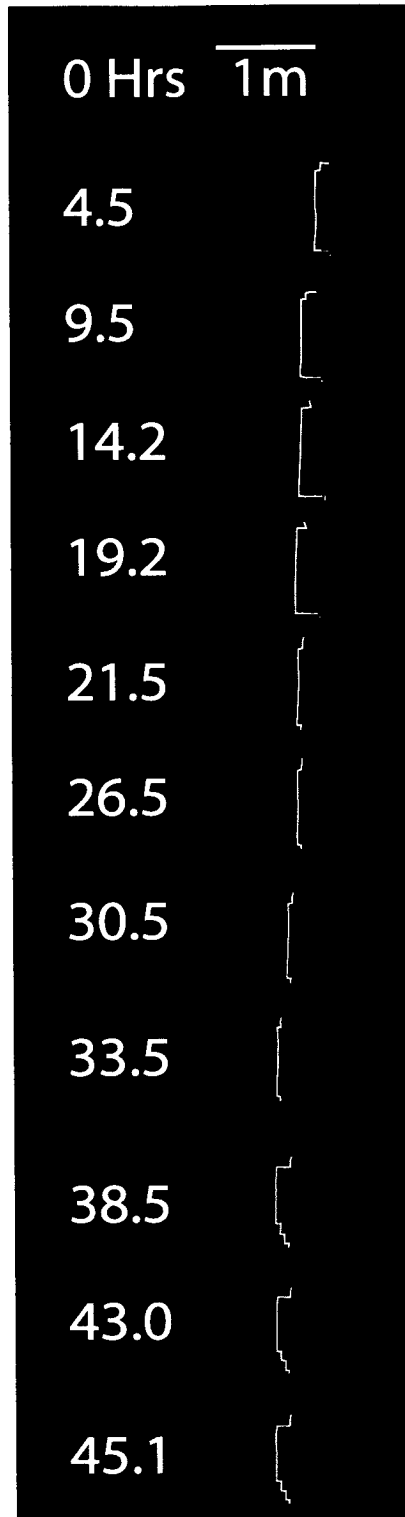


Figure 3.15 Run E – Plan View of Knickpoint Edge Outline over Time. Top layer is in red, middle layer is yellow, bottom layer is blue. Flow is from left to right. Corresponding run time is given in hours to left of outlines.

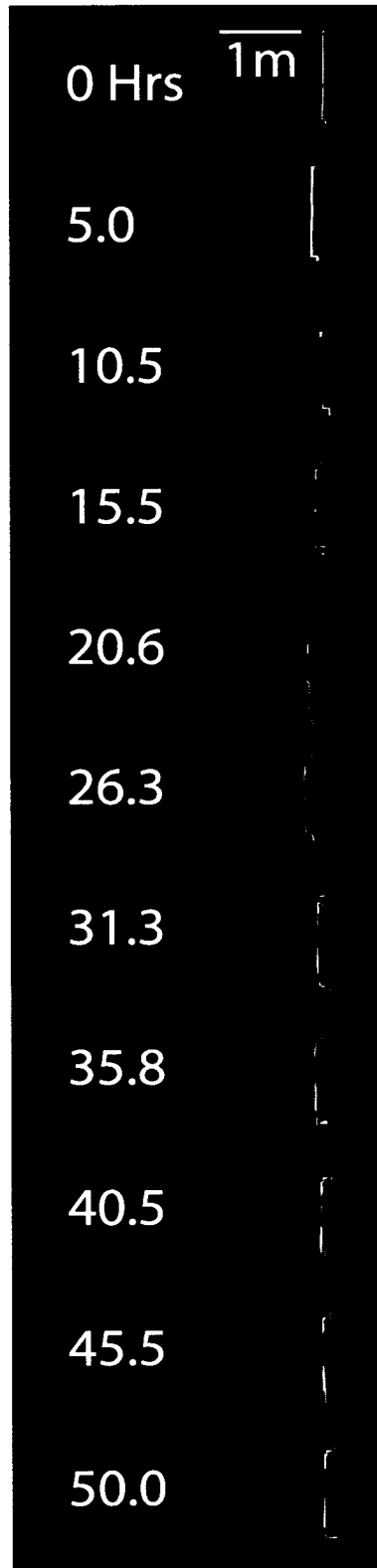


Figure 3.16 Run G – Plan View of Knickpoint Edge Outline over Time. Top layer is in red, middle layer is yellow, bottom layer is blue. Flow is from left to right. Corresponding run time is given in hours to left of outlines.

3.3.1 Linear Face

For all runs, the initial knickpoint edge was a linear face perpendicular to the sidewall of the flume (Figure 3.17). The linear face was present during all flume runs.

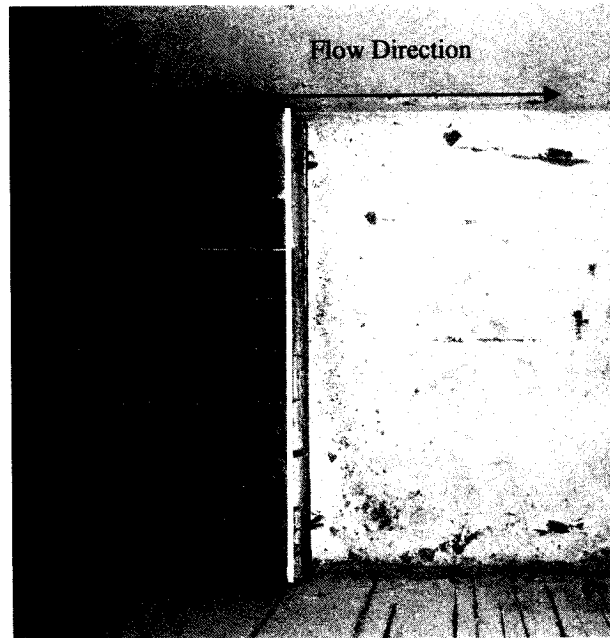


Figure 3.17 Linear Face of Initial Knickpoint Edge - Run B. Flow is from left to right. Outline of face in yellow.

3.3.2 Quasi-Parabolic Curve Opening Upstream

The rows of blocks closest to the knickpoint, especially at the knickpoint edge, are often displaced over time from their original linear alignment perpendicular to the sidewall into a curvilinear form opening upstream, similar to a suspended chain hanging in the air (Figure 3.18 and Figure 3.19). The blocks appear to resist the downstream driving forces through the opposing forces created along the joints between blocks. This may be similar to forces along joints in stone arches where the driving force is opposed by a restoring force along the joints between blocks to form a static curve condition. Such forces are hypothesized to result from the interlocking of the irregular rough boundaries between otherwise physically disjointed blocks when rotation of the blocks

wedges the edges and forms force configurations that oppose the downstream hydraulic driving forces. Blocks that are not disjointed add complexity to any force analysis, but would act in the same manner as individual blocks but with a different geometry. The curve formed by a hanging chain supporting only its own weight forms a catenary or hyperbolic curve. The addition of external forces or non-uniform weight distribution along the wire or chain changes the shape of the static curve to other forms such as parabolas. The curves formed at the knickpoint edge were outlined using overhead photographic surveys of the bed.

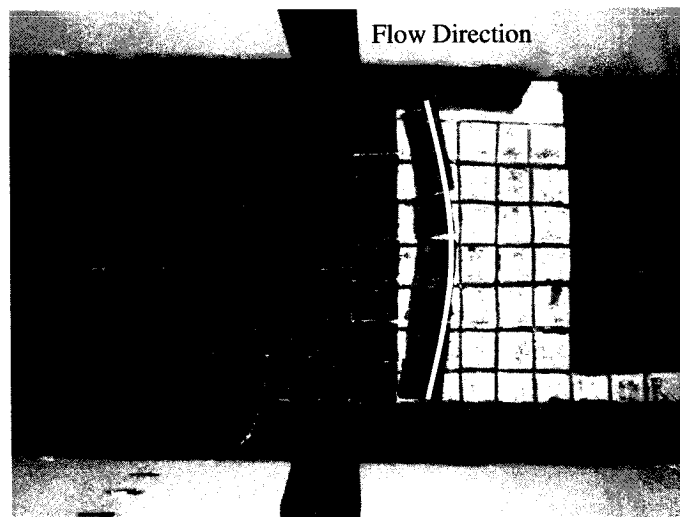


Figure 3.18 Quasi-Parabolic Curve Opening Upstream on Knickpoint Edge - Top Layer in Run B. Flow is from left to right. Outline of curve form in yellow.

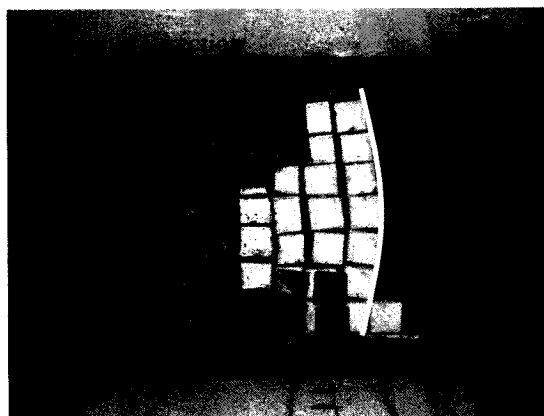


Figure 3.19 Another Example of Arch from Photographic Surveys

3.3.3 Quasi-Parabolic Curve Opening Downstream

The knickpoint geometry also often exhibits a quasi-parabolic curve opening downstream formed by non-mobilized blocks along the flume edge (Figure 3.20). I hypothesize that these blocks are not mobilized because sidewall interactions diminish driving forces along the edge of the channel. Because the highest driving forces are exerted in the center of the channel, center blocks and near-center blocks are eroded first. This occasionally leaves behind blocks near the channel edge that are eroded later when removal of side-reinforcing blocks diminishes resisting force and allows the diminished driving forces to mobilize these blocks. Attempts were made to reduce sidewall interactions by lining the edges with a 6-cm-wide block-bumper of non-jointed concrete on each layer.

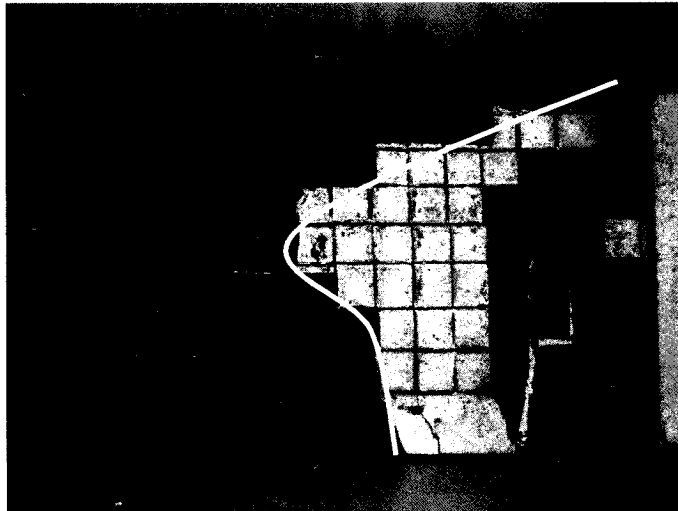


Figure 3.20 Quasi -Parabolic Curve Opening Downstream at Knickpoint Edge -Top Layer in Run B. Flow is from left to right. Outline of curve form in yellow.

3.3.4 Irregular Form

Some of the knickpoint planform geometries are irregularly shaped so that blocks in the channel remain in place while surrounding blocks near the edge are eroded (Figure

3.21). Such forms suggest qualitatively the beginnings of an anabranching channel, but a true sub-channel extending upstream beyond a few blocks never developed.

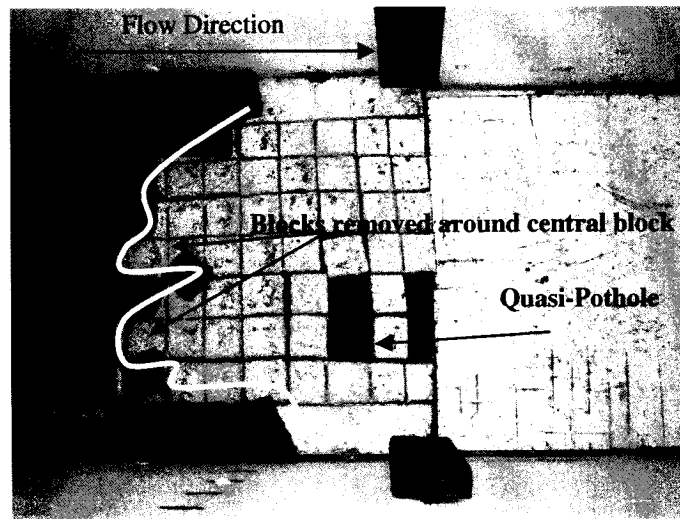


Figure 3.21 Irregular Form at Knickpoint Edge - Top and Middle Layers in Run B. Also note the quasi-pothole in the middle white layer. Flow is from left to right. Outline of curve form in yellow.

3.3.5 Quasi-Potholes

Occasionally blocks or partial blocks located upstream of the knickpoint were plucked, leaving behind a quasi-pothole type feature (Figure 3.22). These features were easily identified by the lack of that layer's color on the concrete.



Figure 3.22 Quasi-Potholes Formed by Hydraulic Removal of Blocks. Flow is from left to right.

The formation process of potholes in the geomorphic literature generally implies that abrasion is the primary formative process (e.g., Hancock et al., 1998; Whipple et al., 2000a). These features are not formed by abrasion, but exhibit similar morphology to potholes in that they are local depressions in the bed surface with vertical sides on the scale of the joint spacing (Wohl, 1993; Hancock et al., 1998; Whipple et al., 2000a; Springer and Wohl, 2002). Quasi-potholes with depths less than the joint spacing sometimes formed where the partial top of a block was physically weak and a partial or full fracture developed between the top and the lower portion of the block (Figure 3.23).

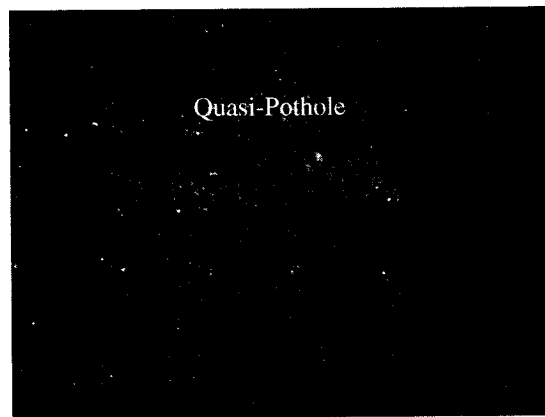


Figure 3.23 Removal of Top of Block

The various morphologic features and overall morphology of the bedrock channel seen during the experiment were the result of water flow interacting with the jointed concrete channel. The next element of analysis focuses on understanding the forces involved in developing these features in the experimental jointed bedrock channel over time.

3.4 Force Analysis for Ideal Block at Knickpoint

The primary observed mode of block removal is sliding. A force diagram was developed for this type of motion for an idealized block at the knickpoint in the flume with bed slope S_b (Figure 3.24).

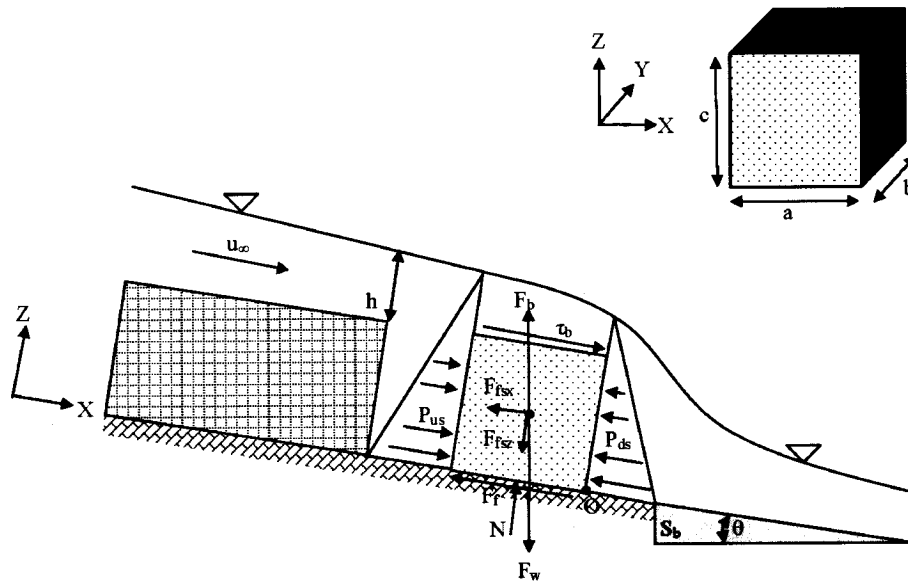


Figure 3.24 Force Diagram for Ideal Block at Knickpoint. An ideal block with sides denoted is in the upper corner of the figure. See notation in Table 3.6.

Table 3.6 Notation for Figure 3.24

Notation	Definition
a, b, c	Length, width, and height of block
h	Flow depth above block
u_{∞}	Approach flow velocity
P_{us}, P_{ds}	Hydrostatic pressure along upstream and downstream face of block
F_{fsx}, F_{fsz}	x and z components of friction force along sides of block
F_f	Friction along base of block
N	Normal force along base of block
F_w	Weight of block
F_b	Buoyancy force acting on block
τ_b	Bed shear stress acting on top of block
θ	Bed slope angle
S_b	Bed slope

The block weight (not submerged) is given by:

Equation 3.14

$$F_w = \rho_s \cdot g \cdot a \cdot b \cdot c$$

The x and z components are:

Equation 3.15

$$x \text{ direction: } F_{wx} = F_w \sin \theta$$

$$z \text{ direction: } F_{wz} = -F_w \cos \theta$$

Gravity is denoted by g . The mass density of the blocks, ρ_s was measured at 1,814 kg/m³.

The bed slope of the flume was surveyed at 0.029 m/m (0.029 radians).

The buoyancy force acting on the block is:

Equation 3.16

$$F_b = \rho_w \cdot g \cdot a \cdot b \cdot c$$

The x and z components are:

Equation 3.17

$$x \text{ direction: } F_{bx} = -F_b \sin \theta$$

$$z \text{ direction: } F_{bz} = F_b \cos \theta$$

The mass density of water, ρ_w , is assumed to be 1,000 kg/m³ at 4°C.

The submerged weight of the block is:

Equation 3.18

$$F_w + F_b = (\rho_s - \rho_w)g \cdot a \cdot b \cdot c$$

The force due to the shear stress of the flow applied to the top surface of the block is:

Equation 3.19

$$F_\tau = \tau_b \cdot a \cdot b$$

The bed shear stress was estimated by:

Equation 3.20

$$\tau_b = \rho_w g h S_b$$

The force due to the hydrostatic pressure distribution along the upstream block side (P_{us}) is integrated over the side surface. Wilcox (2000) provides a solution to the integration of the pressure across the surface to give the pressure force:

Equation 3.21

$$F_{P_{us}} = \rho_w \cdot g \cdot \bar{\zeta} \cdot b \cdot c$$

where $\bar{\zeta}$ is the distance from the water surface to the centroid of the upstream side area (Figure 3.25):

Equation 3.22

$$\bar{\zeta} = h + \frac{c}{2}$$

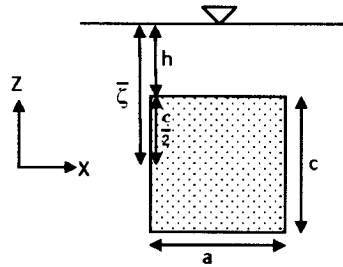


Figure 3.25 Distance from Water Surface to Centroid of Side Area, $\bar{\zeta}$

Similarly, the hydrostatic pressure force along the downstream block side (P_{ds}) is:

Equation 3.23

$$F_{P_{ds}} = -\rho_{wa} \cdot g \cdot \bar{\zeta} \cdot b \cdot c$$

where ρ_{wa} is the mass density of the aerated nappe flow cavity immediately downstream from the edge of the knickpoint. The pressure distribution in the cavity or eddy formed at the downstream face of the knickpoint (aerated nappe flow cavity) is less than the pressure distribution under a no-wake condition (Wilcox, 2000; Toombes and Chanson, 2008). The pressure difference generates a net pressure force on the block equal to the difference between P_{us} and P_{ds} , which is positive in the downstream direction. The force

generated by the net pressure difference is approximated by applying a lower density to the pressure force on the downstream side that accounts for aeration of the volume of water immediately downstream of the knickpoint.

The force due to friction along the base of the block is:

Equation 3.24

$$F_f = C_f \cdot N$$

where C_f is the coefficient of friction and N is the normal force at the base of the block:

Equation 3.25

$$N = F_{wz} + F_{bz}$$

In this study, coefficients were experimentally determined for contact between a block and the base and between blocks under submerged conditions using a spring gage (Figure 3.26). Additional mass (other blocks) were added to a standard block to aid in estimating the coefficient, which is assumed to be independent of mass. The spring was attached via a hook through a metal eyelet attached by adhesive to the standard block (Figure 3.27).

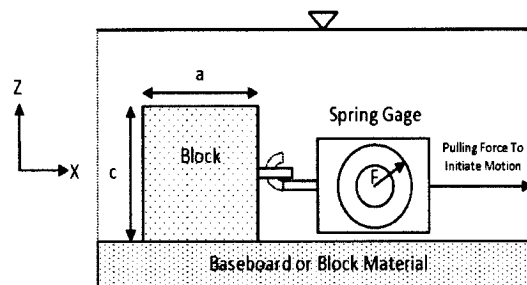


Figure 3.26 Diagram of Spring Gage Setup for Measuring F_f

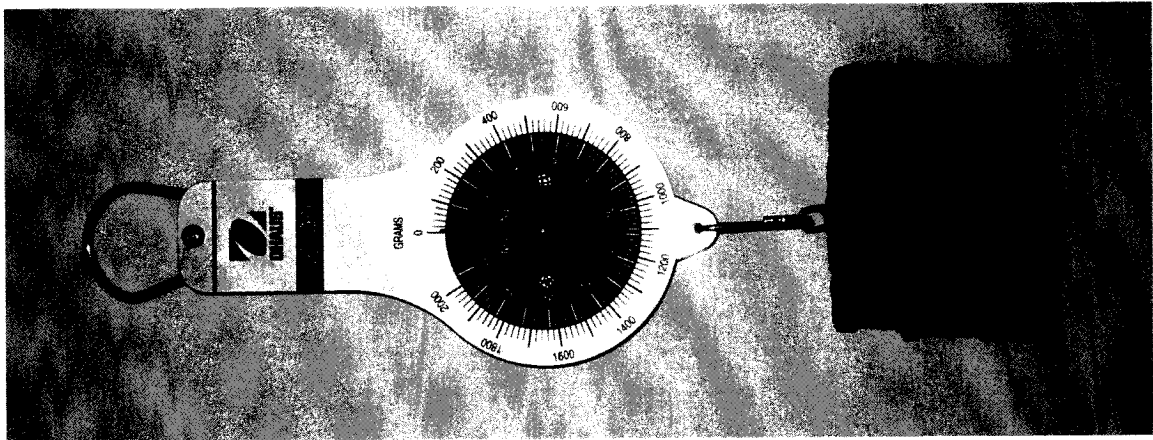


Figure 3.27 Spring Gage Attached to Standard Block via Hook

The spring gage was manually extended horizontally ($\theta = 0$) away from the block to gradually pull on the block parallel to the direction of initial motion. The spring gage was extended until initial motion of the block occurred. The applied force at the moment of initial motion was recorded as the force necessary to initially mobilize the block, F_f . Combined with the known submerged block weight, N gives the coefficient of friction:

Equation 3.26

$$C_f = \frac{F_f}{N} = \frac{F_f}{(\rho_s - \rho) \cdot g \cdot a \cdot b \cdot c \cdot \cos \theta}$$

The mean coefficient of friction for a block on the baseboard is 0.43 (σ : 0.038) (Figure 3.28 and Table B.1) and a block on another block is 0.73 (σ : 0.054) (Figure 3.28 and Table B.2). The visibly rougher surface of the block yields a higher coefficient of friction than the smoother base. A difference in coefficients of friction introduces some complexity.

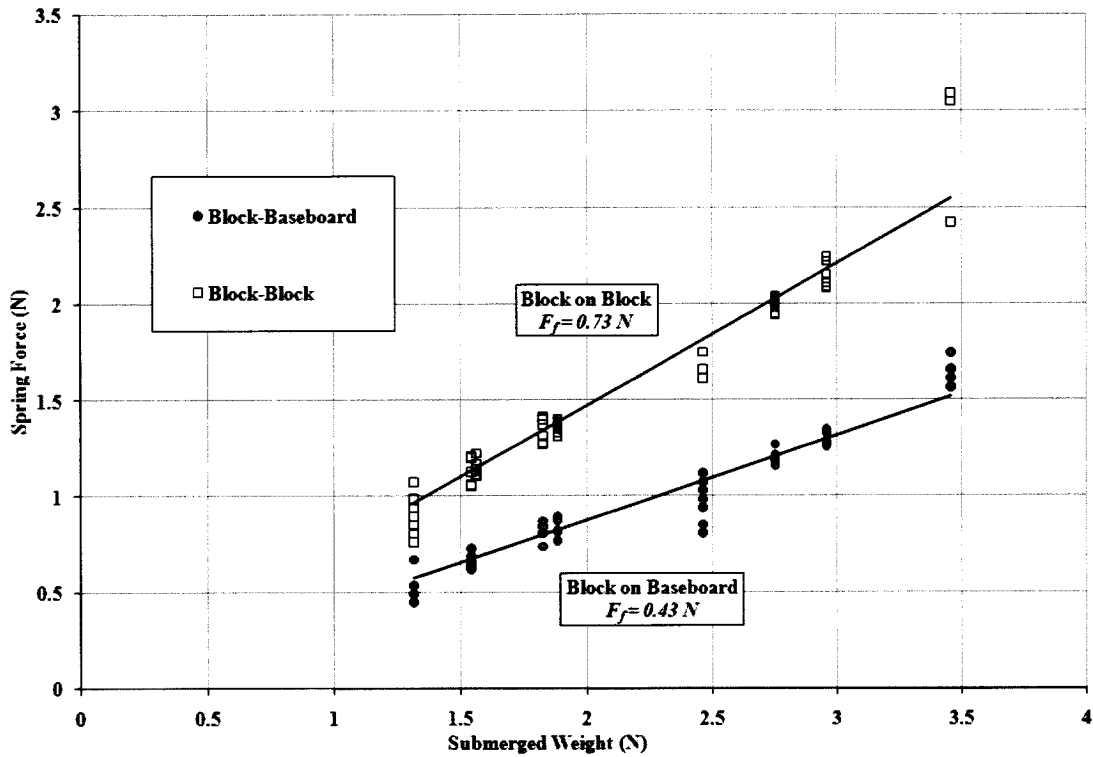


Figure 3.28 Spring Gage Results for C_f

There is also a friction force between blocks, F_{fs} , along the sides of the block parallel to flow in the x direction when blocks contact each other (a in Figure 3.24). This may be decomposed into two components in the x and z direction, F_{fsx} and F_{fsz} , respectively, to express total friction along both sides of the block. For sliding motion in the x -direction, F_{fsz} is considered negligible and the component in the x -direction is used. This force arises from the irregular interlocking edges between blocks and counter net motion from the other forces up to a threshold when exceeded the block is removed. These forces may vary from block to block and over time as the sides rub and break down the rough elements between them. This spatial and temporal variability makes it difficult and complex to estimate the magnitude of these forces *a priori* and will be discussed later.

For the primary observed sliding motion in the x-direction, the sum of forces in the x direction yields:

Equation 3.27

$$x \text{ direction: } \Sigma F_x = F_{wx} + F_{bx} + F_f + F_{fsx} + F_{\tau_b} + F_{p_{as}} + F_{p_{ds}}$$

Replacing each force component with their respective formula yields the sum of forces involved in sliding motion for a block:

Equation 3.28

$$\Sigma F_x = (\gamma_w - \gamma_{wa})\left(h + \frac{c}{2}\right)(b \cdot c) + \tau_b(a \cdot b) + (\gamma_s - \gamma_w)(\sin \theta - C_f \cos \theta)(a \cdot b \cdot c) + F_{fsx}$$

For a first order approximation, we will ignore the friction force along the sides of the block, F_{fsx} . The resultant equation is:

Equation 3.29

$$\Sigma F_x = (\gamma_w - \gamma_{wa})\left(h + \frac{c}{2}\right)(b \cdot c) + \tau_b(a \cdot b) + (\gamma_s - \gamma_w)(\sin \theta - C_f \cos \theta)(a \cdot b \cdot c)$$

This may be divided into three main components in terms of dimensions of the block:

Equation 3.30

$$\Sigma F_x = \underbrace{(\gamma_w - \gamma_{wa})\left(h + \frac{c}{2}\right)(b \cdot c)}_{\text{Front _ and _ Back _ Sides}} + \underbrace{\tau_b(a \cdot b)}_{\text{Top _ Area}} + \underbrace{(\gamma_s - \gamma_w)(\sin \theta - C_f \cos \theta)(a \cdot b \cdot c)}_{\text{Volume}}$$

1. Front and Back Sides: $(\gamma_w - \gamma_{wa})\left(h + \frac{c}{2}\right)(b \cdot c)$
2. Top Area: $\tau_b(a \cdot b)$
3. Volume: $(\gamma_s - \gamma_w)(\sin \theta - C_f \cos \theta)(a \cdot b \cdot c)$

For the flume experiment, the first two components encourage block motion while the third component may restrict motion depending on friction and bed slope. The condition to initiate motion is evaluated by setting the sum of forces equal to zero and solving for the critical bed shear stress.

Equation 3.31

$$0 = \underbrace{(\gamma_w - \gamma_{wa})\left(h + \frac{c}{2}\right)(b \cdot c)}_{\text{Front_and_Back_Sides}} + \underbrace{\tau_b(a \cdot b)}_{\text{Top_Area}} + \underbrace{(\gamma_s - \gamma_w)(\sin \theta - C_f \cos \theta)(a \cdot b \cdot c)}_{\text{Volume}}$$

Equation 3.32

$$\underbrace{\tau_c}_{\text{Critical_}\tau} = \underbrace{(\gamma_s - \gamma_w)(C_f \cos \theta - \sin \theta)(c)}_{\text{Body_Forces}} - \underbrace{(\gamma_w - \gamma_{wa})\left(\frac{h}{a} + \frac{c}{2a}\right)(c)}_{\text{Pressure_Forces}}$$

This may be made dimensionless into a form similar to the Shields parameter.

Equation 3.33

$$\frac{\tau_c}{\gamma_w(G_s - 1)c} = \underbrace{(C_f \cos \theta - \sin \theta)}_{\text{Body_Forces}} - \underbrace{\left(\frac{1 - G_a}{G_s - 1}\right)\left(\frac{h}{a} + \frac{c}{2a}\right)}_{\text{Pressure_Forces}}$$

where G_s is the block specific gravity and G_a is specific gravity of the aerated volume immediately downstream of the block at the knickpoint. This dimensionless relationship for initiation of motion has two components on the right hand side, one from pressure forces due to nappe flow and the other from body forces of the block.

If the bed slope is sufficiently low, then we can ignore the bed slope component. In our experimental setup the bed slope is 0.029, yielding the sine component equal to 0.029, which is over an order of magnitude less than the significantly greater cosine component of 0.43 and 0.73 for coefficients of friction of 0.43 and 0.73, respectively (cosine of 0.029 equal to 0.99958). Ignoring the negligible sine component yields:

Equation 3.34

$$\frac{\tau_c}{\gamma_w(G_s - 1)c} = \underbrace{(C_f \cos \theta)}_{\text{Body_Forces}} - \underbrace{\left(\frac{1 - G_a}{G_s - 1}\right)\left(\frac{h}{a} + \frac{c}{2a}\right)}_{\text{Pressure_Forces}}$$

The above equation shows the critical dimensionless shear stress for a block is the difference between the resisting friction along the base of the block and the pressure forces due to the nappe flow regime. As the nappe flow cavity becomes more aerated,

the critical dimensionless shear stress necessary to move the block is lowered. Regarding block dimensions, increased side width perpendicular to flow (a) increases critical dimensionless shear stress while increased block height (c) lowers critical dimensionless shear stress.

The pressure in the aerated nappe flow cavity in our flume was not directly measured, but a comparison can be made for a range of aeration percentages given as G_a and the calculated critical dimensionless shear stress over the range of the other parameters to the observed small events (1 to 3 blocks), assuming the relationship for critical dimensionless shear stress applies for C_f of 0.43 and 0.73 (Figure 3.29 and Figure 3.30). For C_f of 0.43, small events occurred with 3% to 18% aeration while for C_f of 0.73, aeration ranges from 6% to 30%. These pressure differences for the aerated nappe flow cavity have been measured in other flume experiments with similar hydraulic (nappe flow) conditions (Toombes and Chanson, 2008). The plots show that small percentages of aeration of clear water quickly increase the potential for block movement.

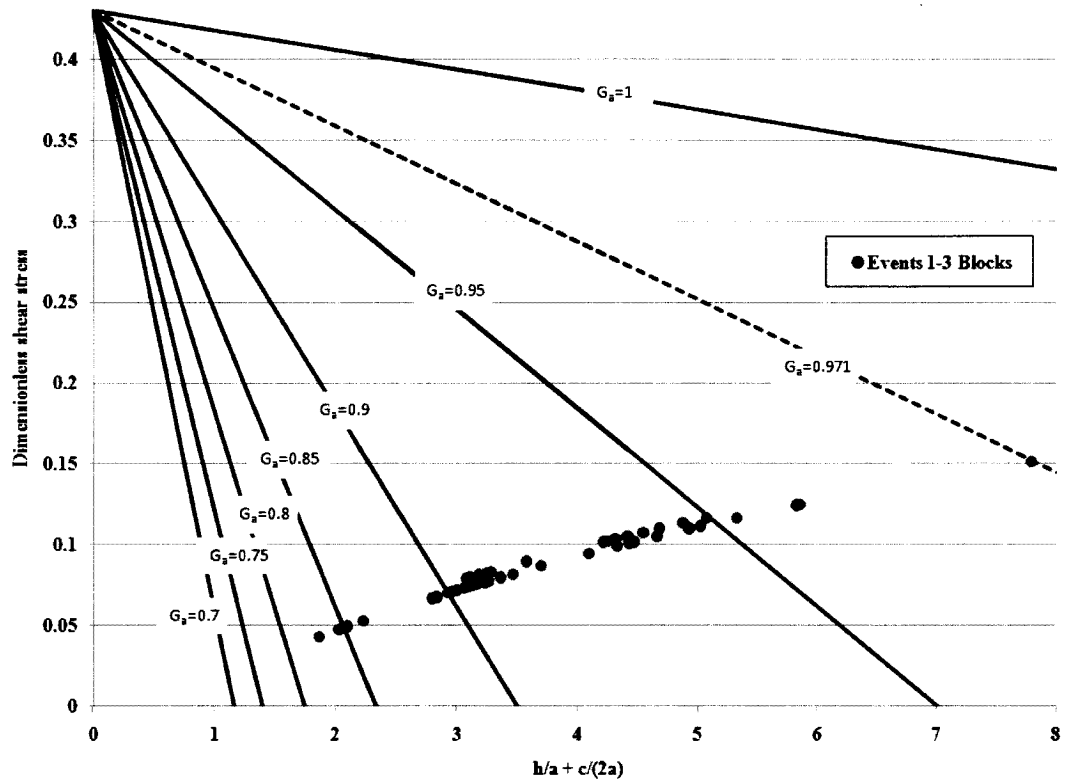


Figure 3.29 Estimated Critical Dimensionless Shear Stress of 1 to 3 Block Events by G_a for $C_f = 0.43$.

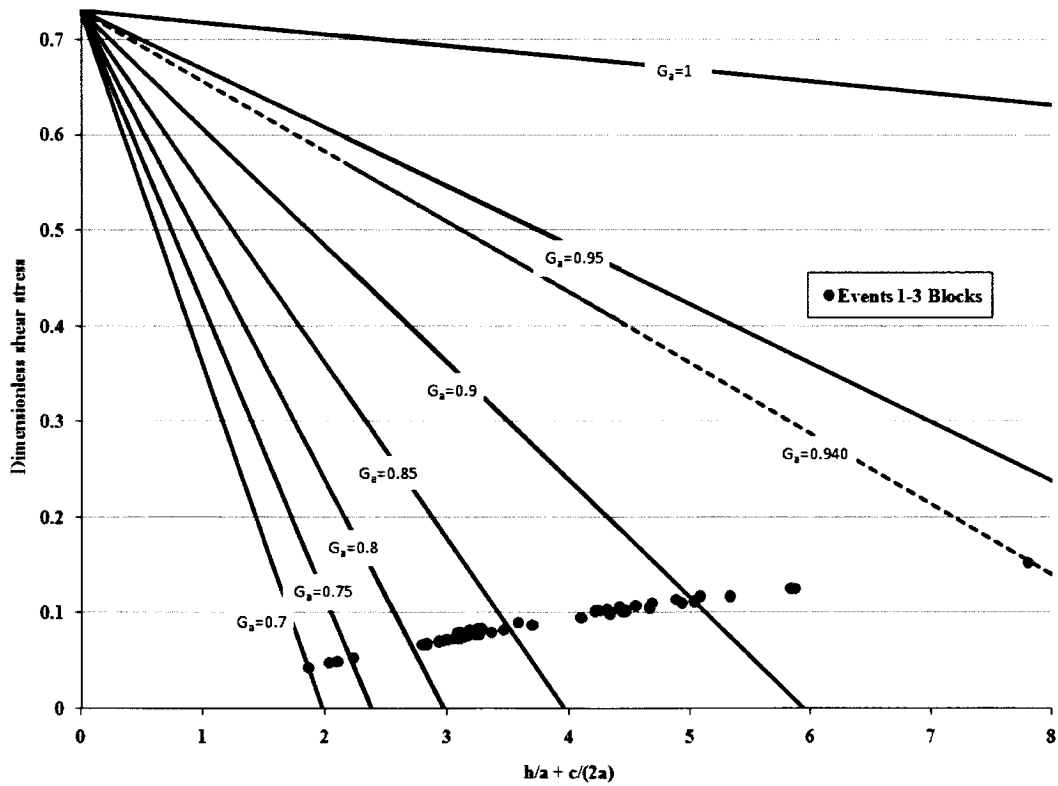


Figure 3.30 Estimated Critical Dimensionless Shear Stress of 1 to 3 Block Events by G_a for $C_f = 0.73$.

3.4.1 Resisting Forces along Sides of Block

In all flume runs, blocks in the same row perpendicular to the sidewall were observed to arch outwards, opening upstream. The center or near-center block served as the keystone in the arch morphology described and illustrated in the earlier discussion of planform geometry seen during the runs. A mechanical linkage between the blocks is theorized to lead to the development of the arch morphology. This mechanical linkage differs from the frictional resistance along the bottom surface of the block in that the linkages along the sides are macroscopic roughness elements, whereas the bottom friction resistance results primarily from smaller scale roughness (Figure 3.31 and Figure 3.32).

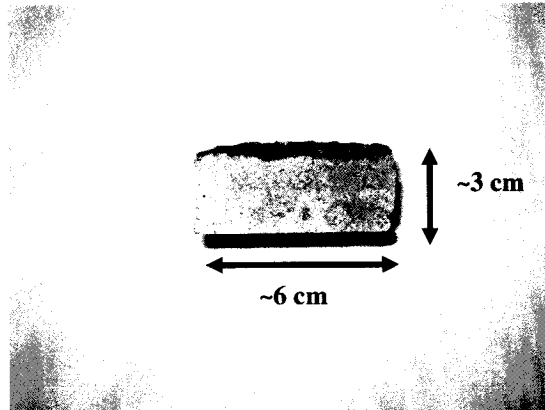


Figure 3.31 Side View of Typical Large Block

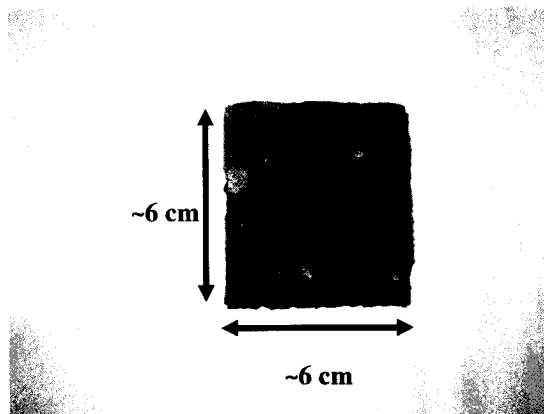


Figure 3.32 Top View of Typical Large Block

When the keystone block is mobilized, it pulls the linked blocks on either side with it in the downstream direction. This dynamic mechanical action cascades through adjoining blocks to form the arch morphology. An example of the arch shape comes from the photographic surveys (Figure 3.20). Closer examination of the joints between blocks shows an irregular jagged joint interface with interlocking teeth (Figure 3.33).



Figure 3.33 Interlocking Joints between Blocks



Figure 3.34 Grains between Blocks

These teeth are part of the linkage between blocks. Presumably, a smooth interface parallel to the driving vector would allow for a single block to be mobilized much more easily without moving adjoining blocks. In addition to the interlocking teeth along the ragged joints, the rotation of the closely packed blocks both forces the neighboring blocks outward or inward and wedges the block in place. This effectively creates a statically unstable structure where the removal of one or a few blocks results in the mobilization of

multiple blocks linked into a chain or arch shape via wedging and interlocking joints. Qualitative examples of the resultant block arch shape are present after a downstream force is applied by a rubber mallet striking the center of the block row perpendicular to the sidewall of the flume (Figure 3.35 and 38). The strength of the mallet force applied was a full swing of the arm but not accelerating beyond the force needed to swing the mallet fully onto the target.

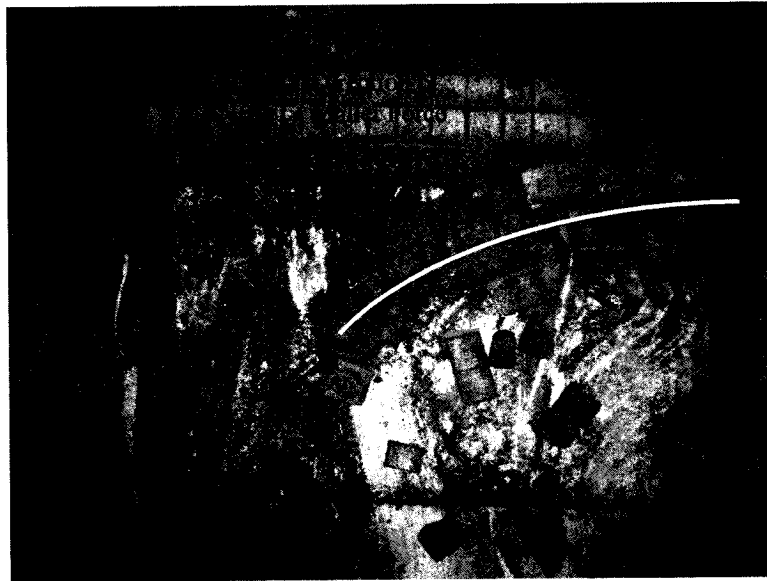


Figure 3.35 Example of Arching Created by Mallet

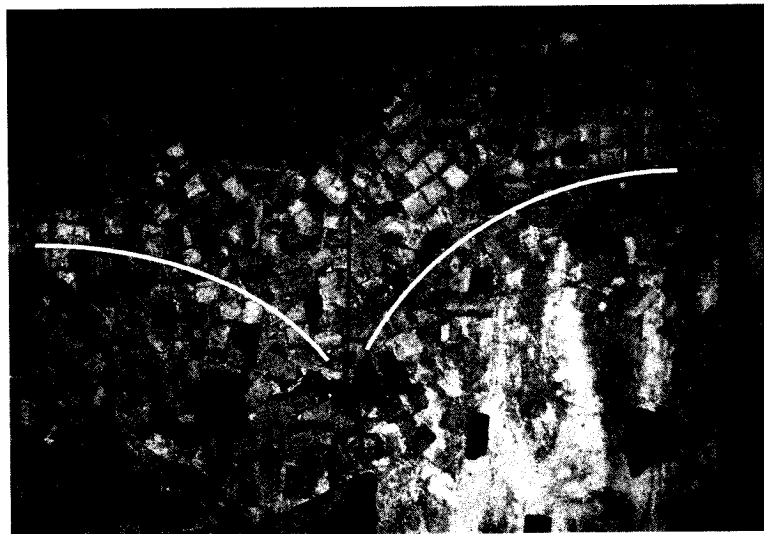


Figure 3.36 Example of Arching Created by Mallet

Key blocks are those which, when removed, allow a larger set of blocks to be mobilized (Warburton, 1987). Warburton (1987), in an examination of rock failure mechanics, defined a key block as a block whose removal would be required for the degradation of a larger mass of blocks. Such a definition also characterizes the erosional kinematics observed in the flume, where the removal of one or a few key blocks results in a more massive immediate failure. The key block definition is incorporated in the geo-engineering literature into block theory, first introduced by Goodman and Shi (1985), where the failure possibilities of a rigid jointed rock mass next to an open space are examined, with particular attention to key blocks formed by the joint configuration in the rock mass of interest (Goodman, 1995). Their examination of key blocks and rock failure was primarily concerned with building structural support, dam support, and tunnel support structures where the primary loading came from the rock mass only. In the quarrying of blocks at the knickpoint, the driving forces produced by flow are the important if not primary loads on the rock mass, including key blocks. However, block theory and especially the concept of a key block provides a plausible framework describing the resistance provided by other blocks to the side of the block of interest. In a summary of block theory, Goodman (1995) discusses the importance of joint resistance to block failure. Joint roughness determines to a great extent the shear force necessary to overcome the resisting force along the joint, defined as the shear strength of the joint. Material present in the joint space will produce lower joint shear strength. Annandale (2006) provides an examination of the hydraulic scouring of jointed bedrock in the context of block theory, providing a link in the geo-engineering literature between block

theory and fluvial processes. According to Annandale (2006), jointed bedrock is classified as a physical gel, where a physical gel consists of elements in adjoining spaces that are connected to each other by touching. Resistance of jointed bedrock to scour is thus heavily influenced by joint resistance, which is primarily a function of joint roughness and presence of material in the joint, and the role of key blocks.

For our previously derived equation for dimensionless shear stress, we discussed the potential for side friction forces but did not include them. We now will introduce a possible approach for the side friction forces. Unlike the friction force along the base of the block, the side friction forces are hypothesized to be the result of interlocking elements along the irregular edges of the blocks. Our approach is to assume a constant force per unit area that results on average for these interlocking edges, f_s with the total side friction force, F_{fs} being the unit force multiplied by the side area of the two sides:

Equation 3.35

$$F_{fs} = f_s \cdot 2(b \cdot c)$$

This force will resist in the direct of motion of the block, which we observed being primarily sliding, so we assume $F_{fs} \sim F_{fsx}$. Adding this into the force balance yields:

Equation 3.36

$$\Sigma F_x = \underbrace{(\gamma_w - \gamma_{wa})(h + \frac{c}{2})(b \cdot c)}_{\text{Front_and_Back_Sides}} + \underbrace{\tau_b(a \cdot b)}_{\text{Top_Area}} + \underbrace{(\gamma_s - \gamma_w)(\sin \theta - C_f \cos \theta)(a \cdot b \cdot c)}_{\text{Volume}} - \underbrace{f_s \cdot 2(b \cdot c)}_{\text{Transverse_Sides}}$$

Setting the sum of forces to zero for critical conditions and solving for the dimensionless shear stress yields:

Equation 3.37

$$\underbrace{\frac{\tau_c}{\gamma_w(G_s - 1)c}}_{\text{Critical_}\tau} = \underbrace{(C_f \cos \theta)}_{\text{Body_Forces}} + \underbrace{\frac{f_s \cdot 2}{\gamma_w(G_s - 1)a}}_{\text{Transverse_Sides}} - \underbrace{\left(\frac{1 - G_a}{G_s - 1}\right)\left(\frac{h}{a} + \frac{c}{2a}\right)}_{\text{Pressure_Forces}}$$

We see the addition of our hypothesized side friction forces means the dimensionless critical shear stress decreases with increased side length, a . This competes with the pressure forces component where increased side length a increases critical shear stress. Our previous equation for dimensionless shear stress represents the end point where the side friction forces decrease to zero. This may occur as blocks are loosened through both extraction of key blocks and breakdown of the rough edges between blocks over time.

3.4.2 Forces Acting over Time and Space

Whipple et al. (2000a) suggest bedrock blocks are loosened over time and theorized that the loosening rate is an empirical function of shear stress. Building on this model of linking changes in the erosional process with forces acting over time with our simple force analysis, loosening of blocks and mobilization are both functions of the work done by the flow on the blocks as well as the body force of the blocks themselves. However, it is difficult to measure precisely and accurately the instantaneous forces operating in the jointed bedrock flume channel and thereby predict for an individual block the unique forces necessary to mobilize the block at a given point in time. This is especially true for the instantaneous pressure forces of turbulent flow acting as a source of effective force in a system such as those described by Graf (1977), Nelson et al. (1995) and Papanicolaou et al. (2001). In this study I have chosen to use averaging and generalization for easy calculation that encapsulates the observed erosional work by the flow over the bedrock channel with some degree of reasonable accuracy.

As described previously, stream power expresses energy expenditure by the flow. Although primarily expended in motion of the flow, some portion is expended on the

river bed (Annandale, 2006). In this case, the bed is jointed bedrock. The force analysis developed an estimate of the threshold critical net force necessary for initiation of block motion. Some of these forces, such as resistance to motion along the sides of the block perpendicular to the bed and parallel to the direction of motion, change over time as the block is exposed to forces near the critical threshold until the net force balance results in motion of the block. In our force balance this is represented by decreasing unit side friction force over time.

In the statistical approach to follow, the block loosening action mentioned by Whipple et al. (2000a) will be included by using expenditure of stream power over time acting on the block. Additional complexity not directly addressed in our force balance for a single block are key block conditions under which, in addition to gradual loosening of an individual block, the removal of a key block results in a sudden change in the net force balance that exceeds the threshold of motion for a set of blocks that then are mobilized at a much more catastrophic rate than the gradual erosion of one block over a period of time. This will be addressed in the statistical approach to follow.

Parameters for the threshold for motion, stream power expenditure to represent block loosening, and key block complexity are three elements incorporated into the following statistical analysis of erosion of the experimental jointed bedrock channel to combine with measured hydraulics and bedrock characteristics into a model of the observed erosion of the jointed bedrock channel over time. The goal is to build onto the critical force evaluation a more time and energy-based dimension for our understanding of block erosion.

3.5 Statistical Analysis

Determinant modeling of erosion of each block over time would require complex modeling and detailed knowledge of the structure of the jointed material over time, including the joint strength of every vertical joint, the rotation of blocks resulting from the loading by the turbulent flow, the wedging forces of the rotated blocks on neighboring blocks, and the spatially and temporally distributed loading applied by the turbulent flow on the jointed bedrock channel. An alternative to a deterministic model is a statistical model where the likelihood of an erosional event of a given magnitude at a given point in time is determined. The model proposed is as follows: At time t , an erosional event may occur with a defined probability distribution. If an event occurs, the event magnitude is m , with a defined probability distribution. If an event does not occur, then the event magnitude is null or zero.

To examine the possibility of applying such a model to erosion of our experimental jointed bedrock channel, a statistical analysis of the flume results was undertaken. Our model is built on two primary questions:

1. At a given time, what is the likelihood that an event occurs?
2. Given that an event occurs, what is the likelihood of a given event magnitude?

Note that the probability of an event magnitude at a given time is conditional on the probability of an event occurring at a given point in time. The discontinuous nature of erosion of the bedrock channel observed during all runs lends itself to this statistical description of the overall erosion time series.

The distribution of joint strength and therefore possible keystone configurations is assumed to be random; hence, the resistance of the bedrock channel is spatially random. The primary loading on the blocks required for failure is hydraulic loading by controlled flow in the flume. The spatial distribution of the hydraulic loading applied by the flow over a given period of time was previously expressed as energy expended per unit area expressed as cumulative unit stream power (*CUSP*) or energy expended per unit length expressed as cumulative total stream power (*CTSP*) of the channel bed. Although time lapse is in theory correlated with block erosion, it is not time lapse in and of itself but work done on the bed which is physically responsible for block erosion. Time lapse is replaced in the statistical model with energy expenditure expressed as *CUSP* or *CTSP*. Event magnitude was found not to be strongly correlated with either. A discussion of the correlation between event magnitude and time lapse or energy expenditure is provided in Appendix C.

The usage of energy expenditure instead of time lapse is not only a more appealing physically-based variable representing the hydraulic loading responsible for failure but also provides one possible way to normalize between different channel widths and discharge conditions as these influence loading on the bed. Such conditions are taken into account in calculating stream power. With the advantage of normalizing between different conditions seen in the experimental runs, the energy expenditure will be used instead of time lapse in determining the likelihood of an event occurrence. Energy expenditure will be expressed as *CUSP* with the random variable denoted by E_e or as *CTSP* with the random variable denoted by T_e .

The assumed independence of $P(B)$ and $P(E_e)$ allows for a simplified estimate of the probability of erosion of a given magnitude after a given energy expenditure.

Assume the energy expended until an event occurs and event magnitudes are independent random variables each characterized by a particular probability distribution. The probability of an event of a given magnitude after a given energy expenditure is then conditional on the joint distribution formed by the independent distributions of the two random variables of event occurrence and event magnitude.

Equation 3.38

$$P(B, E_e) = P(B)P(E_e)$$

A key component of the statistical analysis will be to determine whether a particular probability distribution fits the distribution of the random variables of interest, namely event magnitude (B) and event occurrence (E_e or T_e).

The statistical analysis is divided into three parts. The first part involves determining an appropriate probability distribution to describe the observed probability distribution of *CUSP* required for event occurrence, E_e , examining variation between runs, and investigating any correlation with differing run conditions (e.g., channel width and joint spacing). In the second part, an appropriate probability distribution to describe the observed probability distribution of event magnitude, B , will be determined, followed by examining variation between runs, and investigating any correlation with differing run conditions. The third part of the analysis combines our analysis of event occurrence and magnitude to build a statistical description of erosion in our physical model. A supplemental statistical section with expanded analysis and supporting statistical results is included in Appendix C. The statistical software packages S-Plus 7.0 Student Edition and SPSS v. 15 were used for the statistical analysis (S-Plus, 2005; SPSS, 2006).

3.5.1 Probability of Event Occurrence

The probability of event occurrence is expressed by the continuous random variable E_e , *CUSP* between events. The possible values of E_e lie in the domain from near 0 to infinity. The empirical cumulative distribution functions (CDF) of the results of Runs A, B, D, E, and G were used to accurately fit appropriate probability distributions to the empirical distributions. An example empirical distribution is shown for Run A (Figure 3.37). The cumulative distribution describes the probability of the random variable being equal to or less than a given value. For the empirical data, the CDF expresses the probability of an event occurring after a certain *CUSP* has occurred. For these data, the lognormal distribution appeared to fit best with the data from all runs. This is theoretically an appropriate distribution because by definition the dataset has only positive real numbers representing time measurements between events. The lognormal distribution fitted to each dataset uses the mean and standard deviation of the natural logarithmic transform of the dataset. The previous analysis of energy expenditure showed differences in stream power related to width. Runs with the same width but different discharge and joint spacing have similar values of energy expenditure per event as a result of compensating changes in lapse time per event such that energy expenditure remains relatively constant within width groupings. Event occurrence is only part of determining total erosion. The other part is how much material is removed when an event occurs, or the magnitude of the event. A comparison of the means of the natural log-transformed data by run shows the means of Runs A and B to be closer in value and greater than those of Runs D, E, and G (Figure 3.38 and Table C.4).

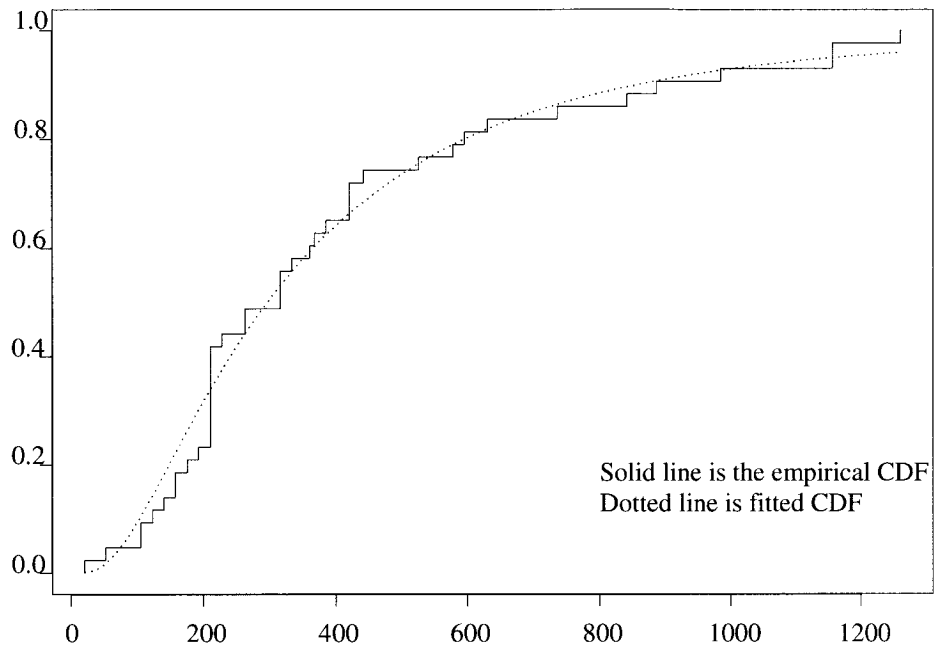


Figure 3.37 Empirical CDF and Fitted (Hypothesized) Lognormal CDF - Run A

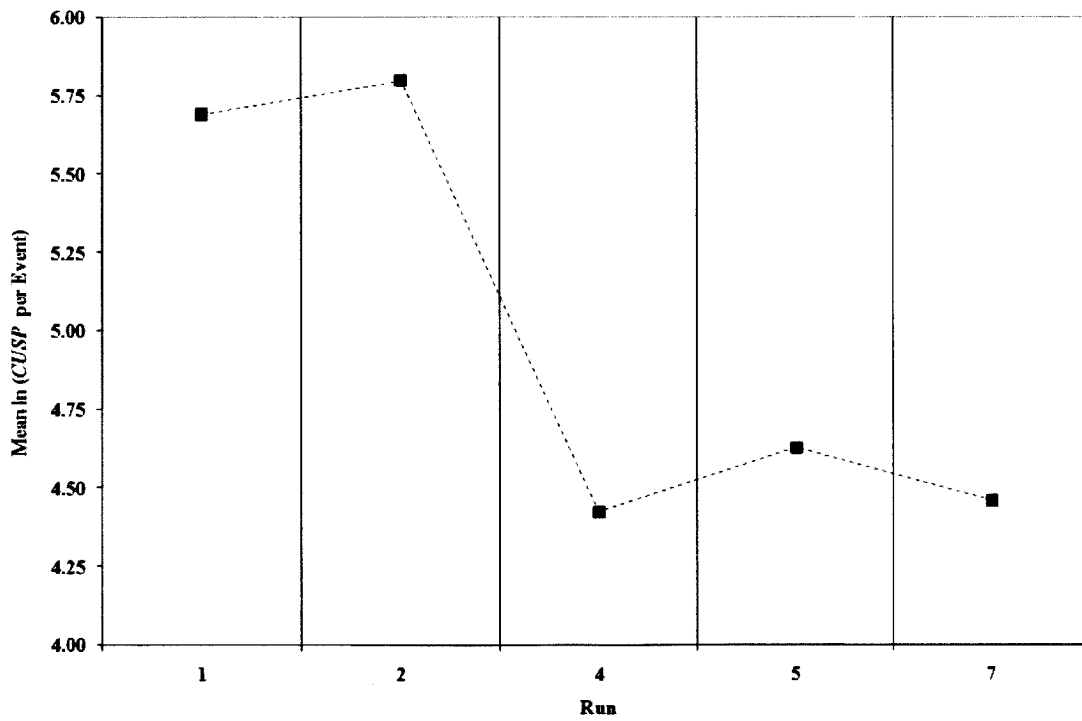


Figure 3.38 Comparison of Mean ln(CUSP per Event) by Run

The results of Dunnett's C multiple comparisons also show the greatest difference between the grouping of Runs A and B and the grouping of Runs D, E, and G (Table C.7). The statistic in the multiple comparisons is significant at the 95% level for all but the comparison of Run B and Run E, which was found to be significant at 94% but not at the 95% level. In particular, the mean *CUSP* required for event occurrence is greater in Runs A and B than in Runs D, E, and G, but similar within each grouping. The only major difference between these two groupings is channel width. The significant difference between groups suggests channel width plays an important role in determining the amount of expended energy necessary for event occurrence.

Given the difference between groupings by channel width, the data by group were examined. After back-transforming the mean of the log transformed data, mean *CUSP* values are 308 kJ/m² for the narrow channel and 88 kJ/m² for the wide channel. The ratio between the calculated *CUSP* for the narrow flume and the wide flume is 3.5:1; in other words, 3.5 times more energy was expended on average per event in the narrow flume runs than in the wide flume runs. Intriguingly, the ratio between narrow and wide channel widths is 1:2 and this energy difference occurs with measured higher flow depths and calculated shear stresses for the narrow flume runs versus the wide flume runs. The ratio of 1:2 seen in the flume widths and the ratio of 3.5:1 seen in the *CUSP* calculations requires more exploration. The unit stream power calculation includes the width through the calculation of hydraulic radius. If the expended discharge, $Q \Delta t$, between events on average is the same for narrow and wide flumes, then the *CUSP* and *CTSP* ratios will be 2:1 and 1:1, respectively. The flume results give a *CUSP* ratio of 3.5:1, indicating there is a difference in $Q \Delta t$ per event (expended discharge per event)

assuming the hydraulic radius is equal to channel width and using the same discharge, water density, and bed slope. After back-transforming the mean of the log transform of the data, the corresponding *CTSP* per event is 285 kJ/m² for the narrow channel and 117 kJ/m² for the wide channel. The ratio between the calculated *CTSP* for the narrow flume and the wide flume is 2.43:1; in other words, 2.43 times more energy was expended on average per event in the narrow flume runs than in the wide flume runs. The theoretical ratio of 1:1 was calculated where group widths differ but mean *CTSP* per event is the same. The theoretical ratio differs from the observed ratio of 2.43:1. An expanded outline of this calculation is provided in Appendix C. This result suggests there is something else leading to differences in expended stream power per event between the width groupings. An expanded outline of this calculation is provided in Appendix C. To provide an explanation, the equations for *CUSP* and *CTSP* were decomposed into a set of ratios between the two width groupings. An expanded outline of this calculation is provided in Appendix C. The overall ratio and product of ratios from the decomposition of the *CUSP* and *CTSP* ratios are equal. Time lapse (Δt) and R_h (~channel width with a small contribution from depth) are the dominant factors differing between groups, with a minor contribution from differences in mean Q between events. The contribution from time lapse with ratio of 2.66:1 indicates there is a difference with regard to the energy expenditure necessary for erosion despite nearly equal discharge expenditure at a ratio of 0.91:1. Differences are seen between individual runs with the same discharge and joint spacing but different widths (e.g., Run A and Run D). Differences within width groupings appear to be negligible because runs with the same width but different joint spacing are not significantly different (e.g., Run E and Runs G).

The dependency of time lapse on width, joint spacing, and mean discharge was further examined by a robust analysis of variance where time lapse is the dependent variable and channel width, joint spacing, and mean discharge are main effects. A detailed analysis and discussion is provided in Appendix C and summarized here. Joint spacing was the least significant effect in the full model with p-value greater than 0.10. A reduced model with only channel width and mean discharge was subsequently constructed with channel width and mean discharge significant at p-values less than 0.05. Unfortunately, both models explain only 8% of the variation seen in the data. The large variation in the data is not sufficiently explained by the model for predicting time lapse between events with any statistical confidence, but the model does provide a framework of significant parameters for further investigation. Despite the large variation in the data and resulting low predictive power of the model, our analysis consistently links qualitatively channel width and mean discharge to time lapse between events, suggesting that increases in these two main effects will lower of lapse time.

The analysis of energy expenditure per event showed differences related primarily to channel width. Runs with the same channel width but different mean discharge and joint spacing have similar values of energy expenditure per event as a result of compensating changes in time lapse per event so that energy expenditure per event remains relatively constant within width groupings. Event occurrence is only part of determining total erosion. The next section examines how much material is removed (i.e., event magnitude) when an event does occur.

3.5.2 Probability of Event Magnitude

In addition to estimating the likelihood of an event occurring, the probability of a given magnitude when an event occurs is the second component of the probability model of erosion. In the previous analysis examining event occurrence, less energy was necessary for event occurrence in the wide flume setup than in the narrow flume. The overall erosion rate may be less in the wide flume if each event is sufficiently smaller than in the narrow flume so more material per unit time is eroded on average in the narrow flume. Alternatively, the erosion rate may be higher in the wide flume than the narrow flume if event magnitudes are sufficiently higher in the wide flume setup. To investigate event magnitudes, a similar approach will be taken as was used for the event occurrence probability analysis. Cumulative density plots of the event volume data were examined and a suitable probability distribution chosen. Further analysis compared mean event volume between runs, with attention to any differences between groupings by joint spacing and channel width of the flume.

For the empirical data, the CDF expresses the probability of equal or lesser event magnitude by volume when an event occurs. The possible values of volume lie in the domain from near 0 to infinity. For these data, the lognormal distribution appeared to best fit the data from all runs. An expanded section is provided in Appendix C. The lognormal distribution fit to each dataset uses the mean and standard deviation of the natural logarithm transform of the dataset (S-Plus, 2005).

Multiple comparisons using Dunnett's *C* show significant differences in event volume between runs, which deserves further inquiry. The results are summarized here with an expanded section in Appendix C. There is a similar pattern as for event

occurrence between width groupings but there are also significant differences within width groupings such as between Runs A and B or between Run E and Runs D and G. Run D and Run G appear to be similar. This is expected because they had nearly the same setups in terms of discharge, width, and joint spacing but different run times. The other non-significant difference resulting from the multiple comparisons tests was between Run A and Run E, where both joint spacing and flume width were different, although the difference was not as great as between Run D and Run G. All other combinations which were significantly different based on the multiple comparisons tests have either different joint spacing but the same flume width (Runs A, D and G; Runs B and E), or the same joint spacing but different flume width (Runs A and B; Runs D, E and G). Flume width and joint spacing both statistically correspond with event magnitude probabilities.

The differences seen in the multiple comparisons test were examined in the context of flume width and joint spacing combinations by qualitatively organizing the different runs in order of highest mean $\ln(\text{Event Volume})$ based on the multiple comparisons test (Table 3.7).

Table 3.7 Ranking of Runs by $\ln(\text{Event Volume})$. Highest Rank is 1

Run	Channel Width	Joint Spacing	Rank
B	Narrow (0.61m)	Wide (0.06m)	1
A	Narrow (0.61m)	Narrow (0.03m)	2
E	Wide (1.17m)	Wide (0.06m)	3
D and G	Wide (1.17m)	Narrow (0.03m)	4

The rankings show runs with the narrow channel width tend toward larger mean event magnitudes. Wide joint spacing contributes to higher event magnitudes than narrow joint spacing given the same channel width. However, decomposing the relationship between

width, joint spacing, and event magnitude is not as easily achieved as in the previous analysis of event occurrence, where width shows a far more dominant influence.

A linear regression of the dummy variables width and joint spacing on the log transform of event volume, V was done to quantitatively clarify the role of width and joint spacing in event magnitude. An expanded section for the results presented here is in Appendix C. The analysis of variance showed channel width and joint spacing with significant correlation to log transform of event volume, with p-values of less than 0.0001. Overall the model had an R-squared value of 0.495 (~ 50%), with width being more strongly correlated than joint spacing.

Event magnitude may also be expressed by the number of blocks eroded instead of total volume of the blocks in the event. As in the previous analysis, runs were compared using log transformed event block count data. A descriptive comparison between runs suggests similar means between Run A and B and between Run D, G, and Run E (Table 3.8).

Table 3.8 Event Block Count by Run

Run	N	Mean ln(Event Block Count)	Std. Dev.	Mean Block Count
A	43	3.89	1.507	49
B	24	3.60	1.512	37
E	61	1.22	1.381	3
D	24	1.77	1.633	6
G	23	1.22	1.449	3
Total	175	2.28	1.894	10

Multiple comparisons were done using Tukey and Dunnett's C and the results are in the expanded section in Appendix C. The multiple comparison results support the initial conclusion from comparison of means that the mean event block counts of Run A

and B are statistically similar but differ from Run D, E, and G, which are similar to each other.

A model with width and joint spacing as factors for \ln (event block count) was constructed because width and joint spacing were significant factors in determining event volume. The results are summarized here with expanded analysis in Appendix C. The analysis of variance showed channel width with significant correlation to log transform of event volume although joint spacing was not significant. An AOV table for the reduced model with only width was then constructed. The reduced model has an R-squared value of 0.396, almost the same as the previous model with 0.397. The analysis of variance suggests that a partial explanation of differences seen in the mean log transform of event block count is channel width; runs with wide channel width had lower mean event block counts than runs in the narrow channel.

At the outset of this statistical analysis, erosion over time was described as probability of event occurrence combined with probability of event magnitude provided an event occurs. The insights from the analyses of event magnitude and event occurrence are next combined to investigate the erosion of blocks over time. The focus will be on the interactions between event volume, event occurrence in terms of stream power expenditure, channel width, and joint spacing in an effort to more fully describe erosion of the experimental jointed bedrock channel.

3.5.3 Modeling Erosion

From the previous analysis of event occurrence, the probability of an event occurring after a given expenditure of energy is correlated with channel width to some

degree, although a great deal of random variation is present, with several outliers. Event magnitude correlates with channel width and joint spacing. Recall that event magnitude was weakly correlated with energy expenditure. The weak yet visually suggestive correlation between energy expenditure and event volume warrants further inquiry. The distributions of energy expenditure as expressed by *CUSP* or *CTSP*, time lapse between events, and event magnitude were best fitted assuming lognormal distributions. The log-transformed datasets were used in all the previous statistical analyses. Inquiring into the possible relationship between event occurrence as expressed by energy expenditure and event magnitude, log-transformed *CTSP* and *CUSP* for each run were plotted against corresponding log-transformed event volume to identify any visible correlation (Figure 3.39 and Figure 3.40). The correlation may be slightly negative as indicated in the earlier analysis of event occurrence, but the correlation is not very strong and a great deal of variation is present. However, the addition of expended energy per event to the previous model could perhaps add significant power after the overlying effects of channel width and joint spacing are taken into account. Such a model would provide a link between event occurrence and event magnitude to yield the magnitude of erosion at a given event occurrence.

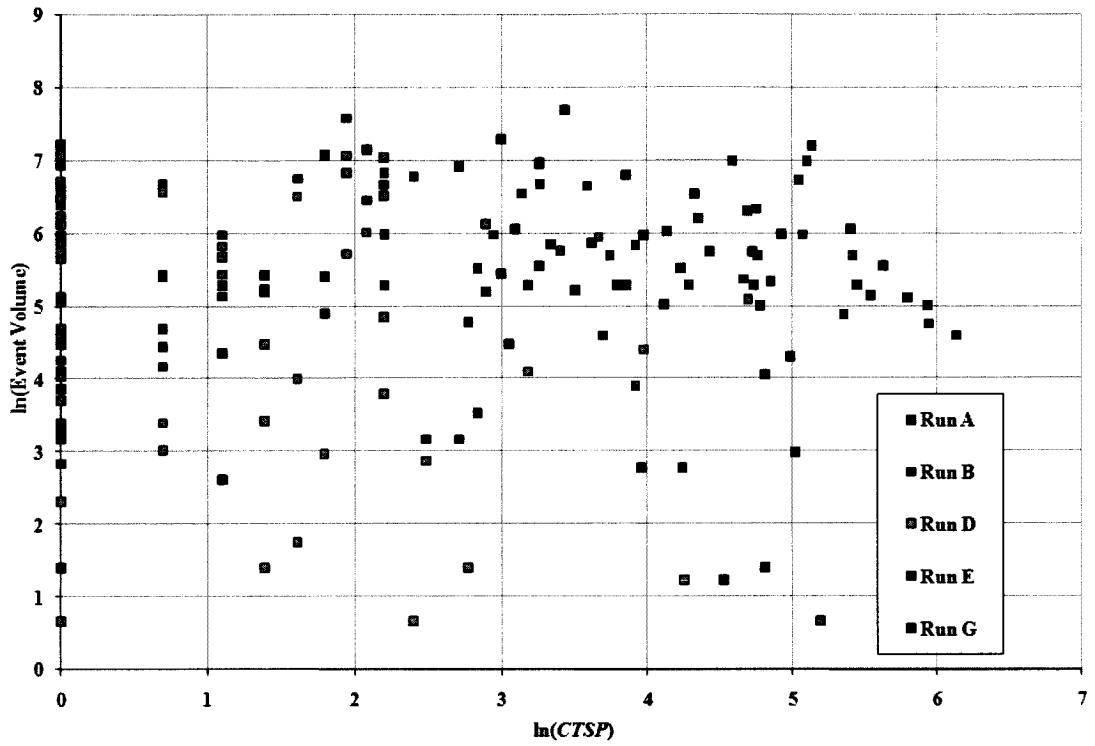


Figure 3.39 Event Volume and CTSP by Run

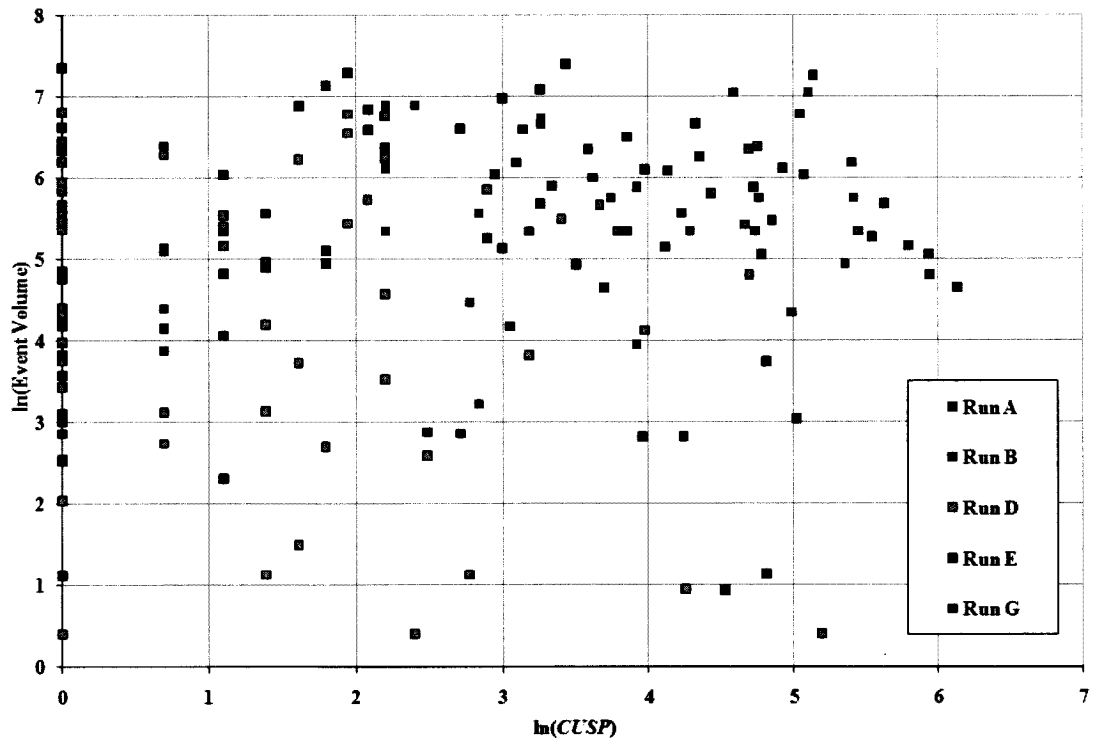


Figure 3.40 Event Volume and CUSP by Run

A linear regression of width, joint spacing, log transform of *CUSP* per event and interaction term between width and the log transform of *CUSP* per event on log transform of event volume, *V* was done and an AOV table constructed. The results are summarized here with the full results and expanded analysis provided in Appendix C.

Final Model of Event Volume:

Equation 3.39

$$\ln(V) = \beta_0 + \beta_1 W + \beta_2 J + \beta_3 \ln(T_e) + \beta_4 \ln(T_e) W$$

The interaction term, despite having a p-value of 0.295, was retained because the term provided significance to the overall model, with F statistic of 4 and p-value of 0.04. Also, because the energy expenditure term was included in the model, the previous correlation between width and energy expenditure suggests including an additional interaction term. The coefficient term for $\ln(CTSP)$ is negative, which indicates longer periods of energy expenditure result in lower event volumes. However, the term is not very significant with a p-value of only 0.322. Overall, the model explains 49.5% of the variation seen in the event magnitude data, which leaves over 50% of the variation in the event magnitude unexplained. A normal *QQ* plot of residuals shows some outliers and greater variation at the extremes of the data set (Figure 3.41). Attempts to bring these elements into the model may yield a better explanation of the variation in event magnitude.

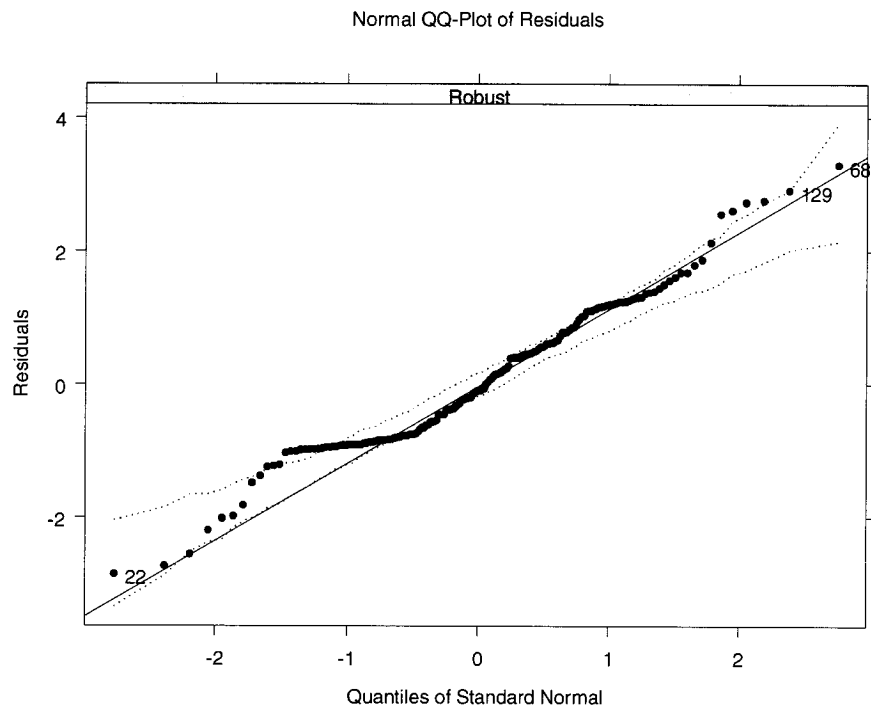


Figure 3.41 Normal QQ Plot of Residuals of Final Model of Event Volume

Key Block Classification

Comparison of the frequencies of different event volumes suggests bimodal tendencies between small events and the largest events (Figure 3.42). Recalling the earlier discussion of key block theory as a model of block motion, the motion of a few blocks is required for a mass movement to occur although such an event may or may not immediately occur. The bimodal tendencies of the event magnitudes suggest grouping of small events, which in the context of key block theory are termed key block events, and large events, denoted as mass failures. The additional grouping factor of key block events and mass failure events was applied to the data, where key blocks events occur at event block counts of less than or equal to three. This was a subjective grouping break based on the observation that mass failures tended to be significantly greater than three

blocks. This reflects the fact that, from a mechanical standpoint, a single block removed has one block attached on either side. Thus if even the one middle block is theoretically the key block, the motion of that block being removed involves the possible simultaneous removal of the block on either side for a total removal of three blocks. This additional classification scheme was not included in the previous analyses because it was performed *post hoc* with regard to the experimental runs.

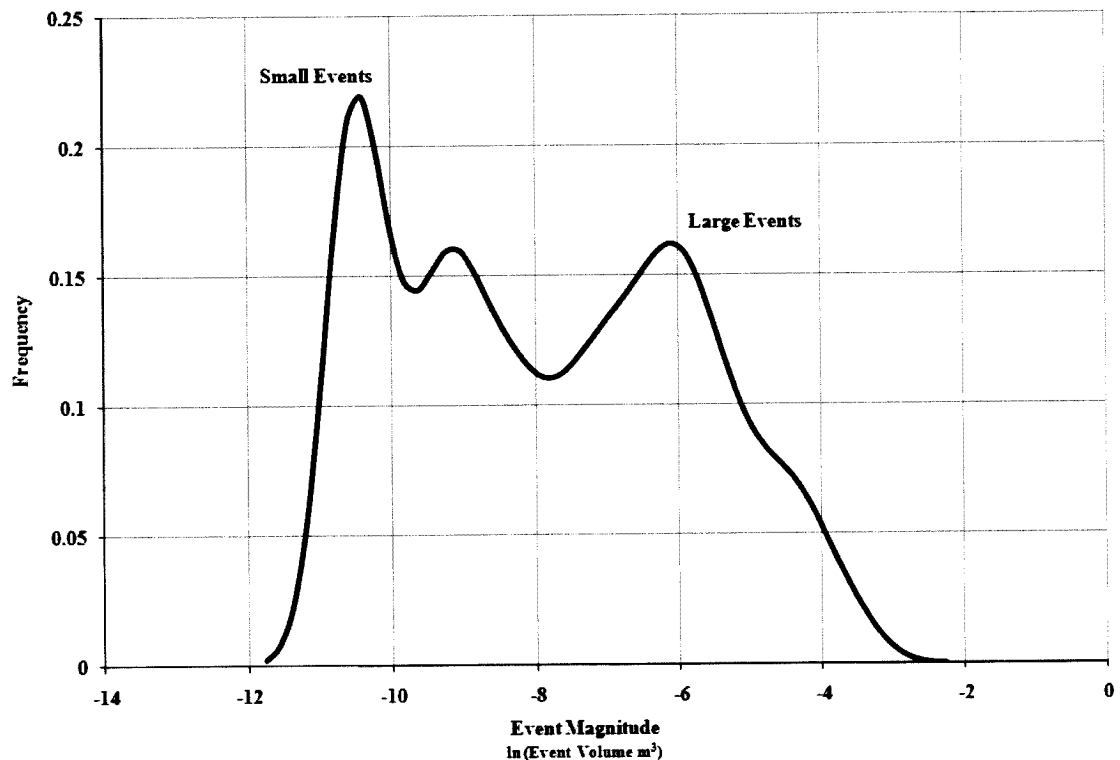


Figure 3.42 Frequency Plot for Event Magnitude

The key block event classification scheme was applied and added to the previous model of event magnitude including width, joint spacing, and energy expenditure, and including an interactions term with energy expenditure. The robust statistical methodology was utilized as in previous models. Overall, the full model provided significantly more explanation of the variation in event magnitude at 66%, compared to

the previous model with explanatory value of 50%. The results are summarized here with the full results and expanded analysis provided in Appendix C.

Full Revised Model of Event Volume:

Equation 3.40

$$\ln(V) = \beta_0 + \beta_1 W + \beta_2 J + \beta_3 M + \beta_4 \ln(T_e) + \beta_5 \ln(T_e) W + \beta_6 \ln(T_e) M$$

The interaction term between key block classification and energy expenditure is fairly insignificant, with p-value of 0.265 and term added significance p-value of 0.279. A reduced model was then analyzed without the inclusion of this interaction term with good results. The results are summarized here with the full results and expanded analysis provided in Appendix C.

Reduced Revised Model of Event Volume:

Equation 3.41

$$\ln(V) = \beta_0 + \beta_1 W + \beta_2 J + \beta_3 M + \beta_4 \ln(T_e) + \beta_5 \ln(T_e) W$$

The removal of the interaction term improved the significance of all the remaining terms with p-values less than 0.05. The reduced model also explains 69% of the variation in event magnitude, which is greater than the full model at 66% and much greater than the previous model with the energy expenditure term at 50%. The residuals are fairly normal and more contained than the previous model with the classification scheme (Figure 3.43 to Figure 3.45). The comparison of event values versus the model values produces a fairly uniform variation around the model predictions, although much variation still exists (Figure 3.46).

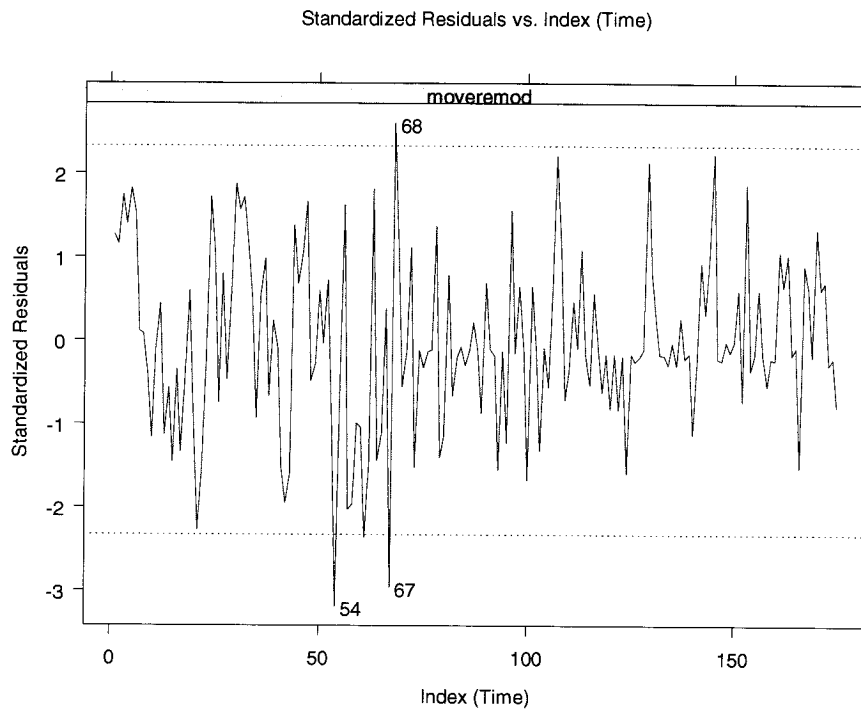


Figure 3.43 Standardized Residuals for Reduced Revised Model of Event Volume

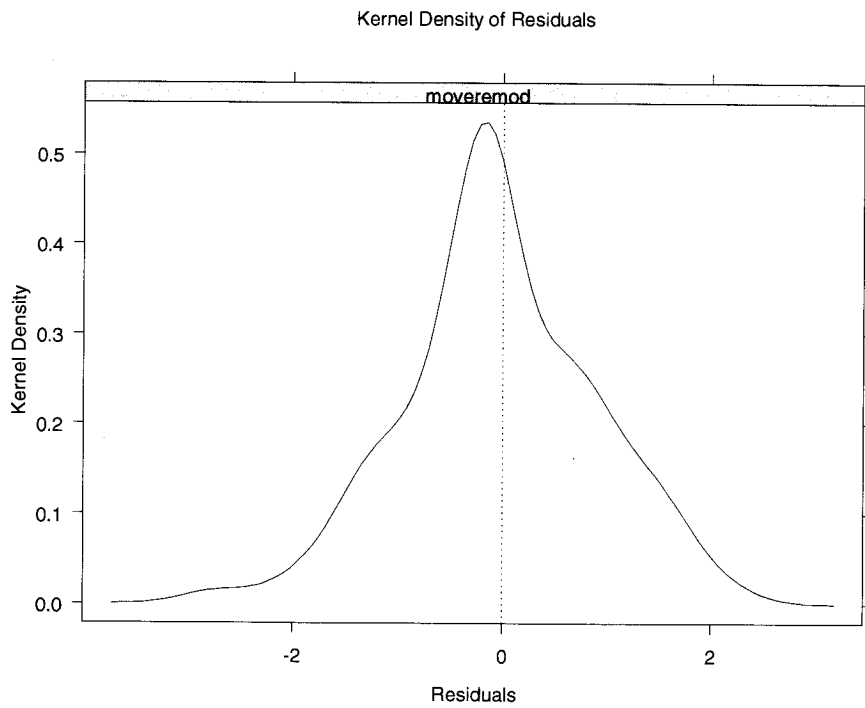


Figure 3.44 Density Plot of Residual for Reduced Revised Model of Event Volume

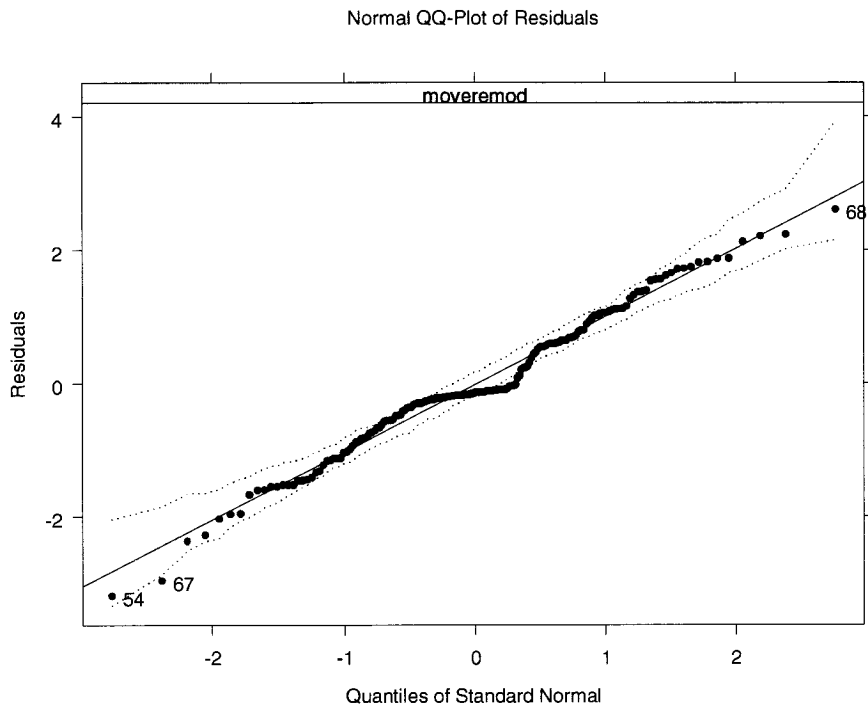


Figure 3.45 Normal QQ Plot of Residuals for Reduced Revised Model of Event Volume

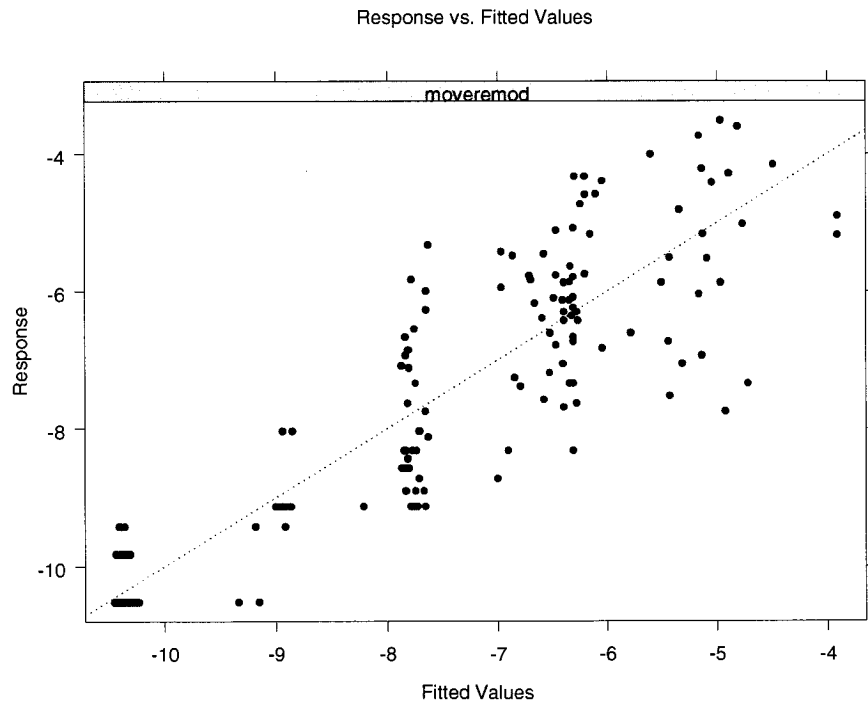


Figure 3.46 Plot of Response versus Fitted Values for Reduced Revised Model of Event Volume

The inclusion of key block classification in the model provides significant explanatory power. Some caution is noted in that the movements defined as key blocks were not specifically tested as to whether these blocks were key blocks in the jointed bedrock. Our approach is somewhat subjective by defining all events with block counts equal to or less than three as key block events. However, the strong bimodal pattern seen in the frequency of event magnitudes and experimental observation of key block action provides evidence supporting the classification scheme. Unfortunately, the predictive power of this model requires classification of blocks as key blocks or mass failures, which may be difficult to define *a priori*. Statistical key block prediction has been done for civil engineering applications relating to rock failure (Annandale, 2006). Perhaps such a scheme may in the future be developed for jointed bedrock channels.

Our statistical analyses suggest that channel width was a primary factor correlating to differences in event occurrence as measured by energy expenditure and event magnitudes. Secondary yet important factors of joint spacing and key block classification were involved in event magnitude. Energy expenditure was weakly correlated with event magnitude, with relative significance after accounting for classification of an event as removal of key blocks or mass failure. Event occurrence was influenced by channel width, but much unexplained variation remains. The interaction of width with energy expenditure, primarily time lapse between events, complicated the determination of the link with event magnitude. The correlation suggests that higher energy expenditures result in smaller event magnitudes, as suggested by key block theory. However, the weakness of the correlation prevents much discussion of this

correlation. Perhaps future experimentation where the primary variable is flume discharge would elucidate such correlation.

One measurement of particular interest is the erosional efficiency of a given set of conditions of loading by flows on a particular jointed bedrock setup. The final model for predicting event magnitude written in equation form is as follows:

Equation 3.42

$$\ln(V) = \beta_0 + \beta_1 W + \beta_2 J + \beta_3 M + \beta_4 \ln(T_e) + \beta_5 \ln(T_e) W$$

Subtracting $\ln(T_e)$, the natural log of *CTSP* from both sides, and then rearranging the terms yields an expression for erosional efficiency in terms of volume eroded per unit energy expenditure, V/T_e where T_e is expressed as *CTSP*:

Equation 3.43

$$\ln\left(\frac{V}{T_e}\right) = \beta_0 + \beta_1 W + \beta_2 J + \beta_3 M + [\beta_4 + \beta_5 W - 1] \ln(T_e)$$

This may be rewritten by taking the exponential of both sides for an expression of energy efficiency as a power function of *CTSP*:

Equation 3.44

$$\frac{V}{T_e} = e^{(\beta_0)} e^{(\beta_1 W + \beta_2 J + \beta_3 M)} T_e^{(\beta_4 + \beta_5 W - 1)}$$

Substituting the coefficients:

Equation 3.45

$$\ln\left(\frac{V}{T_e}\right) = -3.427 + -5.992 W + 48.189 J + 1.301 M + [-1.762 + 0.622W - 1] \ln(T_e)$$

or in exponential form:

Equation 3.46

$$\frac{V}{CTSP} = 0.325 e^{(-5.922 W + 48.189 J + 1.301 M)} T_e^{(-1.762 + 0.622 W)}$$

This model of erosional efficiency allows inferences about the impact of width, joint spacing, key block classification, and energy expenditure on erosional efficiency. The existence of a correlation between stream power expenditure and event magnitude supports the third hypothesis stated earlier, but the nature of the correlation is complex. The coefficients shows that decreases in channel width and increases in joint spacing increase overall erosional efficiency. Events classified as mass block events are 3.7 times more efficient than those classified as key block events. As expected by simple inspection of the equations, a decrease in energy expenditure per event increases overall erosional efficiency. This appears to be influenced by width, such that greater widths require greater decreases in energy expenditure to be achieved for the same erosional efficiency. Additional investigation into the influence of the different parameters may be found in Appendix C.

The important of active channel width may be understood in the context of unit stream power where, given the same total discharge, slope, and thus total stream power, the unit stream power is reduced by half when the width is increased by a factor of two. Recalling from the force analysis the concept of a threshold force necessary to mobilize the block, less net force is applied to the block at lower stream power values, resulting in longer wait times for erosion to occur as less force is available to break down side friction forces of key blocks. Observed reduction in stream power caused by increasing the channel width slightly increased the energy expenditure between events on average.

Wait time between events also was important for the erosional efficiency of the system. Longer wait times and thus higher energy expenditure per event of the same magnitude result in greater energy expenditure per block and lower erosional efficiency

as measured by the amount of erosion per unit energy expenditure. The longest wait times were for the wide flume and wide joint spacing where the unit stream power is reduced and the block size increases. In general, the wider flume had longer wait times, which was interpreted as being related to lower unit stream power and thus longer time needed to expend enough energy to loosen and mobilize blocks.

4. Conclusions

The basic research question is:

What are the characteristics of channel morphology development on jointed, resistant bedrock as a function of joint spacing, sediment discharge, and channel width?

With this basic research question in mind, the study focused on three specific hypotheses concerning jointed bedrock channels:

H1: The erosional threshold for bedrock with more widely spaced joints is higher than for more narrowly spaced joints.

H2: Erosion is discontinuous over time.

H3: A correlation exists between stream power expended on the bed and event magnitudes.

The force analysis directly addresses *H1*. The hydrostatic pressure gradient between the upstream and downstream sides of a hypothetical block at the knickpoint edge is the dominant driving force in the force balance. The frictional forces around the block resist motion. Inclusion of side frictional forces results in competing changes in driving and resisting forces as a function of block side dimensions roughly parallel to flow. As the side frictional forces become negligible, increased side length leads to increased resistance to erosion. A dimensionless critical shear stress relationship was developed and shows that aeration percentages of 3% to 30% covered the range of observed small block events (1 to 3 blocks), assuming negligible resistance along the sides of the block. Justification for assuming negligible resistance is observation that blocks with significant side resistance tend to pull surrounding blocks out to create larger magnitude events than the 1 to 3 block events. Blocks upstream were not exposed to as great a net driving force because they were protected by surrounding blocks, so the highest erosion rates would

most likely be at the knickpoint edge where the net driving forces are likely highest. The force analysis and supporting observed key block-type erosion pattern only partially supports our first hypothesis depending on the dominance of side friction forces versus base friction. While side friction forces between blocks dominate the resistance to motion, increasing the length of the block side parallel to the flow may decrease the erosional threshold, an effect opposite of *H1*. As the base friction force becomes dominant and the side frictional forces negligible, increased side length increases the erosional threshold, which supports *H1*. A transitional stage exists between the states with dominant side friction and dominant base friction, with competing effects from increased side length on the erosional threshold between the two friction sources.

Observed kinematics of block erosion showed the upstream discontinuous migration of the knickpoint over time was the dominant erosional process and morphological feature, enhanced by minor erosional features upstream such as quasi-potholes via quarrying of one or two blocks. These results support hypothesis *H2*. Both the rate of erosion and the rate of upstream migration are characterized by periods of low erosion rates and migration punctuated by rapid rates of erosion over very short time periods (less than a minute) and the knickpoint rapidly migrating upstream a short distance. This pattern of morphological change supports the second hypothesis. The kinematics of block erosion and the statistical model showed a relationship between key block events, classified as events with removal of one to three blocks, which formed a visually distinctive population, with a second population of greater magnitude events. These key block events required greater energy expenditure to occur, hence longer time intervals after which larger magnitude events shortly occur. The force analysis shows

removal of side friction forces reduces the erosional threshold until only the base friction is included to increase the likelihood of block removal. Cascading erosion of adjoining blocks in the transverse direction after removal of the key block creates the larger magnitude events observed.

The force analysis provides a theoretical force threshold for block mobilization necessary for a given block morphology. If the threshold is not reached then the block may not be quarried. Abrasion may occur at discharges below the threshold on bedrock surfaces exposed to the impact of grains being transported by the flow. In this case, abrasion will become the dominant process of channel erosion. A transitional discharge regime above the threshold may exist for block mobilization where the contribution from block quarrying and abrasion to total erosion would vary with block morphology, discharge, and sediment transport. Increased dominance of abrasion would lead to more continuous erosion rates.

The existence of a correlation between energy expenditure and magnitude of events hypothesized in *H3* is supported by statistical analysis of the experimental results but is not always a simple linear relationship. Models of the probability of event occurrence and event magnitude were combined to model the erosional efficiency, expressed as the amount of erosion per unit energy expenditure. The parameters in the final model were active channel width, joint spacing, type of event, and cumulative total stream power. Building on the measured block erosion kinematics and the estimated stream power expenditure between events, the statistical model presented here delineates a definitive relationship between joint spacing, channel width, event magnitude (key blocks and large magnitude events), and energy expenditure as expressed by expended

stream power. Key block events, classified as events with removal of one to three blocks, formed a visually distinctive population, with a second population of greater magnitude events. These key block events required greater energy expenditure to occur, especially per block. If most of the energy expended between events is expended during events that cause the removal of blocks, then the analysis suggests that key blocks require large energy expenditures per unit volume removed. The subsequent larger magnitude events require much less energy expenditure per unit volume because the removal of the key block reduces the erosional threshold of the adjoining blocks. Increasing the stream power may reduce the energy expenditures per unit volume for both types of events, as observed in the developed statistical model of erosion.

The joint spacing and associated block size were also key factors in determining erosional efficiency. After removing key blocks, both large and small blocks were readily mobilized as larger magnitude events. The increased volume of the larger blocks led to a higher erosional efficiency for large blocks than for the small blocks under the same hydraulic conditions despite likely higher threshold for erosion of the larger blocks once the side forces were removed. Note that this is only for blocks along the knickpoint edge. Quasi-potholes occurred more often in small block configurations than in large block configurations but were not numerous in any run, supporting the observation that erosion most often occurs at the knickpoint where the contributing driving forces from pressure gradients and bed shear stress are highest. The force balance indicates the three-dimensional joint pattern controls the potential for vertical plucking of blocks when flow is parallel to the top surface of the block, which in the runs was not often above the threshold. One exception is occasionally-observed lengthening of the knickpoint, which

forced the flow to impinge near-vertically on a lower layer immediately downstream and promoted plucking of lower-layer blocks because hydraulic pressure forces are in the near-vertical direction.

Overall, stream power expenditure, key blocks, and joint spacing were the most significant controls on the rate of erosion of the experimental jointed bedrock channel through block removal. Changes in morphology occurred primarily by knickpoint retreat in the horizontal direction rather than vertical plucking. Block geometry determined by joint spacing plays an important role in determining the driving and resisting forces. The combined effect of joint spacing on the force balance and block volume influences the erosional efficiency as measured by the amount of erosion per unit energy expenditure. The role of key blocks that require high energy expenditure for their removal was also a major control on the erosional dynamics of the bedrock channel. Key blocks are not determined by average joint spacing but by variability in jointing characteristics including spacing, direction, continuity, and roughness. Key blocks are hypothesized to be the cause of the mass failure kinematics seen in the flume runs.

5. Application to Anabranching Bedrock Channels

Insights from the flume experiment developed some intriguing relationships applicable to anabranching channels. Within anabranching channels there are sub-channels which theoretically have a higher unit stream power than shallower flow between channels or the average unit stream power over the entire active channel width. As postulated earlier, these sub-channels may form by preferential erosion along joint weaknesses, but the force analysis and statistical analysis of the flume results suggest that the relationship between preferential erosion and joint weaknesses is not always straightforward. Although no distinctly anabranching channels formed during any experimental runs, relationships developed from the force and statistical analyses may be applied to hypotheses concerning anabranching channels. It is important to note that comparisons between channel forms and joint spacing here assume similar hydraulic histories (e.g., stream power expenditure).

The resulting models from the statistical analysis suggest that more widely spaced vertical joints form blocks that erode at a higher volume per unit stream power than narrower joint spacing when assuming the same horizontal joint spacing (i.e., block height). More widely spaced joints form wider blocks which, when eroded from the channel, leave wider channels that have lower unit stream power than those resulting from removal of smaller blocks from narrower joint spacing. The narrower channels in narrow joint spacing focus flow energy with resulting high stream power. This may encourage incision of a narrower joint spacing, leaving wider blocks as islands where wider blocks without side friction forces have a higher erosional threshold than smaller blocks without side friction forces. If for a given area the narrower joint spacing is

concentrated in one area or sufficiently narrow and uniform over an area, flow may be preferentially concentrated in the initially channelized area. This initially channelized area may erode quickly enough that only a single dominant channel forms between the majority of stationary blocks which, as the channel incises, have decreasing frequency of exposure to flows and thus lower stream power exerted against them. The statistical analysis suggests that higher unit stream power leads to higher erosion; thus, preferentially amplifying unit stream power within the inner channel will amplify erosion of the inner channel compared to surrounding areas. Key block characteristics of the arch-like failure of blocks at the knickpoint edge also suggest that sufficient variability in block erodibility may be necessary for anabranching channels to form. Variations in vertical joint spacing do not necessarily give rise to an anabranching channel because no anabranching channels formed during this study in Run C or Run F, which both had variation in vertical joint spacing. Sufficient variation of joint spacing and balance between erosion rates between sub-channels is necessary for an anabranching channel to exist instead of incision of a single dominant channel.

Block erodibility is controlled not only by jointing characteristics, but also by factors influencing hydraulic forces such as active channel width. The statistical analyses suggest active channel width was an important factor. Restriction on the active channel width such as by landslides or overall valley width may sufficiently increase unit stream power such that an inner channel forms, whereas for a wider active channel and floodplain an anabranching channel may form for the same joint spacing. This may be pertinent for the experimental runs, where no anabranching channels formed. Sufficient exposure of bedrock in the channel and floodplain relative to block spacing may be

necessary in addition to variation in joint spacing for anabranching channels to develop.

This flume study was done as part of a project that included field measurements of joint spacing for several bedrock channel reaches along the Orange River in South Africa where the morphology varied from inner channel and outer bedrock strath to wide anabranching bedrock channel. Data consisted of joint spacing measurements at selected areas along exposed bedrock channel(s) and a qualitative description of the reach site. From these descriptions each site is classified as anabranching (*A*), inner channel with an outer bedrock strath (*S*), or a transition area with characteristics of both (*AS*). Table 5.1 presents descriptive statistics for the field samples. Although there is a great deal of variation in the joint spacing data, with coefficient of variation greater than 1, a comparison of the means suggests the anabranching channels have a slightly greater joint spacing than the inner channel reaches.

Table 5.1 Descriptive Statistics for Joint Spacing by Channel Type - Orange River, South Africa

Channel Type	A	AS	S
Mean Joint Spacing (m)	0.65	0.54	0.55
Std. Dev.	1.53	1.86	0.94
Max	30.95	30.95	10.12
Min	0.01	0.01	0.01
Total Joint Count	1574	872	375
Coeff. Of Variation	2.38	3.46	1.70

The inner channel reaches have a lower overall variation in joint spacing than the anabranching channels, whereas the highest variation is for the transition channels. Also note that the maximum joint spacing for the anabranching channels is greater than any of the inner channels by a factor of ~3.

Assuming similar hydraulic histories between the channel reaches in the field data (e.g., stream power expenditure), the differences in the joint spacing statistics (mean and standard deviation) between channel types is consistent with the previous discussion asserting that narrow joint spacing may lead to a incised dominant main channel while anabranching channels would be found in areas with both a higher mean joint spacing and greater variation. The differences in variation of joint spacing between channel types, however, are much more significant than mean joint spacing. Variation in joint spacing may be a dominant control on the bedrock channel type based both on the field data and application of the experimental results.

The reaches classified as transitional between anabranching and inner channel (AS) showed a mean joint spacing very similar to the anabranching channel data but had the highest variation in joint spacing, suggesting mixing of larger joint spacing and narrower joint spacing similar qualitatively to Run C. In Run C, the presence of irregular joint spacing did correlate with the development of some depressions upstream of the knickpoint face which were defined as quasi-potholes, but no distinct pool-riffle morphology was formed. The higher variation but fairly similar mean joint spacing may indicate a greater imbalance between incision rates among subchannels, with a few subchannels in sufficiently narrower joint spacing having much higher incision rates. As discussed earlier, a balance between erosion of subchannels needs to exist for the anabranching channel to be present instead of an incised channel. The AS channels are transitioning to inner channel morphology where the few subchannels will form the inner channel, possibly leaving relic subchannels and islands on the bedrock strath.

Overall, the field data are consistent with the role of joint spacing in the development of anabranching channels developed from the force and statistical analyses of the flume study results. The strongest difference between channel types in the field data is variation of joint spacing. Less variable and narrower joint spacing is found in inner channel reaches, more variable and wider joint spacing in anabranching reaches, and transitional reaches with aspects of an inner channel and anabranching channels at higher flows correlate with a wider variation in joint spacing that encompasses values found in inner channel and anabranching reaches. Anabranching channels may persist as long as there is sufficient balance between erosion rates of the subchannels in the bedrock channel surface. However, changes to the system may induce preferential erosion of one or a few subchannels, reduce expenditure to other subchannels by dominating flow conveyance, and eventually transitioning from an anabranching to inner channel morphology. Changes to the system include a diminished flood regime, or passing of a knickpoint which may be associated with falling base level. A given set of joint conditions or a given flow regime may not be enough to develop either anabranching or an inner channel; rather, the balance between these is the key to the development and persistence of either bedrock channel morphology.

6. Further Research in Bedrock Erosion

This study highlighted the implications and complications in estimation of rates of erosion of jointed bedrock exposed along river channels. Averages for long time intervals on the order of hundreds to thousands of years provide valuable information about bedrock channel evolution but may not accurately represent the kinematics on smaller time scales. Rates measured on the temporal scale of the length of time between quarrying events will likely be more highly variable than averages over longer time intervals and better capture high variability in the timing of events.

The many possibilities for future research and potential for future flume studies include refined direct force measurements and integrating engineering rock mechanics and rock mass strength theories into models of bedrock erosion. New techniques for mapping joint pattern using ground-scanning LiDAR may be used to develop a detailed dataset of bedrock channel characteristics in three dimensions and use of such a map as the prototype in physical and numerical models. Linking processes and measured erosion across greater spatial and temporal scales will provide a better quantitative model of erosion of bedrock channels and greater understanding of how contemporary channel morphologies developed.

7. References

- Annandale, G.W. 2006. Scour Technology. McGraw-Hill. 430 pp.
- Ahnert, F. 1994. Equilibrium, scale, and inheritance in geomorphology. *Geomorphology*. 11. 125-140.
- Bagnold, R.A. 1960. Sediment discharge and stream power – a preliminary announcement. USGS Circular 421.
- Bagnold, R.A. 1966. An approach to the sediment transport problem from general physics. USGS Professional Paper 422-1.
- Baker, V. 1973. Paleohydrology and Sedimentology of Lake Missoula flooding in eastern Washington. Geological Society of America. Special Paper 144. 79 pp.
- Baker, V. R. 1978. Large-scale erosional and depositional features of the Channeled Scabland. In, V.R. Baker and D Nummedal, eds., *The Channeled Scabland*. NASA. Washington D.C., 81-116.
- Baker, V.R. and Pickup, G. 1987. Flood geomorphology of the Katherine Gorge, Northern Territory, Australia. *Geological Society of America Bulletin*. 98. 635-646.
- Bretz, J.H. 1924. The Dalles type of river channel. *Journal of Geology*. 32. 139-149.
- Burbank, D.W., Leland, J., Fielding E., Anderson, R.S., Brozovic, N., Reid, M.R., and Duncan, C. 1996. Bedrock incision, rock uplift, and threshold hillslopes in the northwestern Himalayas. *Nature*. 379. 505-510.
- Carling, P. and Tinkler, K. 1998. Conditions for the entrainment of cuboid boulders in bedrock streams: an historical review of literature with respect to recent investigations. In, Tinkler and E.E. Wohl, eds., *Rivers over Rock: Fluvial Processes in Bedrock Channels*. AGU Geophysical Monograph 107. 19-34.
- Davis, G.H. and Reynolds, S.J. 1996. *Structural geology of rocks and regions*. John Wiley and Sons, New York. 800p.
- Goodman, R.E., 1995. Block theory and its application. *Geotechnique*. 45. 3. 383-423.
- Goodman, R.E. and Shi, G.H., 1985. *Block theory and its application to rock engineering*. Prentice-Hall, Englewood Cliffs, NJ.
- Graf, W.L. 1977. The rate law in fluvial geomorphology. *American Journal of Science*. 277. 178-191.

Graf, W.L. 1983. Downstream changes in stream power in the Henry Mountains, Utah. *Annals of the Association of American Geographers*. 73. 3. 373-387.

Grant, G.E. 1997. Critical flow constrains flow hydraulics in mobile-bed streams: A new hypothesis. *Water Resources Research*. 33. 349-358.

Gupta, A., Kale, V.S., and Rajaguru, S.N. 1999. The Narmada River, India, through space and time. In. A.J. Miller and A. Gupta, eds., *Varieties of fluvial forms*. Wiley, New York. 113-143.

Hancock, G.S., Anderson, R.S., and Whipple, K.X. 1998. Beyond Power: Bedrock River Incision Process and Form. In, Tinkler and E.E. Wohl, eds., *Rivers over Rock: Fluvial Processes in Bedrock Channels*. AGU Geophysical Monograph 107. 35-60.

Hayakawa, Y. and Matsukura, Y. 2003. Recession rates of waterfalls in Boso Peninsula, Japan, and a predictive equation. *Earth Surf. Process. Landforms* 28. 675-684.

Heritage, G.L., Van Niekerk, A.W., and Moon, B.P. 1999. Geomorphology of the Sabie River, South Africa: an incised bedrock-influenced channel. In. A.J. Miller and A. Gupta, eds., *Varieties of fluvial forms*. Wiley, New York. 113-143.

Holland, W.N., and Pickup, G. 1976. Flume study of knickpoint development in stratified sediment. *Geological Society of America Bulletin*. 87. 76-82.

Kale, V.S., Baker, V.R., and Mishra, S. 1996. Multi-channel patterns of bedrock rivers: an example from the central Narmada basin, India. *Catena*. 26. 85-98.

Kale, V.S. and Shingade, B.S. 1987. A morphological study of potholes of Indrayani Knickpoint (Maharashtra). In. Datya, V.S., et al., eds. *Explorations in the tropics.: Prune, India*, Professor K.R. Dikshit Felicitation Committee , Professor K.R. Dikshit Felicitation Volume. 206-214.

Klassen, G.J., Mosselman, R.E., Masekik, G., Bruhl, H., Huisink, M., Kooman, E., and Seymoursbergen, A.C. 1993. Plan for changes in large braided sand-bed rivers. Delft Hydraulics Publications No. 444, December.

Miller, J.R. 1991. The influence of bedrock geology on knickpoint development and channel-bed degradation along downcutting streams in south-central Indiana. *J. Geology*. 99. 591-605.

Montgomery, D.R. and Gran, K.B. 2001. Downstream variations in the width of bedrock channels. *Water Resources Research*. 37. 1841-1846.

Nelson, J., Shreve, R.L., McLean, S.R., and Drake, T.G. 1995. Role of near-bed turbulence structure in bed load transport and bed form mechanics. *Water Resources Research*. 31. 8. 2071-2086.

- Papanicolaou, A.N., Diplas, P., Dancy, C.L., and Balakrishnan, M. 2001. Surface roughness effects in near-bed turbulence: implications to sediment transport. *Journal of Engineering Mechanics*. 127. 3. 211-218.
- Rhoads, B.L. 1987. Stream power terminology. *Professional Geographer*. 39. 2. 189-195.
- Seidl, M.A. and Dietrich, W.E. 1992. The problem of channel erosion into bedrock. In. K.H. Schmidt and J. de Ploey, eds., *Functional Geomorphology*. Catena Supplement 23. 101-124.
- Sklar, L.S. and Dietrich, W.E. 2001. Sediment and rock strength controls on river incision into bedrock. *Geology* 29. 1087-1090.
- S-Plus 7.0 Guide to Statistics, Volumes I & II. 2005. Insightful Corporation, Seattle, WA.
- Springer, G.S. 2002. Profile maintenance in bedrock streams incising soluble strata. Unpublished PhD. Dissertation, Colorado State University, Ft. Collins.
- Springer, G.S. and Wohl, E.E. 2002. Empirical and theoretical investigations of sculpted forms in Buckeye Creek Cave, West Virginia. *Journal of Geology*. 110. 469-481.
- SPSS Base 15.0 User's Guide. 2006. SPSS Inc., Chicago, IL.
- Stock, G.S. and Montgomery, D.R. 1999. Geologic constraints on bedrock river incision using the stream power law. *Journal of Geophysical Research*. 104B. 4983-4993.
- Thompson, D. and Wohl, E. 1998. Flume experimentation and simulation of bedrock channel processes. In, Tinkler and E.E. Wohl, eds., *Rivers over Rock: Fluvial Processes in Bedrock Channels*. AGU Geophysical Monograph 107. 279-296.
- Tinkler, K.J. 1997a. Critical flow in rockbed streams with estimated values for Manning's n. *Geomorphology*. 20. 147-164.
- Tinkler, K.J. 1997b. Indirect velocity measurement from standing waves in rockbed streams. *Journal of Hydraulic Engineering*. 123. 918-921.
- Tinkler, K.J. and Wohl, E. 1998. A primer on bedrock channels. In, Tinkler and E.E. Wohl, eds., *Rivers over Rock: Fluvial Processes in Bedrock Channels*. AGU Geophysical Monograph 107. 279-296.
- Toombes, L. and Chanson, H. 2008. Flow patterns in nappe flow regime down low gradient stepped chutes. *Journal of Hydraulic Research*. 46. 1. 4-14.
- Tooth, S. and McCarthy, T.S. 2004. Anabranching in mixed bedrock-alluvial rivers: the example of the Orange River above Augrabies Falls, Northern Cape Province, South Africa. *Geomorphology*. 57. 235-262.

Van Niekerk, A.W., Heritage, G.L., and Moon, B.P. 1995. River classification from management: the geomorphology of the Sabie River in eastern Transvaal. *South African Geographical Journal*. 77. 68-76.

Van Niekerk, A.W., Heritage, G.L., Broadhurst, J.L., and Moon, B.P. 1999. Bedrock anastomosing channel systems: morphology and dynamics in the Sabie River, Mpumalanga Province, South Africa. In, A.J. Miller and A. Gupta, eds., *Varieties of fluvial forms*. Wiley, New York. 33-51.

Warburton, P.M. 1987. Implications on keystone action for rock bolt support and block theory. *International Journal of Rock Mechanics and Mineral Science*. 24 283-290.

Wende, R. 1999. Boulder bedforms in jointed-bedrock channels. In, A.J. Miller and A. Gupta, eds., *Varieties of fluvial forms*. Wiley, New York. 189-216.

Whipple, K.X., Snyder, N.P., and Dollenmayer, K. 2000a. Rates and processes of bedrock incision by the Upper Ukak River since the 1912 Novarupta ash flow in the Valley of Ten Thousand Smokes, Alaska. *Geology*. 28. 9. 835-838.

Whipple, K.X., Hancock, G.S., and Anderson, R.S. 2000b. River incision into bedrock: mechanics and relative efficiency of plucking, abrasion, and cavitation. *Geological Society of America Bulletin*. 112. 490-503.

Wilcox, D.C. 2000. *Basic Fluid Mechanics*. DCW Industries. La Canada, CA. 786 p.

Wohl, E.E. 1993. Bedrock channel incision along Piccaninny Creek, Australia. *J. Geology*. 101. 749-761.

Wohl, E.E. 1998. Bedrock channel morphology in relation to erosional processes. In, Tinkler and E.E. Wohl, eds., *Rivers over Rock: Fluvial Processes in Bedrock Channels*. AGU Geophysical Monograph 107. 133-152.

Wohl, E.E. 2000. Substrate influences on step-pool sequences in the Christopher Creek drainage, Arizona. *J. Geology*. 108. 121-129.

Wohl, E.E., Greenbaum, N., Schick, A.P., and Baker, V.R. 1994. Controls on bedrock channel incision along Nahal Paran, Israel. *Earth Surface Processes and Landforms*. 19. 1-13.

Wohl E.E. and Merritt, D.M. 2001. Bedrock channel morphology. *GSA Bulletin* 113. 1205-1212.

Appendix A Flume Data

Table A.1 Event Data for Run A

Run	Run Time (hrs)	Nominal Discharge (m ³ /s)	Channel Width (m)	Joint Spacing (m)	Block Type	Movement Type	Event Block Count	Event Volume (m ³)	CUSP	CTSP	Time Lapse Since Last Event (hrs)
A	2.00	0.2	0.61	0.03	A	m	158	0.004266	420	396	2.00
A	7.50	0.2	0.61	0.03	A	m	97	0.002619	1156	1090	5.50
A	13.00	0.2	0.61	0.03	A	m	163	0.004401	1156	1090	5.50
A	14.00	0.2	0.61	0.03	A	m	230	0.006210	210	198	1.00
A	14.75	0.2	0.61	0.03	A	m	374	0.010098	158	149	0.75
A	16.25	0.2	0.61	0.03	A	m	223	0.006021	315	297	1.50
A	17.50	0.2	0.61	0.03	A	m	68	0.001836	263	248	1.25
A	18.50	0.2	0.61	0.03	A	m	72	0.001944	210	198	1.00
A	19.50	0.2	0.61	0.03	A	m	47	0.001269	210	198	1.00
A	20.50	0.2	0.61	0.03	A	m	24	0.000648	210	198	1.00
A	22.22	0.2	0.61	0.03	A	m	50	0.001350	361	340	1.72
A	23.80	0.2	0.61	0.03	A	m	83	0.002241	333	314	1.58
A	25.80	0.2	0.61	0.03	A	m	19	0.000513	420	396	2.00
A	26.80	0.2	0.61	0.03	A	k	3	0.000081	210	198	1.00
A	28.05	0.2	0.61	0.03	A	m	17	0.000459	263	248	1.25
A	29.55	0.2	0.61	0.03	A	m	42	0.001134	315	297	1.50
A	32.55	0.2	0.61	0.03	A	k	1	0.000027	631	594	3.00
A	33.55	0.2	0.61	0.03	A	m	44	0.001188	210	198	1.00
A	34.55	0.2	0.61	0.03	A	m	113	0.003051	210	198	1.00
A	35.05	0.2	0.61	0.03	A	m	40	0.001080	105	99	0.50
A	36.05	0.2	0.61	0.03	A	m	9	0.000243	210	198	1.00
A	37.88	0.2	0.61	0.03	A	k	1	0.000027	385	363	1.83
A	39.88	0.2	0.61	0.03	A	k	3	0.000081	420	396	2.00
A	40.47	0.2	0.61	0.03	A	m	378	0.010206	123	116	0.58
A	43.30	0.2	0.61	0.03	A	m	115	0.003105	596	561	2.83

Table A.1 Cont.

A	45.05	0.2	0.61	0.03	A	m	28	0.000756	368	347	1.75
A	46.55	0.2	0.61	0.03	A	m	116	0.003132	315	297	1.50
A	50.55	0.2	0.61	0.03	A	m	26	0.000702	841	792	4.00
A	51.63	0.2	0.61	0.03	A	m	105	0.002835	228	215	1.08
A	52.13	0.2	0.61	0.03	A	m	458	0.012366	105	99	0.50
A	56.35	0.2	0.61	0.03	A	m	154	0.004158	886	835	4.22
A	57.18	0.2	0.61	0.03	A	m	326	0.008802	175	165	0.83
A	57.85	0.2	0.61	0.03	A	m	210	0.005670	140	132	0.67
A	58.60	0.2	0.61	0.03	A	m	118	0.003186	158	149	0.75
A	58.85	0.2	0.61	0.03	A	m	50	0.001350	53	50	0.25
A	61.35	0.2	0.61	0.03	A	m	77	0.002079	526	495	2.50
A	64.10	0.2	0.61	0.03	A	m	108	0.002916	578	545	2.75
A	67.60	0.2	0.61	0.03	A	m	23	0.000621	736	693	3.50
A	69.70	0.2	0.61	0.03	A	m	62	0.001674	441	416	2.10
A	69.80	0.2	0.61	0.03	A	m	150	0.004050	21	20	0.10
A	70.72	0.2	0.61	0.03	A	m	18	0.000486	193	182	0.92
A	76.72	0.2	0.61	0.03	A	m	6	0.000162	1261	1189	6.00
A	81.40	0.2	0.61	0.03	A	m	9	0.000243	985	928	4.68

Table A.2 Event Data for Run B

Run	Run Time (hrs)	Nominal Discharge (m ³ /s)	Channel Width (m)	Joint Spacing (m)	Block Type	Movement Type	Event Block Count	Event Volume (m ³)	CUSP	CTSP	Time Lapse Since Last Event (hrs)
B	1.50	0.11	0.61	0.06	B	m	253	0.027324	196	172	1.50
B	3.33	0.11	0.61	0.06	B	m	127	0.013716	239	210	1.83
B	6.83	0.11	0.61	0.06	B	m	137	0.014796	457	402	3.50
B	9.08	0.11	0.61	0.06	B	m	277	0.029916	294	259	2.25
B	12.18	0.11	0.61	0.06	B	m	37	0.003996	405	356	3.10
B	13.51	0.11	0.61	0.06	B	m	61	0.006588	174	153	1.33
B	19.51	0.11	0.61	0.06	B	m	75	0.008100	784	689	6.00
B	22.93	0.11	0.61	0.06	B	m	53	0.005724	447	393	3.42
B	25.68	0.11	0.61	0.06	B	m	112	0.012096	359	316	2.75
B	27.93	0.11	0.61	0.06	B	m	26	0.002808	294	259	2.25
B	29.93	0.11	0.61	0.06	B	m	4	0.000432	261	230	2.00
B	39.10	0.11	0.61	0.06	B	m	26	0.002808	1198	1054	9.17
B	42.85	0.11	0.61	0.06	B	m	221	0.023868	490	431	3.75
B	46.35	0.11	0.61	0.06	B	m	9	0.000972	457	402	3.50
B	51.93	0.11	0.61	0.06	B	m	8	0.000864	729	641	5.58
B	55.68	0.11	0.61	0.06	B	m	22	0.002376	490	431	3.75
B	67.68	0.11	0.61	0.06	B	k	1	0.000108	1567	1379	12.00
B	75.18	0.11	0.61	0.06	B	m	5	0.000540	980	862	7.50
B	81.93	0.11	0.61	0.06	B	m	11	0.001188	987	887	6.75
B	88.93	0.2	0.61	0.06	B	m	169	0.018252	1417	1350	7.00
B	89.01	0.2	0.61	0.06	B	m	52	0.005616	17	16	0.08
B	89.10	0.2	0.61	0.06	B	m	69	0.007452	17	16	0.08
B	89.48	0.2	0.61	0.06	B	m	145	0.015660	78	74	0.38
B	90.18	0.2	0.61	0.06	B	m	6	0.000648	142	135	0.70

Table A.3 Event Data for Run C

Run	Run Time (hrs)	Nominal Discharge (m ³ /s)	Channel Width (m)	Joint Spacing (m)	Block Type	Movement Type	Event Block Count	Event Volume (m ³)	CUSP	CTSP	Time Lapse Since Last Event (hrs)
C	1	0.11	0.61	0.03 & 0.06	A	m	112	0.003024	195	195	1.00
		0.11	0.61	0.03 & 0.06	B	m	91	0.009828			
C	6	0.11	0.61	0.03 & 0.06	A	m	66	0.001782	596	977	5.00
		0.11	0.61	0.03 & 0.06	B	m	42	0.004536			
C	7	0.11	0.61	0.03 & 0.06	B	m	18	0.001944	119	195	1.00
C	13	0.11	0.61	0.03 & 0.06	A	m	101	0.002727	1368	1368	6.00
		0.11	0.61	0.03 & 0.06	B	m	35	0.003780			
C	16	0.11	0.61	0.03 & 0.06	A	m	4	0.000108	358	586	3.00
		0.11	0.61	0.03 & 0.06	B	k	2	0.000216			
C	23	0.11	0.61	0.03 & 0.06	A	k	2	0.000054	835	1368	7.00
		0.11	0.61	0.03 & 0.06	B	m	7	0.000756			
C	24	0.11	0.61	0.03 & 0.06	A	k	1	0.000027	119	195	1.00
		0.11	0.61	0.03 & 0.06	B	k	3	0.000324			
C	26	0.11	0.61	0.03 & 0.06	A	m	24	0.000648	238	391	2.00
		0.11	0.61	0.03 & 0.06	B	m	5	0.000540			
C	33	0.11	0.61	0.03 & 0.06	A	m	15	0.000405	835	1368	7.00
		0.11	0.61	0.03 & 0.06	B	m	45	0.004860			
C	40	0.11	0.61	0.03 & 0.06	A	m	32	0.000864	835	1368	7.00
		0.11	0.61	0.03 & 0.06	B	m	26	0.002808			
C	44	0.11	0.61	0.03 & 0.06	A	m	11	0.000297	477	782	4.00
		0.11	0.61	0.03 & 0.06	B	k	1	0.000108			
C	45	0.11	0.61	0.03 & 0.06	A	k	1	0.000027	195	195	1.00
C	46	0.11	0.61	0.03 & 0.06	A	k	1	0.000027	195	195	1.00
		0.11	0.61	0.03 & 0.06	B	k	1	0.000108	391	391	

Table A.3 Cont.

C	48	0.11	0.61	0.03 & 0.06	A	k	1	0.000027	238	391	2.00
		0.11	0.61	0.03 & 0.06	B	m	20	0.002160			
C	49	0.11	0.61	0.03 & 0.06	A	m	26	0.000702	195	195	1.00
C	62	0.11	0.61	0.03 & 0.06	A	m	47	0.001269	2541	2541	13.00
		0.11	0.61	0.03 & 0.06	B	m	11	0.001188	2737	2737	
C	63	0.11	0.61	0.03 & 0.06	A	m	6	0.000162	119	195	1.00
		0.11	0.61	0.03 & 0.06	B	k	2	0.000216			
C	64	0.11	0.61	0.03 & 0.06	A	k	3	0.000081	119	195	1.00
		0.11	0.61	0.03 & 0.06	B	m	6	0.000648			
C	67	0.11	0.61	0.03 & 0.06	A	k	2	0.000054	586	586	3.00
C	69	0.11	0.61	0.03 & 0.06	A	k	3	0.000081	238	391	2.00
C	70	0.11	0.61	0.03 & 0.06	A	m	26	0.000702	119	195	1.00
		0.11	0.61	0.03 & 0.06	B	m	23	0.002484			
C	72	0.11	0.61	0.03 & 0.06	B	m	6	0.000648	391	391	2.00
C	76	0.11	0.61	0.03 & 0.06	A	m	82	0.002214	477	782	4.00
		0.11	0.61	0.03 & 0.06	B	m	47	0.005076			
C	77	0.11	0.61	0.03 & 0.06	A	k	1	0.000027	195	195	1.00
C	88	0.2	0.61	0.03 & 0.06	B	k	1	0.000108	2433	2433	11.00
C	89	0.2	0.61	0.03 & 0.06	A	m	22	0.000594	210	344	1.00
		0.2	0.61	0.03 & 0.06	B	k	1	0.000108			
C	91	0.2	0.61	0.03 & 0.06	A	m	63	0.001701	420	689	2.00
		0.2	0.61	0.03 & 0.06	B	m	36	0.003888			
C	93	0.2	0.61	0.03 & 0.06	A	m	117	0.003159	420	689	2.00
		0.2	0.61	0.03 & 0.06	B	m	37	0.003996			
C	94	0.2	0.61	0.03 & 0.06	A	m	17	0.000459	210	344	1.00
		0.2	0.61	0.03 & 0.06	B	m	4	0.000432			
C	95	0.2	0.61	0.03 & 0.06	A	m	121	0.003267	210	344	1.00
		0.2	0.61	0.03 & 0.06	B	m	41	0.004428			

Table A.3 Cont.

C	102	0.2	0.61	0.03 & 0.06	A	m	18	0.000486	1470	2410	7.00
		0.2	0.61	0.03 & 0.06	B	m	20	0.002160			
C	108	0.2	0.61	0.03 & 0.06	A	m	20	0.000540	1260	2066	6.00
		0.2	0.61	0.03 & 0.06	B	m	33	0.003564			
C	109	0.2	0.61	0.03 & 0.06	B	m	16	0.001728	210	344	1.00
C	110	0.2	0.61	0.03 & 0.06	A	k	2	0.000054	210	344	1.00
		0.2	0.61	0.03 & 0.06	B	m	4	0.000432			
C	116	0.2	0.61	0.03 & 0.06	A	m	53	0.001431	1260	2066	6.00
		0.2	0.61	0.03 & 0.06	B	m	8	0.000864			
C	120	0.2	0.61	0.03 & 0.06	A	k	2	0.000054	840	1377	4.00

Table A.4 Event Data for Run D

Run	Run Time (hrs)	Nominal Discharge (m ³ /s)	Channel Width (m)	Joint Spacing (m)	Block Type	Movement Type	Event Block Count	Event Volume (m ³)	CUSP	CTSP	Time Lapse Since Last Event (hrs)
D	0.02	0.11	1.17	0.03	A	m	180	0.004860	1	2	0.02
D	2.00	0.11	1.17	0.03	A	k	3	0.000081	177	231	1.98
D	2.02	0.11	1.17	0.03	A	m	11	0.000297	1	2	0.02
D	4.52	0.11	1.17	0.03	A	k	1	0.000027	223	292	2.50
D	7.02	0.11	1.17	0.03	A	k	3	0.000081	223	292	2.50
D	8.63	0.11	1.17	0.03	A	m	4	0.000108	144	189	1.62
D	11.50	0.11	1.17	0.03	A	k	1	0.000027	256	334	2.87
D	11.52	0.11	1.17	0.03	A	k	1	0.000027	1	2	0.02
D	14.02	0.11	1.17	0.03	A	k	1	0.000027	223	292	2.50
D	17.95	0.11	1.17	0.03	A	k	1	0.000027	351	459	3.93
D	18.65	0.11	1.17	0.03	A	m	53	0.001431	62	82	0.70
D	18.70	0.11	1.17	0.03	A	m	5	0.000135	4	6	0.05
D	18.87	0.11	1.17	0.03	A	m	6	0.000162	15	19	0.17
D	21.62	0.11	1.17	0.03	A	m	30	0.000810	245	321	2.75
D	22.00	0.11	1.17	0.03	A	m	9	0.000243	34	45	0.38
D	22.35	0.11	1.17	0.03	A	k	1	0.000027	31	41	0.35
D	32.50	0.11	1.17	0.03	A	k	1	0.000027	917	1201	10.15
D	32.52	0.11	1.17	0.03	A	k	1	0.000027	3	4	0.02
D	34.25	0.2	1.17	0.03	A	k	1	0.000027	268	354	1.73
D	36.52	0.2	1.17	0.03	A	m	18	0.000486	351	465	2.27
D	39.00	0.2	1.17	0.03	A	k	1	0.000027	384	508	2.48
D	40.50	0.2	1.17	0.03	A	m	7	0.000189	232	307	1.50
D	44.00	0.2	1.17	0.03	A	k	2	0.000054	541	717	3.50
D	44.02	0.2	1.17	0.03	A	m	16	0.000432	3	4	0.02

Table A.4 Cont.

D	44.37	0.2	1.17	0.03	A	k	1	0.000027	54	71	0.35
D	44.80	0.2	1.17	0.03	A	m	4	0.000108	67	89	0.43
D	46.20	0.2	1.17	0.03	A	k	1	0.000027	217	287	1.40
D	49.50	0.2	1.17	0.03	A	m	5	0.000135	510	676	3.30
D	49.52	0.2	1.17	0.03	A	m	70	0.001890	3	3	0.02
D	50.35	0.2	1.17	0.03	A	k	1	0.000027	129	171	0.83
D	51.45	0.2	1.17	0.03	A	k	2	0.000054	170	225	1.10
D	53.00	0.2	1.17	0.03	A	k	1	0.000027	240	317	1.55
D	53.02	0.2	1.17	0.03	A	m	4	0.000108	3	4	0.02
D	54.13	0.2	1.17	0.03	A	k	2	0.000054	172	228	1.11
D	56.65	0.2	1.17	0.03	A	k	1	0.000027	389	515	2.52
D	56.92	0.2	1.17	0.03	A	m	5	0.000135	42	55	0.27
D	61.00	0.2	1.17	0.03	A	k	1	0.000027	631	835	4.08
D	64.35	0.2	1.17	0.03	A	m	9	0.000243	518	686	3.35
D	64.45	0.2	1.17	0.03	A	k	2	0.000054	15	20	0.10
D	65.25	0.2	1.17	0.03	A	m	109	0.002943	124	164	0.80
D	66.92	0.2	1.17	0.03	A	k	3	0.000081	258	341	1.67
D	68.93	0.2	1.17	0.03	A	m	8	0.000216	312	413	2.02
D	69.02	0.2	1.17	0.03	A	m	12	0.000324	13	18	0.09
D	69.32	0.2	1.17	0.03	A	m	24	0.000648	46	61	0.30
D	72.52	0.2	1.17	0.03	A	k	1	0.000027	495	656	3.20
D	74.40	0.2	1.17	0.03	A	m	39	0.001053	291	385	1.88
D	74.88	0.2	1.17	0.03	A	k	1	0.000027	75	99	0.48
D	80.52	0.2	1.17	0.03	A	m	9	0.000243	872	1154	5.64
D	80.67	0.2	1.17	0.03	A	k	2	0.000054	23	30	0.15
D	84.52	0.2	1.17	0.03	A	k	1	0.000027	596	789	3.85
D	85.15	0.2	1.17	0.03	A	m	9	0.000243	97	129	0.63
D	85.65	0.2	1.17	0.03	A	k	1	0.000027	77	102	0.50
D	91.43	0.2	1.17	0.03	A	m	7	0.000189	894	1184	5.78

Table A.4 Cont.

D	91.97	0.2	1.17	0.03	A	k	1	0.000027	82	109	0.53
D	96.54	0.2	1.17	0.03	A	m	7	0.000189	707	936	4.57
D	96.82	0.2	1.17	0.03	A	k	1	0.000027	43	57	0.28
D	96.97	0.2	1.17	0.03	A	m	4	0.000108	23	31	0.15
D	97.50	0.2	1.17	0.03	A	k	1	0.000027	82	109	0.53
D	97.55	0.2	1.17	0.03	A	k	1	0.000027	8	10	0.05
D	97.75	0.2	1.17	0.03	A	k	1	0.000027	31	41	0.20
D	100.00	0.2	1.17	0.03	A	k	1	0.000027	348	461	2.25

Table A.5 Event Data for Run E

Run	Run Time (hrs)	Nominal Discharge (m ³ /s)	Channel Width (m)	Joint Spacing (m)	Block Type	Movement Type	Event Block Count	Event Volume (m ³)	CUSP	CTSP	Time Lapse Since Last Event (hrs)
E	0.03	0.11	1.17	0.06	B	m	122	0.013176	3	4	0.03
E	1.35	0.2	1.17	0.06	B	m	33	0.003564	139	184	1.32
E	2.48	0.2	1.17	0.06	B	m	20	0.002160	171	231	1.13
E	2.60	0.2	1.17	0.06	B	m	15	0.001620	18	24	0.12
E	4.53	0.2	1.17	0.06	B	k	1	0.000108	291	394	1.93
E	4.65	0.2	1.17	0.06	B	k	1	0.000108	18	24	0.12
E	5.23	0.2	1.17	0.06	B	m	16	0.001728	88	119	0.58
E	5.32	0.2	1.17	0.06	B	k	1	0.000108	13	17	0.08
E	5.75	0.2	1.17	0.06	B	m	21	0.002268	65	88	0.43
E	6.57	0.2	1.17	0.06	B	k	1	0.000108	123	166	0.82
E	10.33	0.2	1.17	0.06	B	k	1	0.000108	568	768	3.77
E	11.43	0.2	1.17	0.06	B	m	6	0.000648	166	224	1.10
E	11.88	0.2	1.17	0.06	B	k	1	0.000108	68	92	0.45
E	11.95	0.2	1.17	0.06	B	k	3	0.000324	10	14	0.07
E	19.17	0.2	1.17	0.06	B	m	20	0.002160	1087	1471	7.22
E	20.00	0.2	1.17	0.06	B	k	3	0.000324	126	170	0.83
E	20.28	0.2	1.17	0.06	B	m	122	0.013176	43	58	0.28
E	21.07	0.2	1.17	0.06	B	k	1	0.000108	118	160	0.78
E	21.50	0.2	1.17	0.06	B	k	1	0.000108	65	88	0.43
E	21.67	0.2	1.17	0.06	B	m	17	0.001836	25	34	0.17
E	26.68	0.2	1.17	0.06	B	k	1	0.000108	756	1023	5.02
E	31.63	0.2	1.17	0.06	B	m	15	0.001620	746	1009	4.95
E	36.88	0.2	1.17	0.06	B	m	26	0.002808	791	1070	5.25
E	43.13	0.2	1.17	0.06	B	m	8	0.000864	942	1274	6.25

Table A.6 Event Data for Run G

Run	Run Time (hrs)	Nominal Discharge (m ³ /s)	Channel Width (m)	Joint Spacing (m)	Block Type	Movement Type	Event Block Count	Event Volume (m ³)	CUSP	CTSP	Time Lapse Since Last Event (hrs)
G	0.02	0.2	1.17	0.03	A	m	92	0.002484	3	3	0.02
G	0.13	0.2	1.17	0.03	A	m	12	0.000324	18	24	0.12
G	0.58	0.2	1.17	0.03	A	k	1	0.000027	69	92	0.45
G	0.90	0.2	1.17	0.03	A	k	2	0.000054	48	65	0.32
G	1.20	0.2	1.17	0.03	A	k	1	0.000027	46	61	0.30
G	5.05	0.2	1.17	0.03	A	m	9	0.000243	588	786	3.85
G	5.18	0.2	1.17	0.03	A	k	1	0.000027	20	27	0.13
G	5.27	0.2	1.17	0.03	A	k	1	0.000027	13	17	0.08
G	5.65	0.2	1.17	0.03	A	k	3	0.000081	59	78	0.38
G	6.73	0.2	1.17	0.03	A	k	2	0.000054	165	221	1.08
G	10.50	0.2	1.17	0.03	A	m	36	0.000972	575	769	3.77
G	10.93	0.2	1.17	0.03	A	k	1	0.000027	66	88	0.43
G	14.62	0.2	1.17	0.03	A	k	1	0.000027	562	752	3.68
G	15.50	0.2	1.17	0.03	A	m	4	0.000108	135	180	0.88
G	26.27	0.2	1.17	0.03	A	m	31	0.000837	1644	2198	10.77
G	26.80	0.2	1.17	0.03	A	k	2	0.000054	81	108	0.53
G	27.03	0.2	1.17	0.03	A	k	1	0.000027	36	48	0.23
G	31.42	0.2	1.17	0.03	A	m	47	0.001269	669	895	4.38
G	31.83	0.2	1.17	0.03	A	k	2	0.000054	64	85	0.42
G	35.75	0.2	1.17	0.03	A	k	2	0.000054	598	799	3.92
G	35.77	0.2	1.17	0.03	A	k	1	0.000027	3	4	0.02
G	35.92	0.2	1.17	0.03	A	k	1	0.000027	22	30	0.15
G	45.52	0.2	1.17	0.03	A	m	7	0.000189	1466	1960	9.60

Table A.7 Discharge Data for Run A

Run	Nominal Discharge (m ³ /s)	Channel Width (m)	Run Time (hrs)	Discharge (m ³ /s) from Pressure Gage	Unit Discharge (m ² /s)	Unit Stream Power (W/m ²)	CUSP	Total Stream Power (W/m)	CTSP
A	0.2	0.61	0.25	0.171	0.28	52	46	49	44
A	0.2	0.61	1.67	0.172	0.28	52	311	49	293
A	0.2	0.61	2.50	0.169	0.28	51	464	48	437
A	0.2	0.61	2.67	0.173	0.28	52	495	49	467
A	0.2	0.61	3.50	0.170	0.28	51	649	48	612
A	0.2	0.61	4.75	0.171	0.28	51	881	49	830
A	0.2	0.61	5.75	0.171	0.28	51	1066	49	1005
A	0.2	0.61	6.75	0.170	0.28	51	1252	48	1180
A	0.2	0.61	7.42	0.166	0.27	50	1372	47	1293
A	0.2	0.61	9.22	0.198	0.32	60	1758	56	1657
A	0.2	0.61	9.50	0.197	0.32	60	1819	56	1714
A	0.2	0.61	10.50	0.197	0.32	60	2033	56	1916
A	0.2	0.61	11.50	0.197	0.32	59	2247	56	2118
A	0.2	0.61	12.50	0.197	0.32	60	2462	56	2320
A	0.2	0.61	13.00	0.197	0.32	60	2569	56	2421
A	0.2	0.61	14.92	0.199	0.33	60	2984	57	2812
A	0.2	0.61	15.42	0.194	0.32	58	3089	55	2911
A	0.2	0.61	15.50	0.197	0.32	59	3107	56	2928
A	0.2	0.61	15.83	0.197	0.32	59	3178	56	2995
A	0.2	0.61	16.25	0.197	0.32	59	3267	56	3079
A	0.2	0.61	16.72	0.198	0.32	60	3368	56	3174
A	0.2	0.61	17.55	0.194	0.32	59	3544	55	3340
A	0.2	0.61	18.55	0.197	0.32	60	3758	56	3542
A	0.2	0.61	19.55	0.199	0.33	60	3974	57	3745
A	0.2	0.61	21.55	0.199	0.33	60	4407	57	4153
A	0.2	0.61	21.88	0.199	0.33	60	4479	57	4221

Table A.7 Cont.

A	0.2	0.61	22.27	0.118	0.19	39	4532	33	4267
A	0.2	0.61	22.68	0.200	0.33	60	4622	57	4352
A	0.2	0.61	23.85	0.200	0.33	60	4876	57	4591
A	0.2	0.61	24.85	0.199	0.33	60	5092	56	4794
A	0.2	0.61	25.85	0.199	0.33	60	5308	57	4998
A	0.2	0.61	26.85	0.201	0.33	61	5526	57	5204
A	0.2	0.61	28.02	0.197	0.32	60	5776	56	5439
A	0.2	0.61	28.43	0.198	0.32	60	5866	56	5524
A	0.2	0.61	29.60	0.199	0.33	60	6118	57	5762
A	0.2	0.61	30.60	0.199	0.33	60	6335	57	5965
A	0.2	0.61	31.60	0.199	0.33	60	6551	57	6169
A	0.2	0.61	32.60	0.199	0.33	60	6767	57	6373
A	0.2	0.61	33.60	0.199	0.33	60	6984	57	6577
A	0.2	0.61	34.93	0.199	0.33	60	7271	56	6848
A	0.2	0.61	35.93	0.199	0.33	60	7488	57	7052
A	0.2	0.61	36.93	0.199	0.33	60	7704	57	7256
A	0.2	0.61	37.93	0.200	0.33	60	7921	57	7461
A	0.2	0.61	38.93	0.200	0.33	60	8138	57	7665
A	0.2	0.61	39.93	0.200	0.33	60	8355	57	7870
A	0.2	0.61	40.85	0.201	0.33	61	8556	57	8058
A	0.2	0.61	41.52	0.202	0.33	61	8702	57	8196
A	0.2	0.61	43.35	0.201	0.33	61	9103	57	8574
A	0.2	0.61	46.55	0.197	0.32	60	9789	56	9220
A	0.2	0.61	47.13	0.198	0.32	60	9914	56	9339
A	0.2	0.61	48.55	0.198	0.32	60	10219	56	9626
A	0.2	0.61	49.55	0.197	0.32	60	10434	56	9828
A	0.2	0.61	50.80	0.199	0.33	60	10704	57	10083
A	0.2	0.61	51.38	0.200	0.33	60	10831	57	10202
A	0.2	0.61	53.80	0.198	0.33	60	11352	56	10693

Table A.7 Cont.

A	0.2	0.61	54.80	0.198	0.33	60	11568	56	10897
A	0.2	0.61	55.80	0.201	0.33	61	11786	57	11103
A	0.2	0.61	56.35	0.127	0.21	42	11869	36	11174
A	0.2	0.61	57.02	0.098	0.16	32	11946	28	11241
A	0.2	0.61	59.02	0.198	0.33	60	12377	56	11647
A	0.2	0.61	60.02	0.198	0.32	60	12593	56	11850
A	0.2	0.61	64.85	0.198	0.32	60	13632	56	12830
A	0.2	0.61	65.43	0.198	0.33	60	13758	56	12949
A	0.2	0.61	66.18	0.199	0.33	60	13921	57	13102
A	0.2	0.61	66.85	0.199	0.33	60	14065	57	13237
A	0.2	0.61	68.22	0.198	0.32	60	14359	56	13515
A	0.2	0.61	69.22	0.198	0.33	60	14575	56	13718
A	0.2	0.61	70.55	0.199	0.33	60	14862	56	13989
A	0.2	0.61	71.97	0.199	0.33	60	15169	57	14278
A	0.2	0.61	73.22	0.199	0.33	60	15439	57	14533
A	0.2	0.61	74.47	0.199	0.33	60	15710	57	14788
A	0.2	0.61	75.72	0.199	0.33	60	15981	57	15043
A	0.2	0.61	76.72	0.199	0.33	60	16197	57	15247
A	0.2	0.61	77.05	0.122	0.20	40	16245	35	15289
A	0.2	0.61	77.55	0.120	0.20	39	16316	34	15350
A	0.2	0.61	78.40	0.199	0.33	60	16500	57	15523
A	0.2	0.61	79.40	0.198	0.33	60	16715	56	15726
A	0.2	0.61	80.40	0.196	0.32	59	16929	56	15927
A	0.2	0.61	81.90	0.200	0.33	60	17255	57	16235
A	0.2	0.61	82.40	0.200	0.33	60	17364	57	16337
A	0.2	0.61	83.10	0.199	0.33	60	17515	57	16480
A	0.2	0.61	83.82	0.199	0.33	60	17670	57	16626
A	0.2	0.61	84.65	0.199	0.33	60	17850	56	16795
A	0.2	0.61	85.23	0.198	0.32	60	17975	56	16913

Table A.7 Cont.

A	0.2	0.61	86.23	0.199	0.33	60	18191	57	17117
A	0.2	0.61	87.23	0.199	0.33	60	18407	56	17320
A	0.2	0.61	88.65	0.199	0.33	60	18713	57	17609
A	0.2	0.61	90.15	0.199	0.33	60	19038	57	17915
A	0.2	0.61	90.90	0.199	0.33	60	19200	57	18068
A	0.2	0.61	91.55	0.198	0.32	60	19340	56	18200
A	0.2	0.61	92.22	0.198	0.32	60	19484	56	18335
A	0.2	0.61	93.52	0.198	0.33	60	19764	56	18599
A	0.2	0.61	94.52	0.200	0.33	60	19981	57	18804
A	0.2	0.61	95.52	0.199	0.33	60	20197	57	19007
A	0.2	0.61	96.52	0.199	0.33	60	20414	57	19211
A	0.2	0.61	97.52	0.199	0.33	60	20630	57	19415

Table A.8 Discharge Data for Run B

Run	Nominal Discharge (m ³ /s)	Channel Width (m)	Run Time (hrs)	Discharge (m ³ /s) from Pressure Gage	Unit Discharge (m ² /s)	Unit Stream Power (W/m ²)	CUSP	Total Stream Power (W/m)	CTSP
B	0.11	0.61	0.78	0.067	0.00	22	61	19	53
B	0.11	0.61	2.48	0.113	0.00	37	284	32	250
B	0.11	0.61	3.58	0.113	0.00	37	429	32	377
B	0.11	0.61	3.65	0.113	0.00	36	437	32	385
B	0.11	0.61	5.16	0.114	0.00	37	638	32	561
B	0.11	0.61	6.16	0.114	0.00	37	770	32	678
B	0.11	0.61	7.41	0.113	0.00	37	935	32	823
B	0.11	0.61	8.41	0.113	0.00	37	1067	32	939
B	0.11	0.61	9.91	0.113	0.00	36	1264	32	1112
B	0.11	0.61	10.91	0.111	0.00	36	1393	32	1226
B	0.11	0.61	11.91	0.112	0.00	36	1523	32	1340
B	0.11	0.61	12.76	0.117	0.00	38	1639	33	1442
B	0.11	0.61	13.68	0.114	0.00	37	1760	32	1549
B	0.11	0.61	14.34	0.114	0.00	37	1849	32	1626
B	0.11	0.61	15.34	0.114	0.00	37	1981	32	1743
B	0.11	0.61	16.34	0.114	0.00	37	2114	32	1860
B	0.11	0.61	17.34	0.113	0.00	37	2246	32	1976
B	0.11	0.61	18.34	0.113	0.00	37	2377	32	2091
B	0.11	0.61	19.34	0.112	0.00	36	2508	32	2206
B	0.11	0.61	19.93	0.112	0.00	36	2584	32	2273
B	0.11	0.61	21.01	0.112	0.00	36	2725	32	2398
B	0.11	0.61	22.01	0.112	0.00	36	2856	32	2512
B	0.11	0.61	23.18	0.112	0.00	36	3008	32	2647
B	0.11	0.61	24.18	0.113	0.00	36	3139	32	2762
B	0.11	0.61	25.43	0.113	0.00	36	3303	32	2906

Table A.8 Cont.

B	0.11	0.61	26.18	0.113	0.00	36	3402	32	2993
B	0.11	0.61	27.18	0.113	0.00	36	3533	32	3108
B	0.11	0.61	27.68	0.113	0.00	36	3598	32	3166
B	0.11	0.61	28.43	0.113	0.00	37	3697	32	3253
B	0.11	0.61	29.43	0.112	0.00	36	3827	32	3367
B	0.11	0.61	30.68	0.114	0.00	37	3993	32	3513
B	0.11	0.61	31.68	0.113	0.00	37	4125	32	3629
B	0.11	0.61	32.68	0.114	0.00	37	4257	32	3745
B	0.11	0.61	33.85	0.112	0.00	36	4409	32	3879
B	0.11	0.61	35.10	0.113	0.00	36	4573	32	4023
B	0.11	0.61	37.77	0.114	0.00	37	4928	32	4336
B	0.11	0.61	38.77	0.113	0.00	36	5059	32	4451
B	0.11	0.61	39.93	0.113	0.00	37	5212	32	4586
B	0.11	0.61	41.02	0.113	0.00	37	5355	32	4711
B	0.11	0.61	42.02	0.113	0.00	37	5486	32	4827
B	0.11	0.61	43.35	0.113	0.00	36	5661	32	4980
B	0.11	0.61	44.10	0.113	0.00	37	5760	32	5067
B	0.11	0.61	47.10	0.113	0.00	37	6155	32	5415
B	0.11	0.61	48.10	0.113	0.00	37	6287	32	5531
B	0.11	0.61	49.93	0.113	0.00	37	6529	32	5744
B	0.11	0.61	50.93	0.113	0.00	37	6661	32	5860
B	0.11	0.61	52.76	0.112	0.00	36	6900	32	6070
B	0.11	0.61	53.76	0.112	0.00	36	7030	32	6184
B	0.11	0.61	57.10	0.110	0.00	36	7458	31	6562
B	0.11	0.61	58.10	0.110	0.00	36	7587	31	6674
B	0.11	0.61	59.93	0.113	0.00	37	7828	32	6887
B	0.11	0.61	60.93	0.112	0.00	36	7959	32	7002
B	0.11	0.61	61.51	0.113	0.00	37	8035	32	7069

Table A.8 Cont.

B	0.11	0.61	62.51	0.112	0.00	36	8166	32	7184
B	0.11	0.61	65.18	0.114	0.00	37	8519	32	7495
B	0.11	0.61	66.18	0.114	0.00	37	8652	33	7612
B	0.11	0.61	67.18	0.114	0.00	37	8785	33	7729
B	0.11	0.61	69.43	0.113	0.00	37	9082	32	7990
B	0.11	0.61	71.68	0.113	0.00	36	9377	32	8250
B	0.11	0.61	73.68	0.112	0.00	36	9638	32	8480
B	0.11	0.61	75.53	0.113	0.00	36	9881	32	8693
B	0.11	0.61	77.51	0.115	0.00	37	10145	33	8926
B	0.11	0.61	79.51	0.112	0.00	36	10406	32	9155
B	0.11	0.61	81.01	0.113	0.00	37	10604	32	9329
B	0.2	0.61	82.51	0.197	0.00	58	10919	56	9632
B	0.2	0.61	84.43	0.197	0.00	58	11322	56	10018
B	0.2	0.61	86.43	0.198	0.00	59	11744	56	10422
B	0.2	0.61	88.18	0.197	0.00	58	12113	56	10776
B	0.2	0.61	89.26	0.121	0.00	39	12265	34	10910
B	0.2	0.61	90.01	0.198	0.00	59	12424	56	11062
B	0.2	0.61	92.18	0.197	0.00	58	12879	56	11499

Table A.9 Discharge Data for Run C

Run	Nominal Discharge (m ³ /s)	Channel Width (m)	Run Time (hrs)	Discharge (m ³ /s) from Pressure Gage	Unit Discharge (m ² /s)	Unit Stream Power (W/m ²)	CUSP	Total Stream Power (W/m)	CTSP
C	0.11	0.61	0.17	0.121	0.00	40	24	34	21
C	0.11	0.61	0.67	0.115	0.00	38	92	33	79
C	0.11	0.61	2.67	0.110	0.00	36	352	31	305
C	0.11	0.61	4.67	0.112	0.00	37	618	32	535
C	0.11	0.61	6.42	0.114	0.00	38	855	33	740
C	0.11	0.61	9.83	0.116	0.00	38	1323	33	1145
C	0.11	0.61	11.25	0.116	0.00	38	1516	33	1313
C	0.11	0.61	12.00	0.116	0.00	38	1619	33	1402
C	0.11	0.61	12.58	0.106	0.00	35	1692	30	1465
C	0.11	0.61	13.08	0.113	0.00	37	1759	32	1523
C	0.11	0.61	14.83	0.113	0.00	37	1993	32	1725
C	0.11	0.61	16.08	0.114	0.00	37	2161	32	1870
C	0.11	0.61	17.17	0.114	0.00	37	2307	32	1997
C	0.11	0.61	18.83	0.114	0.00	37	2532	32	2191
C	0.11	0.61	20.33	0.113	0.00	37	2731	32	2364
C	0.11	0.61	22.83	0.110	0.00	36	3057	31	2646
C	0.11	0.61	24.33	0.115	0.00	38	3261	33	2822
C	0.11	0.61	25.58	0.112	0.00	37	3427	32	2966
C	0.11	0.61	27.83	0.112	0.00	37	3726	32	3225
C	0.11	0.61	29.33	0.112	0.00	37	3925	32	3397
C	0.11	0.61	30.83	0.113	0.00	37	4125	32	3571
C	0.11	0.61	32.50	0.112	0.00	37	4347	32	3762
C	0.11	0.61	34.59	0.112	0.00	37	4622	32	4001
C	0.11	0.61	36.09	0.112	0.00	37	4821	32	4173
C	0.11	0.61	38.59	0.112	0.00	37	5151	32	4458

Table A.9 Cont.

C	0.11	0.61	39.09	0.119	0.00	39	5221	34	4519
C	0.11	0.61	39.34	0.113	0.00	37	5255	32	4548
C	0.11	0.61	40.34	0.116	0.00	38	5393	33	4668
C	0.11	0.61	41.42	0.113	0.00	37	5538	32	4793
C	0.11	0.61	42.42	0.113	0.00	37	5672	32	4909
C	0.11	0.61	43.42	0.110	0.00	36	5802	31	5022
C	0.11	0.61	43.62	0.112	0.00	37	5829	32	5045
C	0.11	0.61	44.67	0.112	0.00	37	5968	32	5166
C	0.11	0.61	45.54	0.113	0.00	37	6084	32	5266
C	0.11	0.61	46.54	0.112	0.00	37	6217	32	5381
C	0.11	0.61	47.45	0.112	0.00	37	6339	32	5487
C	0.11	0.61	47.95	0.112	0.00	37	6405	32	5544
C	0.11	0.61	48.27	0.115	0.00	38	6448	33	5581
C	0.11	0.61	50.27	0.107	0.00	35	6701	30	5800
C	0.11	0.61	51.27	0.112	0.00	37	6834	32	5915
C	0.11	0.61	53.27	0.110	0.00	36	7095	31	6141
C	0.11	0.61	54.59	0.112	0.00	37	7268	32	6291
C	0.11	0.61	56.59	0.109	0.00	36	7525	31	6514
C	0.11	0.61	58.59	0.112	0.00	37	7791	32	6744
C	0.11	0.61	60.17	0.113	0.00	37	8002	32	6926
C	0.11	0.61	61.17	0.115	0.00	38	8138	33	7044
C	0.11	0.61	61.75	0.113	0.00	37	8216	32	7112
C	0.11	0.61	63.92	0.113	0.00	37	8506	32	7363
C	0.11	0.61	66.09	0.113	0.00	37	8795	32	7613
C	0.11	0.61	67.09	0.112	0.00	37	8928	32	7728
C	0.11	0.61	68.09	0.113	0.00	37	9061	32	7843
C	0.11	0.61	68.96	0.112	0.00	37	9176	32	7943
C	0.11	0.61	70.59	0.113	0.00	37	9394	32	8131

Table A.9 Cont.

C	0.11	0.61	72.09	0.113	0.00	37	9594	32	8304
C	0.11	0.61	73.59	0.112	0.00	37	9792	32	8475
C	0.11	0.61	75.09	0.112	0.00	37	9991	32	8647
C	0.11	0.61	75.79	0.108	0.00	35	10080	31	8725
C	0.11	0.61	75.91	0.113	0.00	37	10095	32	8738
C	0.11	0.61	76.54	0.114	0.00	38	10181	33	8812
C	0.11	0.61	77.54	0.114	0.00	37	10315	32	8929
C	0.11	0.61	78.62	0.114	0.00	37	10461	32	9055
C	0.11	0.61	80.59	0.114	0.00	37	10726	32	9284
C	0.11	0.61	79.62	0.113	0.00	37	10596	32	9172
C	0.11	0.61	81.09	0.111	0.00	37	10789	32	9339
C	0.11	0.61	83.17	0.110	0.00	36	11061	31	9574
C	0.11	0.61	83.84	0.115	0.00	38	11152	33	9652
C	0.11	0.61	85.17	0.110	0.00	36	11325	31	9803
C	0.11	0.61	86.17	0.110	0.00	36	11455	31	9915
C	0.11	0.61	87.17	0.113	0.00	37	11589	32	10031
C	0.2	0.61	87.67	0.198	0.00	61	11699	56	10132
C	0.2	0.61	88.54	0.199	0.00	61	11890	57	10309
C	0.2	0.61	90.26	0.198	0.00	61	12266	56	10656
C	0.2	0.61	92.01	0.198	0.00	61	12650	56	11011
C	0.2	0.61	93.01	0.198	0.00	61	12870	56	11214
C	0.2	0.61	94.34	0.198	0.00	61	13164	56	11486
C	0.2	0.61	95.59	0.198	0.00	61	13438	56	11739
C	0.2	0.61	97.51	0.197	0.00	61	13857	56	12126
C	0.2	0.61	98.51	0.197	0.00	61	14076	56	12328
C	0.2	0.61	99.51	0.197	0.00	61	14295	56	12530
C	0.2	0.61	100.51	0.197	0.00	61	14513	56	12732
C	0.2	0.61	101.34	0.198	0.00	61	14696	56	12901

Table A.9 Cont.

C	0.2	0.61	102.34	0.199	0.00	61	14916	56	13104
C	0.2	0.61	104.68	0.198	0.00	61	15429	56	13578
C	0.2	0.61	105.68	0.198	0.00	61	15649	56	13781
C	0.2	0.61	106.68	0.198	0.00	61	15868	56	13983
C	0.2	0.61	107.93	0.198	0.00	61	16143	56	14237
C	0.2	0.61	109.26	0.198	0.00	61	16436	56	14508
C	0.2	0.61	110.26	0.198	0.00	61	16655	56	14710
C	0.2	0.61	112.26	0.196	0.00	61	17091	56	15112
C	0.2	0.61	113.26	0.196	0.00	60	17309	56	15313
C	0.2	0.61	114.26	0.198	0.00	61	17528	56	15516
C	0.2	0.61	115.03	0.198	0.00	61	17696	56	15671
C	0.2	0.61	115.86	0.226	0.00	70	17905	64	15864
C	0.2	0.61	116.11	0.197	0.00	61	17959	56	15915
C	0.2	0.61	116.81	0.197	0.00	61	18112	56	16056
C	0.2	0.61	117.78	0.197	0.00	61	18324	56	16251
C	0.2	0.61	119.39	0.197	0.00	61	18677	56	16577
C	0.2	0.61	119.74	0.197	0.00	61	18753	56	16648

Table A.10 Discharge Data for Run D

Run	Nominal Discharge (m ³ /s)	Channel Width (m)	Run Time (hrs)	Discharge (m ³ /s) from Pressure Gage	Unit Discharge (m ² /s)	Unit Stream Power (W/m ²)	CUSP	Total Stream Power (W/m)	CTSP
D	0.11	1.17	0.17	0.114	0.00	44	26	33	20
D	0.11	1.17	0.78	0.113	0.00	43	122	32	91
D	0.11	1.17	1.75	0.113	0.00	43	271	32	203
D	0.11	1.17	2.00	0.113	0.00	43	310	32	232
D	0.11	1.17	2.12	0.115	0.00	44	328	33	246
D	0.11	1.17	2.72	0.113	0.00	43	421	32	315
D	0.11	1.17	3.53	0.113	0.00	43	548	32	410
D	0.11	1.17	4.53	0.114	0.00	43	703	32	526
D	0.11	1.17	5.63	0.113	0.00	43	874	32	654
D	0.11	1.17	6.42	0.113	0.00	43	995	32	745
D	0.11	1.17	6.95	0.114	0.00	43	1078	32	807
D	0.11	1.17	7.27	0.116	0.00	44	1128	33	844
D	0.11	1.17	8.12	0.114	0.00	43	1261	32	944
D	0.11	1.17	9.15	0.112	0.00	42	1419	32	1062
D	0.11	1.17	10.05	0.112	0.00	43	1556	32	1165
D	0.11	1.17	11.10	0.111	0.00	42	1716	32	1285
D	0.11	1.17	11.50	0.111	0.00	42	1777	32	1330
D	0.11	1.17	11.62	0.116	0.00	44	1796	33	1344
D	0.11	1.17	11.97	0.114	0.00	44	1851	33	1385
D	0.11	1.17	12.80	0.114	0.00	43	1981	32	1482
D	0.11	1.17	14.00	0.113	0.00	43	2166	32	1621
D	0.11	1.17	14.23	0.116	0.00	44	2203	33	1649
D	0.11	1.17	14.97	0.115	0.00	44	2319	33	1735
D	0.11	1.17	15.97	0.115	0.00	44	2476	33	1853
D	0.11	1.17	16.77	0.115	0.00	44	2601	33	1947

Table A.10 Cont.

D	0.11	1.17	18.05	0.114	0.00	43	2802	32	2097
D	0.11	1.17	18.50	0.114	0.00	43	2872	33	2150
D	0.11	1.17	18.58	0.119	0.00	45	2886	34	2160
D	0.11	1.17	18.83	0.118	0.00	45	2926	34	2190
D	0.11	1.17	19.10	0.118	0.00	45	2969	34	2222
D	0.11	1.17	20.12	0.117	0.00	45	3132	33	2344
D	0.11	1.17	21.17	0.118	0.00	45	3301	33	2471
D	0.11	1.17	22.00	0.117	0.00	45	3435	33	2571
D	0.11	1.17	22.07	0.117	0.00	44	3446	33	2579
D	0.11	1.17	22.38	0.115	0.00	44	3495	33	2616
D	0.11	1.17	23.38	0.113	0.00	43	3651	32	2732
D	0.11	1.17	24.52	0.113	0.00	43	3826	32	2864
D	0.11	1.17	25.00	0.114	0.00	43	3902	32	2920
D	0.11	1.17	25.05	0.123	0.00	47	3910	35	2927
D	0.11	1.17	25.18	0.115	0.00	44	3931	33	2942
D	0.11	1.17	25.52	0.114	0.00	43	3983	33	2981
D	0.11	1.17	26.48	0.114	0.00	43	4134	32	3094
D	0.11	1.17	27.73	0.114	0.00	43	4330	33	3241
D	0.11	1.17	27.93	0.114	0.00	43	4361	32	3264
D	0.11	1.17	28.13	0.118	0.00	45	4393	34	3288
D	0.11	1.17	28.42	0.116	0.00	44	4438	33	3322
D	0.11	1.17	29.20	0.116	0.00	44	4563	33	3415
D	0.11	1.17	31.28	0.113	0.00	43	4885	32	3656
D	0.11	1.17	32.12	0.115	0.00	44	5016	33	3754
D	0.11	1.17	32.47	0.114	0.00	43	5070	33	3795
D	0.2	1.17	33.00	0.199	0.00	74	5213	57	3904
D	0.2	1.17	33.70	0.198	0.00	74	5399	56	4046
D	0.2	1.17	34.88	0.199	0.00	74	5715	57	4287
D	0.2	1.17	35.95	0.198	0.00	74	5998	56	4504

Table A.10 Cont.

D	0.2	1.17	36.47	0.199	0.00	74	6136	57	4609
D	0.2	1.17	37.00	0.200	0.00	75	6279	57	4718
D	0.2	1.17	37.95	0.200	0.00	75	6535	57	4913
D	0.2	1.17	38.97	0.200	0.00	75	6807	57	5122
D	0.2	1.17	40.00	0.200	0.00	75	7085	57	5334
D	0.2	1.17	40.50	0.201	0.00	75	7220	57	5437
D	0.2	1.17	40.92	0.199	0.00	74	7331	57	5522
D	0.2	1.17	41.32	0.198	0.00	74	7438	56	5603
D	0.2	1.17	42.42	0.199	0.00	74	7731	57	5827
D	0.2	1.17	43.32	0.199	0.00	74	7971	57	6010
D	0.2	1.17	44.00	0.199	0.00	74	8153	57	6149
D	0.2	1.17	44.48	0.201	0.00	75	8283	57	6249
D	0.2	1.17	44.83	0.201	0.00	75	8378	57	6321
D	0.2	1.17	45.73	0.201	0.00	75	8620	57	6506
D	0.2	1.17	46.83	0.200	0.00	74	8915	57	6731
D	0.2	1.17	47.85	0.200	0.00	74	9187	57	6939
D	0.2	1.17	48.97	0.200	0.00	75	9487	57	7168
D	0.2	1.17	49.45	0.200	0.00	74	9617	57	7267
D	0.2	1.17	49.93	0.200	0.00	75	9747	57	7366
D	0.2	1.17	50.38	0.200	0.00	74	9867	57	7459
D	0.2	1.17	51.28	0.200	0.00	74	10108	57	7643
D	0.2	1.17	52.28	0.200	0.00	74	10376	57	7847
D	0.2	1.17	52.85	0.200	0.00	74	10528	57	7963
D	0.2	1.17	53.33	0.202	0.00	75	10659	58	8064
D	0.2	1.17	53.72	0.203	0.00	76	10764	58	8143
D	0.2	1.17	54.55	0.202	0.00	75	10990	58	8316
D	0.2	1.17	55.57	0.202	0.00	75	11265	58	8527
D	0.2	1.17	56.67	0.203	0.00	75	11564	58	8755
D	0.2	1.17	56.92	0.203	0.00	75	11632	58	8807

Table A.10 Cont.

D	0.2	1.17	57.30	0.199	0.00	74	11734	56	8885
D	0.2	1.17	57.70	0.198	0.00	74	11841	56	8966
D	0.2	1.17	58.62	0.198	0.00	74	12084	56	9152
D	0.2	1.17	59.70	0.199	0.00	74	12373	57	9373
D	0.2	1.17	60.68	0.199	0.00	74	12635	56	9573
D	0.2	1.17	60.95	0.199	0.00	74	12706	57	9627
D	0.2	1.17	61.22	0.198	0.00	74	12777	56	9681
D	0.2	1.17	61.40	0.199	0.00	74	12826	57	9719
D	0.2	1.17	61.75	0.200	0.00	74	12920	57	9790
D	0.2	1.17	62.77	0.200	0.00	74	13192	57	9998
D	0.2	1.17	63.02	0.227	0.00	85	13269	65	10057
D	0.2	1.17	63.33	0.227	0.00	85	13365	65	10130
D	0.2	1.17	64.30	0.226	0.00	84	13659	64	10354
D	0.2	1.17	64.48	0.201	0.00	75	13708	57	10392
D	0.2	1.17	64.98	0.200	0.00	75	13842	57	10495
D	0.2	1.17	66.02	0.200	0.00	75	14120	57	10706
D	0.2	1.17	66.92	0.200	0.00	75	14361	57	10891
D	0.2	1.17	67.90	0.200	0.00	74	14625	57	11092
D	0.2	1.17	68.97	0.201	0.00	75	14912	57	11311
D	0.2	1.17	69.37	0.200	0.00	74	15019	57	11393
D	0.2	1.17	69.93	0.199	0.00	74	15170	57	11509
D	0.2	1.17	70.95	0.198	0.00	74	15440	56	11715
D	0.2	1.17	72.03	0.199	0.00	74	15729	57	11936
D	0.2	1.17	72.48	0.200	0.00	74	15850	57	12028
D	0.2	1.17	72.65	0.198	0.00	74	15894	56	12062
D	0.2	1.17	72.83	0.198	0.00	74	15943	56	12099
D	0.2	1.17	73.93	0.198	0.00	74	16235	56	12323
D	0.2	1.17	74.92	0.198	0.00	74	16496	56	12522
D	0.2	1.17	75.62	0.198	0.00	74	16682	56	12663

Table A.10 Cont.

D	0.2	1.17	76.38	0.199	0.00	74	16887	57	12820
D	0.2	1.17	76.70	0.198	0.00	74	16971	56	12884
D	0.2	1.17	78.17	0.198	0.00	74	17361	56	13182
D	0.2	1.17	78.88	0.198	0.00	74	17551	56	13328
D	0.2	1.17	79.80	0.198	0.00	74	17794	56	13513
D	0.2	1.17	80.48	0.198	0.00	74	17975	56	13651
D	0.2	1.17	80.70	0.201	0.00	75	18034	57	13696
D	0.2	1.17	81.03	0.201	0.00	75	18123	57	13764
D	0.2	1.17	81.65	0.200	0.00	74	18288	57	13890
D	0.2	1.17	82.57	0.195	0.00	73	18528	56	14074
D	0.2	1.17	83.68	0.188	0.00	70	18809	53	14288
D	0.2	1.17	84.43	0.191	0.00	71	19002	54	14435
D	0.2	1.17	84.68	0.199	0.00	74	19068	57	14486
D	0.2	1.17	85.27	0.199	0.00	74	19224	57	14605
D	0.2	1.17	85.88	0.198	0.00	74	19387	56	14730
D	0.2	1.17	86.17	0.198	0.00	74	19462	56	14787
D	0.2	1.17	87.18	0.196	0.00	73	19729	56	14991
D	0.2	1.17	88.23	0.197	0.00	73	20007	56	15203
D	0.2	1.17	88.47	0.197	0.00	73	20068	56	15250
D	0.2	1.17	88.65	0.198	0.00	74	20117	56	15287
D	0.2	1.17	89.27	0.199	0.00	74	20281	56	15412
D	0.2	1.17	89.55	0.199	0.00	74	20357	57	15470
D	0.2	1.17	90.47	0.199	0.00	74	20601	57	15657
D	0.2	1.17	91.45	0.199	0.00	74	20864	57	15858
D	0.2	1.17	92.43	0.199	0.00	74	21127	57	16059
D	0.2	1.17	92.78	0.200	0.00	74	21221	57	16130
D	0.2	1.17	93.47	0.199	0.00	74	21404	57	16270
D	0.2	1.17	94.48	0.196	0.00	73	21671	56	16474
D	0.2	1.17	95.52	0.198	0.00	74	21945	56	16683

Table A.10 Cont.

D	0.2	1.17	96.55	0.199	0.00	74	22220	57	16894
D	0.2	1.17	96.87	0.198	0.00	74	22305	56	16958
D	0.2	1.17	97.42	0.198	0.00	74	22451	56	17070
D	0.2	1.17	97.77	0.198	0.00	74	22544	56	17141
D	0.2	1.17	99.00	0.198	0.00	74	22871	56	17391
D	0.2	1.17	99.97	0.199	0.00	74	23129	57	17588

Table A.11 Discharge Data for Run E

Run	Nominal Discharge (m ³ /s)	Channel Width (m)	Run Time (hrs)	Discharge (m ³ /s) from Pressure Gage	Unit Discharge (m ² /s)	Unit Stream Power (W/m ²)	CUSP	Total Stream Power (W/m)	CTSP
E	0.11	1.17	0.15	0.120	0.00	46	25	34	18
E	0.11	1.17	1.00	0.118	0.00	45	163	34	122
E	0.2	1.17	1.15	0.198	0.00	71	202	56	152
E	0.2	1.17	1.75	0.196	0.00	70	353	56	272
E	0.2	1.17	2.73	0.197	0.00	71	604	56	470
E	0.2	1.17	3.78	0.197	0.00	71	871	56	683
E	0.2	1.17	4.48	0.197	0.00	71	1050	56	824
E	0.2	1.17	4.68	0.201	0.00	72	1102	57	865
E	0.2	1.17	5.15	0.200	0.00	72	1222	57	961
E	0.2	1.17	6.20	0.198	0.00	71	1492	56	1175
E	0.2	1.17	7.18	0.195	0.00	70	1740	56	1371
E	0.2	1.17	8.25	0.202	0.00	72	2018	57	1592
E	0.2	1.17	9.25	0.201	0.00	72	2278	57	1798
E	0.2	1.17	9.48	0.202	0.00	72	2338	57	1846
E	0.2	1.17	9.70	0.203	0.00	73	2395	58	1891
E	0.2	1.17	10.02	0.199	0.00	72	2477	57	1956
E	0.2	1.17	10.48	0.200	0.00	72	2597	57	2051
E	0.2	1.17	11.48	0.200	0.00	72	2855	57	2256
E	0.2	1.17	11.98	0.200	0.00	72	2984	57	2358
E	0.2	1.17	12.25	0.200	0.00	72	3053	57	2412
E	0.2	1.17	13.15	0.199	0.00	71	3284	57	2596
E	0.2	1.17	14.12	0.200	0.00	72	3534	57	2793
E	0.2	1.17	14.33	0.200	0.00	72	3590	57	2838
E	0.2	1.17	14.77	0.199	0.00	71	3701	57	2926
E	0.2	1.17	15.12	0.199	0.00	72	3791	57	2998
E	0.2	1.17	16.12	0.199	0.00	71	4048	57	3201

Table A.11 Cont.

E	0.2	1.17	17.13	0.199	0.00	71	4309	56	3408
E	0.2	1.17	18.22	0.198	0.00	71	4586	56	3628
E	0.2	1.17	19.05	0.198	0.00	71	4800	56	3797
E	0.2	1.17	19.42	0.199	0.00	71	4894	57	3872
E	0.2	1.17	19.82	0.198	0.00	71	4996	56	3953
E	0.2	1.17	20.25	0.198	0.00	71	5107	56	4041
E	0.2	1.17	21.27	0.197	0.00	71	5366	56	4247
E	0.2	1.17	21.47	0.198	0.00	71	5418	56	4287
E	0.2	1.17	21.70	0.199	0.00	71	5478	57	4335
E	0.2	1.17	22.18	0.199	0.00	71	5602	57	4433
E	0.2	1.17	22.53	0.198	0.00	71	5691	56	4504
E	0.2	1.17	23.55	0.194	0.00	70	5946	55	4706
E	0.2	1.17	24.50	0.198	0.00	71	6189	56	4899
E	0.2	1.17	25.60	0.200	0.00	72	6473	57	5124
E	0.2	1.17	26.47	0.201	0.00	72	6698	57	5303
E	0.2	1.17	26.70	0.199	0.00	72	6759	57	5350
E	0.2	1.17	27.17	0.199	0.00	71	6879	57	5445
E	0.2	1.17	27.55	0.199	0.00	71	6977	57	5524
E	0.2	1.17	28.57	0.199	0.00	71	7238	57	5731
E	0.2	1.17	29.68	0.199	0.00	72	7526	57	5959
E	0.2	1.17	30.48	0.199	0.00	71	7731	57	6122
E	0.2	1.17	30.63	0.201	0.00	72	7770	57	6153
E	0.2	1.17	31.05	0.201	0.00	72	7878	57	6238
E	0.2	1.17	31.68	0.201	0.00	72	8042	57	6368
E	0.2	1.17	32.70	0.201	0.00	72	8307	57	6578
E	0.2	1.17	33.47	0.201	0.00	72	8506	57	6736
E	0.2	1.17	33.63	0.199	0.00	72	8549	57	6770
E	0.2	1.17	34.23	0.198	0.00	71	8702	56	6891
E	0.2	1.17	35.55	0.198	0.00	71	9039	56	7159

Table A.11 Cont.

E	0.2	1.17	36.53	0.198	0.00	71	9291	56	7358
E	0.2	1.17	37.43	0.198	0.00	71	9522	56	7541
E	0.2	1.17	38.48	0.199	0.00	71	9791	57	7755
E	0.2	1.17	38.73	0.202	0.00	72	9856	57	7806
E	0.2	1.17	39.18	0.201	0.00	72	9973	57	7899
E	0.2	1.17	39.72	0.201	0.00	72	10112	57	8009
E	0.2	1.17	40.73	0.201	0.00	72	10376	57	8218
E	0.2	1.17	41.73	0.201	0.00	72	10636	57	8424
E	0.2	1.17	42.75	0.201	0.00	72	10900	57	8634
E	0.2	1.17	42.97	0.201	0.00	72	10956	57	8678
E	0.2	1.17	43.18	0.197	0.00	71	11011	56	8722
E	0.2	1.17	43.90	0.198	0.00	71	11195	56	8868
E	0.2	1.17	45.03	0.198	0.00	71	11485	56	9097

Table A.12 Discharge Data for Run F

Run	Nominal Discharge (m ³ /s)	Channel Width (m)	Run Time (hrs)	Discharge (m ³ /s) from Pressure Gage	Unit Discharge (m ² /s)	Unit Stream Power (W/m ²)	CUSP	Total Stream Power (W/m)	CTSP
F	0.2	1.17	0.20	0.197	0.00	74	53	56	40
F	0.2	1.17	0.67	0.197	0.00	74	177	56	135
F	0.2	1.17	1.35	0.197	0.00	74	359	56	273
F	0.2	1.17	1.80	0.198	0.00	74	479	56	364
F	0.2	1.17	2.73	0.198	0.00	74	728	56	554
F	0.2	1.17	3.02	0.198	0.00	74	804	56	611
F	0.2	1.17	3.23	0.199	0.00	74	862	57	655
F	0.2	1.17	3.88	0.199	0.00	75	1037	57	788
F	0.2	1.17	4.82	0.200	0.00	75	1288	57	979
F	0.2	1.17	5.78	0.200	0.00	75	1548	57	1177
F	0.2	1.17	6.82	0.199	0.00	75	1826	57	1388
F	0.2	1.17	8.15	0.199	0.00	75	2184	57	1660
F	0.2	1.17	8.30	0.202	0.00	76	2224	57	1691
F	0.2	1.17	9.12	0.202	0.00	76	2447	57	1860
F	0.2	1.17	10.28	0.202	0.00	76	2764	57	2102
F	0.2	1.17	11.45	0.202	0.00	75	3081	57	2343
F	0.2	1.17	12.15	0.202	0.00	76	3272	57	2487
F	0.2	1.17	12.75	0.201	0.00	75	3434	57	2611
F	0.2	1.17	13.75	0.201	0.00	75	3704	57	2816
F	0.2	1.17	14.30	0.201	0.00	75	3852	57	2929
F	0.2	1.17	14.48	0.199	0.00	74	3901	57	2966
F	0.2	1.17	15.37	0.200	0.00	75	4139	57	3147
F	0.2	1.17	16.38	0.200	0.00	75	4413	57	3356
F	0.2	1.17	17.65	0.200	0.00	75	4754	57	3615
F	0.2	1.17	17.87	0.200	0.00	75	4813	57	3659
F	0.2	1.17	18.15	0.200	0.00	75	4889	57	3717

Table A.12 Cont.

F	0.2	1.17	19.12	0.200	0.00	75	5149	57	3915
F	0.2	1.17	20.08	0.197	0.00	74	5406	56	4110
F	0.2	1.17	21.10	0.198	0.00	74	5677	56	4316
F	0.2	1.17	22.37	0.199	0.00	74	6016	57	4574

Table A.13 Discharge Data for Run G

Run	Nominal Discharge (m ³ /s)	Channel Width (m)	Run Time (hrs)	Discharge (m ³ /s) from Pressure Gage	Unit Discharge (m ² /s)	Unit Stream Power (W/m ²)	CUSP	Total Stream Power (W/m)	CTSP
G	0.2	1.17	0.32	0.199	0.00	73	83	57	65
G	0.2	1.17	1.32	0.200	0.00	73	347	57	269
G	0.2	1.17	2.48	0.200	0.00	73	654	57	508
G	0.2	1.17	3.43	0.204	0.00	75	909	58	707
G	0.2	1.17	4.48	0.200	0.00	73	1187	57	922
G	0.2	1.17	4.93	0.200	0.00	73	1305	57	1015
G	0.2	1.17	5.20	0.199	0.00	73	1376	57	1069
G	0.2	1.17	6.20	0.198	0.00	73	1637	56	1272
G	0.2	1.17	7.20	0.198	0.00	73	1899	56	1476
G	0.2	1.17	8.20	0.198	0.00	72	2159	56	1678
G	0.2	1.17	9.28	0.198	0.00	72	2442	56	1898
G	0.2	1.17	10.45	0.198	0.00	73	2747	56	2135
G	0.2	1.17	10.63	0.198	0.00	72	2795	56	2172
G	0.2	1.17	10.97	0.198	0.00	72	2882	56	2240
G	0.2	1.17	11.92	0.198	0.00	73	3130	56	2433
G	0.2	1.17	12.62	0.203	0.00	74	3317	58	2578
G	0.2	1.17	13.82	0.198	0.00	73	3631	56	2822
G	0.2	1.17	14.68	0.197	0.00	72	3855	56	2996
G	0.2	1.17	15.43	0.197	0.00	72	4050	56	3147
G	0.2	1.17	15.65	0.198	0.00	73	4106	56	3191
G	0.2	1.17	16.67	0.199	0.00	73	4373	57	3399
G	0.2	1.17	17.70	0.199	0.00	73	4644	57	3609
G	0.2	1.17	18.62	0.198	0.00	73	4883	56	3795
G	0.2	1.17	19.73	0.197	0.00	72	5174	56	4021
G	0.2	1.17	20.53	0.200	0.00	73	5385	57	4185
G	0.2	1.17	20.78	0.201	0.00	74	5451	57	4236

Table A.13 Cont.

G	0.2	1.17	21.80	0.202	0.00	74	5721	57	4446
G	0.2	1.17	22.75	0.201	0.00	74	5973	57	4642
G	0.2	1.17	23.67	0.203	0.00	74	6219	58	4833
G	0.2	1.17	24.73	0.198	0.00	72	6496	56	5049
G	0.2	1.17	25.77	0.198	0.00	73	6766	56	5259
G	0.2	1.17	26.18	0.197	0.00	72	6874	56	5343
G	0.2	1.17	26.40	0.200	0.00	73	6931	57	5387
G	0.2	1.17	27.42	0.198	0.00	73	7197	56	5594
G	0.2	1.17	28.52	0.198	0.00	73	7484	56	5817
G	0.2	1.17	29.48	0.198	0.00	73	7737	56	6013
G	0.2	1.17	30.45	0.199	0.00	73	7990	57	6210
G	0.2	1.17	31.18	0.199	0.00	73	8182	57	6359
G	0.2	1.17	31.45	0.200	0.00	73	8253	57	6414
G	0.2	1.17	31.78	0.200	0.00	73	8341	57	6482
G	0.2	1.17	32.97	0.200	0.00	73	8652	57	6725
G	0.2	1.17	33.85	0.201	0.00	73	8886	57	6906
G	0.2	1.17	34.93	0.201	0.00	73	9172	57	7129
G	0.2	1.17	35.72	0.201	0.00	74	9380	57	7290
G	0.2	1.17	35.93	0.201	0.00	73	9437	57	7335
G	0.2	1.17	36.33	0.201	0.00	73	9543	57	7417
G	0.2	1.17	37.37	0.202	0.00	74	9818	57	7631
G	0.2	1.17	38.45	0.199	0.00	73	10102	57	7851
G	0.2	1.17	39.42	0.199	0.00	73	10356	57	8048
G	0.2	1.17	40.40	0.198	0.00	73	10613	56	8248
G	0.2	1.17	40.63	0.200	0.00	73	10674	57	8296
G	0.2	1.17	40.97	0.199	0.00	73	10762	57	8364
G	0.2	1.17	42.12	0.197	0.00	72	11061	56	8596
G	0.2	1.17	43.13	0.197	0.00	72	11325	56	8802
G	0.2	1.17	44.08	0.199	0.00	73	11574	57	8995

Table A.13 Cont.

G	0.2	1.17	45.03	0.198	0.00	73	11822	56	9188
G	0.2	1.17	45.48	0.200	0.00	73	11941	57	9280
G	0.2	1.17	45.63	0.201	0.00	74	11980	57	9311
G	0.2	1.17	45.95	0.202	0.00	74	12065	57	9377
G	0.2	1.17	46.82	0.198	0.00	72	12290	56	9552
G	0.2	1.17	47.73	0.199	0.00	73	12531	57	9739
G	0.2	1.17	48.80	0.203	0.00	74	12817	58	9961
G	0.2	1.17	49.95	0.200	0.00	73	13120	57	10197

Appendix B Block Coefficient of Friction Test

Table B.1 Coefficient of Friction for Block on Baseboard

Trial	Submerged Weight (N)	Force to Initiate Motion (N)	C_f
1	1.32	0.7	0.51
2	1.32	0.4	0.34
3	1.32	0.5	0.38
4	1.32	0.5	0.41
5	1.32	0.5	0.41
6	1.32	0.5	0.38
7	2.46	1.1	0.46
8	2.46	1.0	0.42
9	2.46	1.1	0.44
10	2.46	1.0	0.42
11	2.46	0.9	0.38
12	2.46	1.0	0.40
13	2.46	0.9	0.35
14	2.46	0.8	0.33
15	3.46	1.8	0.51
16	3.46	1.6	0.45
17	3.46	1.7	0.48
18	3.46	1.6	0.45
19	3.46	1.6	0.47
20	3.46	1.7	0.48
21	1.55	0.7	0.47
22	1.55	0.6	0.41
23	1.55	0.7	0.43
24	1.55	0.6	0.40
25	1.55	0.7	0.45
26	1.55	0.6	0.42
27	1.88	0.8	0.44
28	1.88	0.9	0.47
29	1.88	0.9	0.48
30	1.88	0.8	0.43
31	1.88	0.9	0.47
32	1.88	0.8	0.41
33	2.75	1.2	0.44
34	2.75	1.2	0.43
35	2.75	1.2	0.44
36	2.75	1.2	0.42
37	2.75	1.2	0.43
38	2.75	1.3	0.46
39	1.83	0.8	0.46
40	1.83	0.8	0.44
41	1.83	0.7	0.40
42	1.83	0.8	0.44
43	1.83	0.8	0.46
44	1.83	0.9	0.48
45	2.96	1.3	0.43
46	2.96	1.3	0.45
47	2.96	1.3	0.46
48	2.96	1.3	0.44
49	2.96	1.3	0.43
50	2.96	1.3	0.43
Mean C_f			0.43
St Dev C_f			0.038

Table B.2 Coefficient of Friction for Block on Block

Trial	Submerged Weight (N)	Force to Initiate Motion (N)	C_f
1	1.32	0.8	0.58
2	1.32	0.9	0.72
3	1.32	0.9	0.65
4	1.32	0.9	0.68
5	1.32	1.1	0.82
6	1.32	0.8	0.61
7	2.46	1.6	0.66
8	2.46	1.8	0.71
9	2.46	1.7	0.67
10	3.46	3.1	0.90
11	3.46	3.1	0.88
12	3.46	2.4	0.70
13	1.55	1.2	0.78
14	1.55	1.1	0.68
15	1.55	1.1	0.69
16	1.55	1.1	0.73
17	1.55	1.1	0.69
18	1.55	1.2	0.78
19	1.88	1.4	0.72
20	1.88	1.3	0.71
21	1.88	1.4	0.73
22	1.88	1.3	0.70
23	1.88	1.4	0.74
24	1.88	1.4	0.74
25	2.75	2.0	0.73
26	2.75	2.0	0.74
27	2.75	2.0	0.71
28	2.75	2.0	0.74
29	2.75	2.0	0.73
30	2.75	1.9	0.71
31	1.83	1.4	0.77
32	1.83	1.4	0.75
33	1.83	1.3	0.70
34	1.83	1.4	0.78
35	1.83	1.3	0.72
36	1.83	1.3	0.70
37	2.96	2.1	0.73
38	2.96	2.1	0.71
39	2.96	2.1	0.71
40	2.96	2.1	0.71
41	2.96	2.2	0.76
42	2.96	2.2	0.75
43	1.56	1.1	0.71
44	1.56	1.1	0.73
45	1.56	1.1	0.71
46	1.56	1.2	0.75
47	1.56	1.2	0.78
48	1.56	1.1	0.73
49	1.32	1.0	0.75
50	1.32	0.9	0.71
		Mean C_f	0.73
		St Dev C_f	0.054

Appendix C Statistical Analysis

The purpose of this appendix is to provide supporting results and additional analysis to supplement and expand on the statistical analysis presented in the main text.

C.1 Further Description of Probabilities of Event Occurrence and Magnitude

C.2 Correlation between Event Magnitude and Time Lapse Between Events

C.3 Correlation between Event Magnitude and Energy Expenditure per Event

C.4 Probability of Event Occurrence Supplement

C.5 Probability of Event Magnitude Supplement

C.6 Modeling Erosion Supplement

C.1 Further Description of Probabilities of Event Occurrence and Magnitude

Our first interest is the probability that at a given point in time the bedrock channel material will fail. Because time is a continuous variable and assuming the interval between events is random, the time taken between failures is a continuous random variable of interest with an underlying probability distribution function to be denoted by T_i . The magnitude of the failure event is the probability of a discrete number of blocks being removed. We assume the magnitude of an event is a random variable B . Because the block dimensions are assumed uniform, the volume of material removed is always expressed as a discrete number of blocks. This value will approach a continuous value as the block size is reduced or diverges from uniform dimensions. Foreseeing application of the probability model to all possible joint patterns where an infinite number of possible block dimensions are possible, B is treated as a continuous random variable for the purposes of fitting a probability distribution to the empirical distribution.

Because the occurrence of an event is a random variable with dimension of time while the magnitude of an event is a random variable with volume dimensions, it is appropriate to separate the erosion record into the two random variables where the probability of an event of a given magnitude at a given time is conditional on the probability of event magnitude and probability of an event occurrence at a point in time. If an event does not occur then the probability of any magnitude is null (0). If an event does occur then the probability of the event magnitude is always positive even if extremely small.

C.2 Correlation between Event Magnitude and Time Lapse Between Events

The goal of our statistical model is to determine the probability of an event magnitude at a point in time given that an event has occurred at a point in time.

Difficulties in estimating the erosion probability distribution arise from the blocks potentially loosening over time so that the magnitude of an event potentially increases with time as more blocks are loosened by the applied hydraulic load. Lowering of joint strength over time may lead to greater magnitude events. The null hypothesis from this potential scenario is that longer time lapses between events correlate with larger magnitude events.

To address this null hypothesis, we first test for correlation between time lapse and event magnitude. If insignificant correlation is found, then for our results the magnitude of an event in the physical model depends only on the joint strength distribution and the hydraulic load applied by the flow. The correlation coefficients between time lapse and event magnitude are low for Runs A, B, D, E, and G (Table C.1).

The low correlation provides empirical support for the alternative hypothesis that event magnitude for the experimental runs is fairly independent of time lapse between events.

Table C.1 Correlation between Time Lapse Between Events and Event Magnitude

Run	Correlation Coefficient	r^2
A	-0.26	0.07
B	-0.28	0.08
D	-0.17	0.03
E	-0.15	0.02
G	0.20	0.04

Interestingly, the weak correlation is negative for four out of the five runs included in the analysis. Recall the earlier discussion of the keystone theory of block failure. A larger event requires a small keystone event, even a single keystone block, to be removed prior to a larger event occurring. Once the keystone event occurs, a larger event can then occur. The negative correlations between time lapse and event magnitude in Runs A, B, D, and E suggest smaller events require a longer time lapse to occur than larger events. This is the same correlation which may be expected using the keystone theory of block removal. The correlation is not very strong because of the additional occurrence of many small events occurring at short time lapses, outlined in red in the plot of time lapse and event magnitude (Figure C.1). The correlation for Run G is positive, but a visual inspection of time lapse versus event magnitude suggests a negative correlation between largest events at longer time lapses, as indicated by the dotted line. The occurrence of many more small events occurring at short time lapses (outlined in red), however, has a greater influence on the overall correlation (Figure C.2).

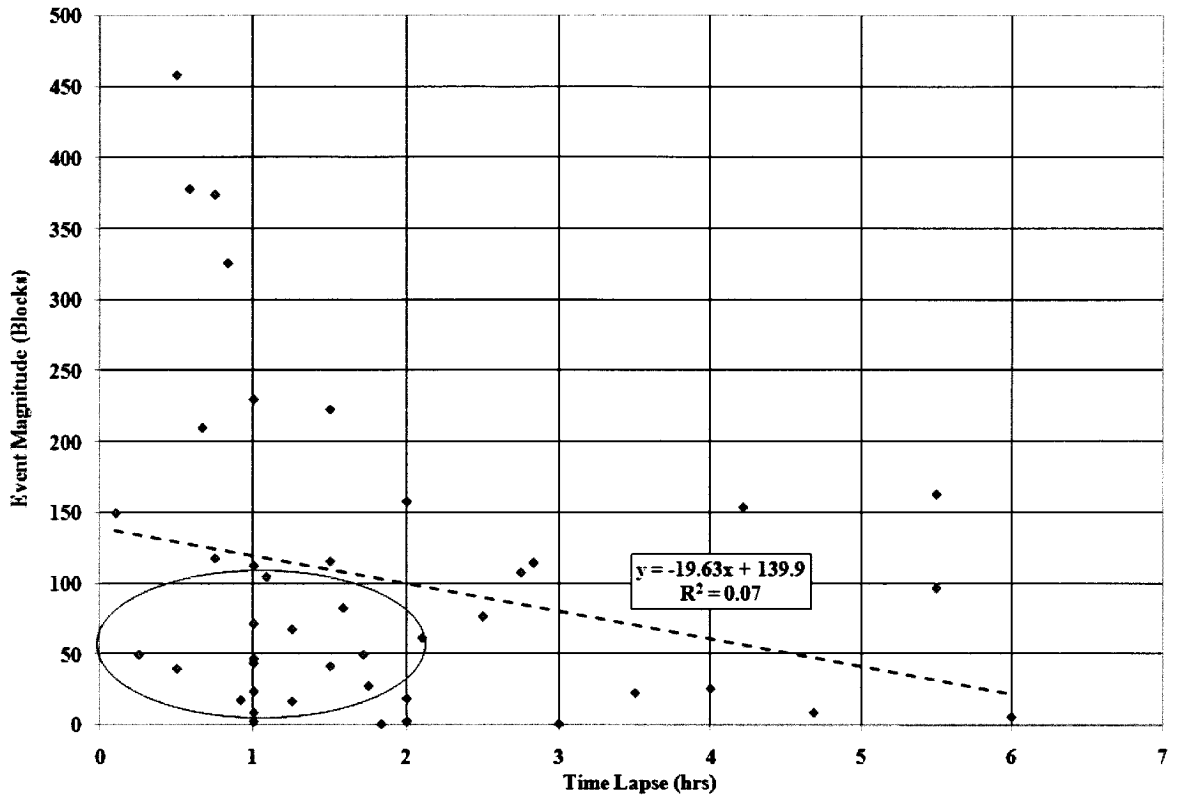


Figure C.1 Correlations between Time Lapse Between Events and Block Count - Run A

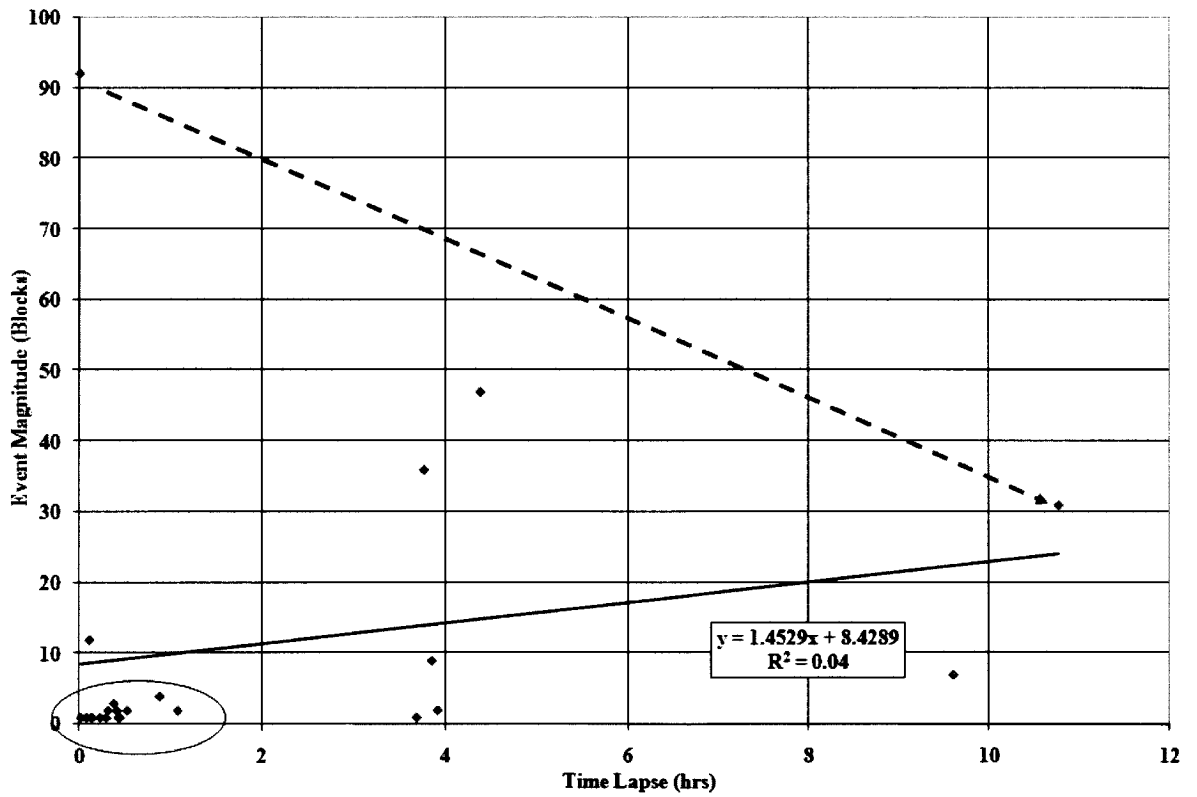


Figure C.2 Correlations between Time Lapse Between Events and Block Count - Run G

C.3 Correlation between Event Magnitude and Energy Expenditure per Event

The correlations between *CUSP* and event magnitude were low but generally negative, with the exception of Run G, as was the previous case for time lapse (Table C.2). The correlations are similar to correlations for time lapse because energy expenditure is linear as a result of relatively constant flow discharge. The competing influences of small events and large events at short time intervals on the correlation seen for time lapse also occur in the *CUSP* correlations.

Table C.2 Correlation between *CUSP* per Event and Event Magnitude

Run	Correlation Coefficient	r^2
A	-0.26	0.07
B	-0.22	0.05
D	-0.17	0.03
E	-0.16	0.02
G	0.20	0.04

C.4 Probability of Event Occurrence Supplement

The probability of event occurrence is expressed by the continuous random variable E_e , *CUSP* between events. The possible values of E_e lie in the domain from near 0 to infinity. The empirical cumulative distribution functions (CDF) of the results of Runs A, B, D, E, and G were used to accurately fit appropriate probability distributions to the empirical distributions. An example empirical distribution is shown for Run A (Figure C.3). The cumulative distribution describes the probability of the random variable being equal to or less than a given value. For the empirical data, the CDF expresses the probability of an event occurring after a certain *CUSP* has occurred. The lognormal distribution appeared to fit best with the data from all runs. This is theoretically an appropriate distribution because by definition the dataset has only positive real numbers representing time measurements between events. The lognormal

distribution fitted to each dataset uses the mean and standard deviation of the natural logarithmic transform of the dataset.

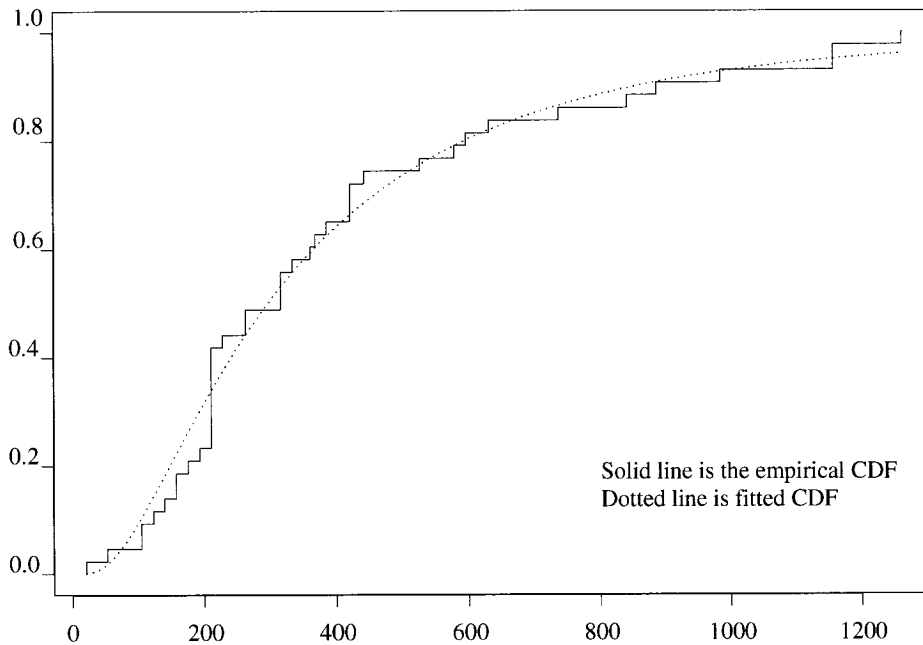


Figure C.3 Empirical CDF and Fitted (Hypothesized) Lognormal CDF - Run A

The Kolmogorov-Smirnov goodness of fit test (KS GOF) was applied to each fitted distribution to assess fit of lognormal distribution to the data (S-Plus, 2005). The KS GOF alternative hypothesis is that at least one data point does not match the fitted distribution and thus a high p-value indicates not to reject the null hypothesis that the fitted distribution describes the empirical dataset. The KS GOF results for all runs support the hypothesis that the fitted distribution describes the empirical data (Table C.3).

Table C.3 KS GOF for Fitted CDF to *CUSP* per Event by Run

Run	KS Statistic	p-value
A	0.1064	0.676
B	0.1424	0.663
D	0.1453	0.152
E	0.1077	0.916
G	0.5877	0.155

Usage of standard methods such as analysis of variance requires the data to be normally distributed. The *CUSP* data are accurately described by a lognormal distribution, so a natural log transform was applied to the data for comparisons between runs and by the width and joint spacing groupings. A comparison of means between runs using the lognormal transformed data validated a normal distribution assumption (Table C.4). A comparison of means and standard deviations of the lognormal-transformed data shows the means and standard deviations of Runs A and B to be closer in value and greater than those of Runs D, E, and G. Comparison of the variances and sample size by run shows differences that may be significant. Levene's test for homogeneity of variances detected significant difference in variances between runs (Table C.5). Both unequal variances and sample sizes are violations of assumptions necessary for confident use of statistical multiple comparisons methods such as Tukey (S-Plus, 2005). However, robust analysis of variance and multiple comparison methodologies such as Welch (Table C.6), respectively, may be used with confidence when there are unequal variances between runs as well as unequal sample sizes (S-Plus, 2005). Exploratory descriptive comparisons were also made graphically between the empirical CDFs of each run and using the KS GOF test to determine whether the actual distributions appear to differ. The results of the KS GOF test support the general observation that the empirical CDFs of Runs A and B differ significantly from Runs D, E, and G (Table C.8).

Table C.4 *CUSP* per Event by Run

Run	N	Mean ln (<i>CUSP</i> per Event)	Std. Dev.	<i>CUSP</i> per Event
A	43	5.69	0.826	296
B	24	5.80	1.179	330
D	61	4.43	1.801	84
E	24	4.63	1.600	102
G	23	4.46	1.804	86

Table C.5 Levene's Test of Homogeneity of Variances for ln (CUSP per Event)

Levene Statistic	df1	df2	Significance
0.920	4	170	0.000

Table C.6 Welch's Robust Test of Equality of Means for ln (CUSP per Event)

Welch Statistic	df1	df2	Significance
9.054	4	64.089	0.000

Table C.7 Multiple Comparisons by Run of ln (CUSP per Event) using Dunnett's C

(I) Run	(J) Run	Mean Difference (I-J)	Std. Error	90% Confidence Interval	
				Lower Bound	Upper Bound
A	B	-0.10729	0.27175	-0.8143	0.5997
	D	1.26584(*)	0.26276	0.6025	1.9292
	E	1.06198(*)	0.35010	0.1490	1.9750
	G	1.23182(*)	0.39672	0.1937	2.2699
B	A	0.10729	0.27175	-0.5997	0.8143
	D	1.37312(*)	0.33336	0.5164	2.2299
	E	1.16927(*)	0.40577	0.1072	2.2313
	G	1.33910(*)	0.44662	0.1678	2.5104
D	A	-1.26584(*)	0.26276	-1.9292	-0.6025
	B	-1.37312(*)	0.33336	-2.2299	-0.5164
	E	-0.20386	0.39981	-1.2372	0.8295
	G	-0.03402	0.44121	-1.1793	1.1113
E	A	-1.06198(*)	0.35010	-1.9750	-0.1490
	B	-1.16927(*)	0.40577	-2.2313	-0.1072
	D	0.20386	0.39981	-0.8295	1.2372
	G	0.16983	0.49819	-1.1362	1.4759
G	A	-1.23182(*)	0.39672	-2.2699	-0.1937
	B	-1.33910(*)	0.44662	-2.5104	-0.1678
	D	0.03402	0.44121	-1.1113	1.1793
	E	-0.16983	0.49819	-1.4759	1.1362

* The mean difference is significant at the 0.10 level.

Table C.8 KS GOF Comparison of Fitted CDFs of CUSP per Event by Run

Comparison	KS Statistic	p-value
A-B	0.244	0.2608
A-D	0.413	0.0002
A-E	0.522	0.0002
A-G	0.562	0.0001
B-D	0.413	0.0036
B-E	0.542	0.0014
B-G	0.529	0.0018
D-E	0.184	0.5016
D-G	0.206	0.3847
E-G	0.192	0.6860

The multiple comparison results show greatest differences between the grouping of Runs A and B and the grouping of Runs D, E, and G (Table C.7). The statistic in the multiple comparisons is significant at the 95% level for all but the comparison of Run B and Run E (significant at 94%). The graphical displays of the comparisons clearly show that there is diminished difference between runs within these two groups, but an observably greater difference when comparing runs between groups (Figure 3.38). In particular, the mean *CUSP* required for event occurrence is greater in Runs A and B than in Runs D, E, and G but similar within each grouping, as noted earlier in the comparison of means.

The only major difference between these two groupings is channel width. The stark difference between groups suggests channel width plays an important role in determining the amount of expended energy necessary for event occurrence. The empirical mean and standard deviation of the lognormal-transformed data for each channel width group was compared next (Table C.9).

Table C.9 *CUSP* per Event by Channel Width Groups

Group	Mean ln(<i>CUSP</i> per Event)	Std. Dev.	<i>CUSP</i> per Event
Narrow (A, B)	5.73	0.960	308
Wide (D, E, G)	4.48	1.745	88
		Ratio	3.50

After back-transforming the mean of the log transformed data, mean *CUSP* values are 308 kJ/m² for the narrow channel and 88 kJ/m² for the wide channel grouping. The ratio between the calculated *CUSP* for the narrow flume and the wide flume is 3.5:1, meaning 3.5 times more energy was expended on average per event in the narrow flume runs than in the wide flume runs. Intriguingly, the ratio between narrow and wide channel widths is 1:2 and this energy difference occurs with measured higher flow depths and calculated shear stresses for the narrow flume runs versus the wide flume runs.

The ratio of 1:2 seen in the flume widths and the ratio of 3.5:1 seen in the *CUSP* calculations requires more exploration. The unit stream power, ω , calculation includes the width through the calculation of hydraulic radius. Assuming the hydraulic radius is equal to channel width and using the same discharge, water density, and bed slope, the ratio of ω between narrow and wide flumes where W is the width of the narrow flume is:

Equation C.47

$$\frac{\omega_{\text{narrow}}}{\omega_{\text{wide}}} = \frac{\left(\frac{\rho g QS}{W}\right)}{\left(\frac{\rho g QS}{2W}\right)} = 2$$

and the ratio of total stream power, Ω , between narrow and wide flumes is:

Equation C.48

$$\frac{\Omega_{\text{narrow}}}{\Omega_{\text{wide}}} = \frac{\rho g QS}{\rho g QS} = 1$$

If the expended discharge, $Q \Delta t$ between events on average is the same for narrow and wide flumes then the *CUSP* and *CTSP* ratios will be 2:1 and 1:1, respectively. The experimental *CUSP* ratio is 3.5:1, indicating there is a difference in $Q \Delta t$ per event, the expended discharge per event. The mean *CTSP* per event was calculated for the flume channel width groups using the log-transformed data (Table C.10 and Table C.11).

Table C.10 *CTSP* per Event by Run

Run	Mean ln(<i>CTSP</i> per Event)	Std. Dev.	<i>CTSP</i> per Event
A	5.63	0.826	279
B	5.69	1.161	295
D	4.70	1.802	110
E	4.93	1.604	138
G	4.75	1.804	116

Table C.11 *CTSP* per Event by Channel Width Groups

Group	Mean ln(<i>CTSP</i> per Event)	Std. Dev.	<i>CTSP</i> per Event
Narrow (A, B)	5.65	0.951	285
Wide (D, E, G)	4.76	1.747	117
		Ratio	2.43

After back-transforming the mean of the log transform of the data, the mean *CTSP* per event is 285 kJ/m² for the narrow channel and 117 kJ/m² for the wide channel. The ratio between the mean *CTSP* for the narrow and the wide channel widths is 2.43:1, indicating that 2.43 times more energy was expended on average per event in the narrow than in the wide channel width runs. The theoretical ratio of 1:1 was calculated where group widths differ but mean *CTSP* per event is the same, which differs from the observed ratio of 2.43:1. This suggests some effect is leading to differences in expended stream power per event between the groupings.

The only variable in the calculation of *CTSP* possibly differing between groups is mean expended discharge, $Q \Delta t$ between events. The discharge was held fairly constant between runs except for Run B, which had a lower average discharge of 0.11 m³/s most of the time. Runs with the same discharge but different flume width such as Run A and Run G are in differing groups. Time elapsed between events rather than the discharge rate may explain the differences in energy expenditure per event. The mean time lapse between events for the log-transformed data was compared by run and channel width groups (Table C.12).

Table C.12 Time Lapse Between Events by Channel Width Groups

Group	Mean ln(Time Lapse Between Events)	Std. Dev.	Time Lapse Between Events (hrs.)
Narrow (A, B)	0.52	1.036	1.7
Wide (D, E, G)	-0.46	1.721	0.6
		Ratio	2.66

After back-transforming the means of the lognormal data, the mean time lapse is 1.7 hr for the narrow and 0.6 hr for the wide channel width. The ratio between the mean time lapse for the narrow flume and the wide flume is approximately 2.66:1, indicating that approximately 2.66 times as much time elapsed between events on average in the narrow

channel width runs as in the wide channel width runs. This closely matches the observed ratio for *CTSP* of 2.5:1, but the theoretical ratio for *CUSP* is twice the ratio of *CTSP* at 4.86:1 given a calculated *CTSP* ratio of 2.43:1.

To provide an explanation, recall from the calculation for *CUSP* that the hydraulic radius, Q , and time were used. The equations for *CUSP* and *CTSP* are decomposed into a set of ratios between the two channel width groupings.

Equation C.49

$$\begin{aligned} \text{CUSP Ratio} &= \frac{E \left[\frac{\rho g Q S_b}{R_h} \Delta t \right]_{\text{narrow}}}{E \left[\frac{\rho g Q S_b}{R_h} \Delta t \right]_{\text{wide}}} \\ &= \frac{\text{Ratio} [Q \Delta t]_{\text{narrow:wide}}}{\text{Ratio} [R_h]_{\text{narrow:wide}}} \text{ or } \frac{\text{Ratio} [Q]_{\text{narrow:wide}} \text{Ratio} [\Delta t]_{\text{narrow:wide}}}{\text{Ratio} [R_h]_{\text{narrow:wide}}} \end{aligned}$$

Equation C.50

$$\begin{aligned} \text{CTSP Ratio} &= \frac{E [\rho g Q S_b \Delta t]_{\text{narrow}}}{E [\rho g Q S_b \Delta t]_{\text{wide}}} \\ &= \frac{E [Q \Delta t]_{\text{narrow}}}{E [Q \Delta t]_{\text{wide}}} \\ &= \text{Ratio} [Q \Delta t]_{\text{narrow:wide}} \text{ or } \text{Ratio} [Q]_{\text{narrow:wide}} \text{Ratio} [\Delta t]_{\text{narrow:wide}} \end{aligned}$$

The low width to depth ratios observed suggest width might not be equivalent to hydraulic radius, so hydraulic radius is used in the calculation of unit stream power instead of width alone. The mean hydraulic radius was calculated for the two flume width groups for the log-transformed data (Table C.13).

Table C.13 Hydraulic Radius (R_h) by Channel Width Groups

Group	Mean $\ln(R_h)$	Std. Dev.	R_h (m)
Narrow (A, B)	-0.078	0.0315	0.93
Wide (D, E, G)	0.285	0.0110	1.33
		Ratio	0.70

The ratio between flume width groups is approximately 0.7:1, equivalent to 1:2.05 as expected based on the ratio of flume widths under the assumption of equal expended discharge per event. Flume width dominates the hydraulic radius, with a small contribution from flow depth, as seen in comparing the hydraulic radii and flume widths of 0.61 m and 1.17 m for narrow and wide flume channels, respectively.

Building on the ratio of time lapse, the ratios of the expended discharge per event, $Q \Delta t$ and average discharge experienced during Δt , Q were compared by the two channel width groupings (Table C.14 and Table C.15).

Table C.14 Cumulative Discharge per Event ($Q\Delta t$) by Channel Width Groups

Group	Mean $\ln(Q \Delta t)$	Std. Dev.	$Q \Delta t$
Narrow (A, B)	-1.28	0.951	0.278
Wide (D, E, G)	-2.17	1.747	0.114
		Ratio	2.43

Table C.15 Discharge (Q) Between Events by Channel Width Groups

Group	Mean $\ln(Q)$	Std. Dev.	Q
Narrow (A, B)	-1.80	0.244	0.17
Wide (D, E, G)	-1.71	0.210	0.18
		Ratio	0.91

The individual variable ratios from the decomposition of the stream power ratios were substituted into the ratios of *CUSP* and *CTSP* and compared with the overall ratios of 3.42 for *CUSP* ratio and 2.43 for *CTSP* ratio.

Equation C.51

$$\begin{aligned} \text{CUSP Ratio of 3.42} &= \frac{\text{Ratio } [Q \Delta t]_{\text{narrow:wide}}}{\text{Ratio } [R_h]_{\text{narrow:wide}}} \text{ or } \frac{\text{Ratio } [Q]_{\text{narrow:wide}} \text{ Ratio } [\Delta t]_{\text{narrow:wide}}}{\text{Ratio } [R_h]_{\text{narrow:wide}}} \\ &= \frac{2.43}{0.711} \text{ or } \frac{(0.91)(2.66)}{0.711} \\ &= 3.42 \end{aligned}$$

Equation C.52

$$\begin{aligned} \text{CTSP Ratio of 2.43} &= \text{Ratio } [Q \Delta t]_{\text{narrow:wide}} \text{ or } \text{Ratio } [Q]_{\text{narrow:wide}} \text{ Ratio } [\Delta t]_{\text{narrow:wide}} \\ &= 2.43 \end{aligned}$$

The overall ratio and product of ratios from the decomposition of the *CUSP* and *CTSP* ratios are equal, as expected. Time lapse, Δt and hydraulic radius, R_h (\sim channel width) are the dominant factors differing between groups, with a minor contribution from differences in mean Q between events. The contribution from time lapse with ratio of 2.66:1 suggests a difference in energy expenditure necessary for erosion despite nearly equal discharge expenditure at a ratio of 0.91:1. Such differences are seen between individual runs with the same discharge and joint spacing but different widths; e.g., Run A and Run D. Runs within the same width grouping but with different joint spacing are not significantly different; e.g., Run E and Runs D.

To model mean energy expenditure and further demonstrate the negligible effects of joint spacing, a robust analysis of variance of the dummy variables channel width, joint spacing, and their interaction term on the log transform of *CTSP* per event was done. *CTSP* was used instead of *CUSP* because channel width is used in the calculation of *CUSP*. The analysis of variance (AOV) tables from the regressions using full and reduced models show channel width with significant correlation to *CTSP* per event whereas joint spacing and the interaction term had insignificant p-values (Table C.16 and Table C.17).

Full Model:

Equation C.53

$$\ln(T_e) = \beta_0 + \beta_1 \ln(W) + \beta_2 J$$

Table C.16 AOV of Full Model of *CTSP* per Event

Variable	df	Sum of Squares	F	p-value
$\ln(W)$	1	141.9518	5.4759	0.0171
J	1	0.0394	0.0024	0.9599
Residuals	172	403.487		

Reduced Model:

Equation C.54

$$\ln(T_e) = \beta_0 + \beta_1 \ln(W)$$

Table C.17 AOV of Reduced Model of CTSP per Event

Variable	df	Sum of Squares	F	p-value
$\ln(W)$	1	142	5.4759	0.0171
Residuals	173	403.4891		

The joint factor is fairly insignificant with a p-value of nearly 1. The reduced model includes only the width term. As expected, channel width is a significant term in explaining the measured expended energy necessary for event occurrence. Channel width was a significant indicator of the energy expenditure per event but there remains much unexplained random variation in the residuals with several outliers after accounting for width (Figure C.4).

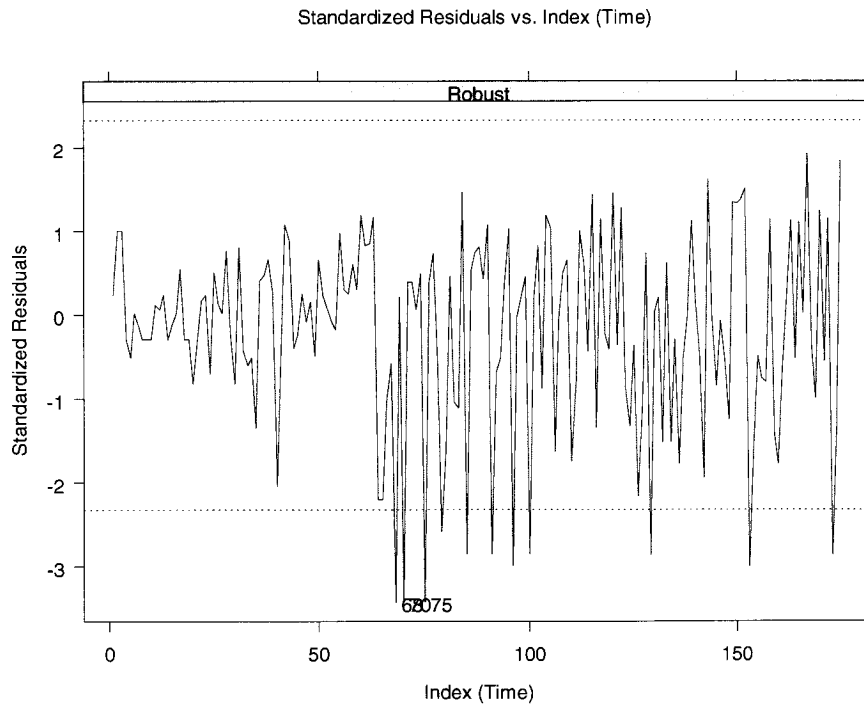


Figure C.4 Standardized Residuals for Reduced Model of CTSP per Event

The greatest difference between width groups was time lapse between events, which deserves greater attention. Recall from the equations for *CUSP* and *CTSP* that discharge, time lapse, and hydraulic radius are the main parameters. Much of the variation in *CUSP* and *CTSP* results from variation in time lapse between events because time lapse was the most variable parameter within runs. The time lapse data were log transformed as previously done with *CUSP* and *CTSP* to satisfy the near-normal distribution assumption. A comparison of means suggests differences between width groups but similarity within width groups, although there is greater variation within groups than seen with *CTSP* or *CUSP* (Figure C.5 and Table C.18).

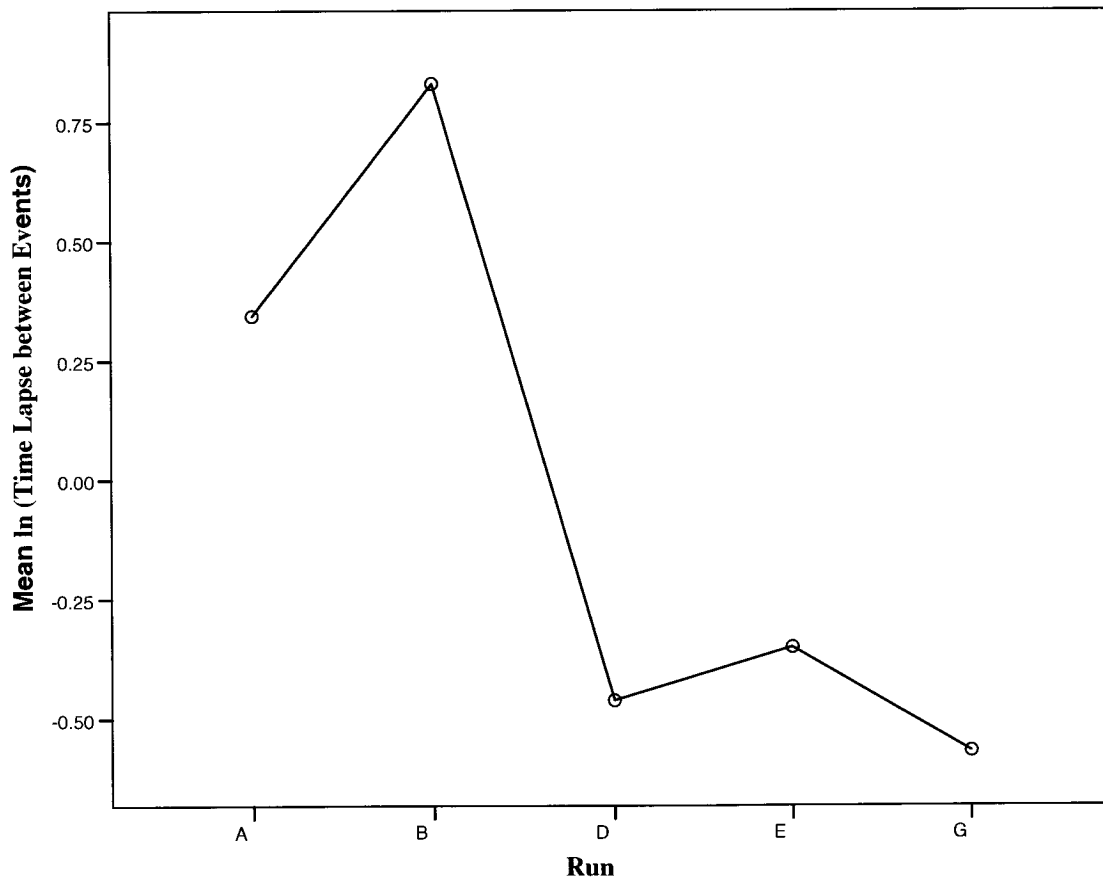


Figure C.5 Comparison of Mean ln(Time Lapse Between Events) by Run

Levene's test for homogeneity of variances detected significant difference in variances between runs so multiple comparison between runs of the log-transformed time lapse between events was done with the same robust methods previously used (Table C.19 to Table C.22). There are significant differences between runs in different channel width groups but none within channel width groups. Run A was found to be marginally but not significantly different from the runs with wide channel width at the 90% level but the difference is much greater than Run A and Run B in the same channel width group. Channel width again appears to be a dominant factor differentiating runs.

Table C.18 Descriptive Statistics of Time Lapse Between Events by Run

Run	N	Mean ln(Time Lapse Between Events)	Std. Dev.	Time Lapse Between Events (hrs)
A	43	0.3432	0.826	1.41
B	24	0.8304	1.293	2.29
D	61	-0.4624	1.773	0.63
E	24	-0.3509	1.562	0.70
G	175	-0.5683	1.804	0.57

Table C.19 Levene's Test of Homogeneity of Variances for ln(Time Lapse Between Events) by Run

Levene Statistic	df1	df2	Significance
6.758	4	170	0.000

Table C.20 Welch Robust Test of Equality of Means for ln(Time Lapse Between Events) by Run

Welch Statistic	df1	df2	Significance
5.426	4	63.679	0.001

Table C.21 ANOVA for ln(Time Lapse Between Events) by Run

Source	Sum of Squares	df	Mean Square	F	Sig.
Between Groups	43.75	4	10.937	4.848	0.001
Within Groups	383.495	170	2.256		
Total	427.245	174			

Table C.22 Multiple Comparisons by Run of ln(Time Lapse Between Events) using Dunnett's C

(I) Run	(J) Run	Mean Difference (I-J)	Std. Error	90% Confidence Interval	
				Lower Bound	Upper Bound
A	B	-0.48717	0.29246	-1.2487	0.2743
	D	0.80556(*)	0.25968	0.1499	1.4612
	E	0.69412	0.34275	-0.1996	1.5878
	G	0.91150	0.39672	-0.1266	1.9496
B	A	0.48717	0.29246	-0.2743	1.2487
	D	1.29273(*)	0.34814	-0.3961	2.1893
	E	1.18129(*)	0.41382	0.0982	2.2644
	G	1.39867(*)	0.45952	0.1937	2.6037
D	A	-0.80556(*)	0.25968	-1.4612	-0.1499
	B	-1.29273(*)	0.34814	-2.1893	-0.3961
	E	-0.11143	0.39134	-1.1227	0.8998
	G	0.10594	0.43938	-1.0349	1.2468
E	A	-0.69412	0.34275	-1.5878	0.1996
	B	-1.18129(*)	0.41382	-2.2644	-0.0982
	D	0.11143	0.39134	-0.8998	1.1227
	G	0.21738	0.49305	-1.0752	1.5100
G	A	-0.91150	0.39672	-1.9496	0.1266
	B	-1.39867(*)	0.45952	-2.6037	-0.1937
	D	-0.10594	0.43938	-1.2468	1.0349
	E	-2.738	0.49305	-1.5100	1.0752

* The mean difference is significant at the 0.10 level.

The mean ln(Discharge Between Events) was calculated for each run (Table C.23).

Comparison of means show Runs A, D, E, and G have similar values at approximately 0.2 m³/s, whereas Run B has a lower mean at approximately 0.1 m³/s.

Table C.23 Comparison of Discharge Between Events by Run

Run	Mean ln(Discharge Between Events)	N	Std. Dev.
A	-1.6428	43	0.00000
B	-2.0740	24	0.21371
D	-1.7664	61	0.25386
E	-1.6516	24	0.12820
G	-1.6132	23	0.00000
Total	-1.7423	175	0.22715

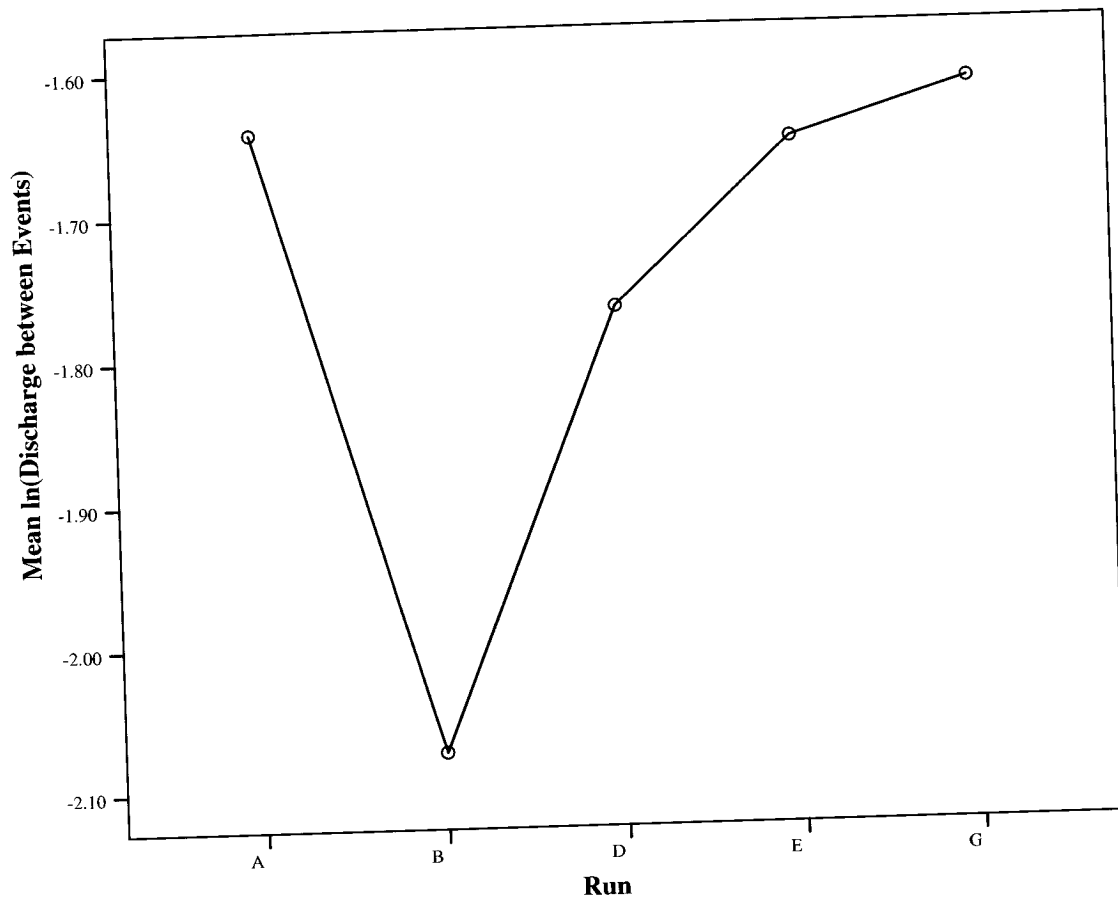


Figure C.6 Comparison of Mean ln(Discharge Between Events) by Run

Runs A and B have similar *CUSP* and *CTSP* values despite having significantly different mean discharge values. Run B does have a higher mean time lapse between events than Run A, although not significantly higher, while having a lower mean discharge. The mean time lapse between events in Run D was slightly higher than Run G, which has similar channel width and joint spacing but different mean discharge. The mean time lapse between events for Run E is slightly higher than Run G, which has higher discharge.

Although not statistically significant in determining mean energy expenditure per event, joint spacing hypothetically may also play a role in the differences in time lapse

between events based on the analysis of forces. The mean time lapse between events for channel width and joint spacing groupings were compared (Table C.24). The combinations of channel width and joint spacing were ranked from highest to lowest mean time lapse between events (Table C.25).

Table C.24 Comparison of Time Lapse Between Events by Width and Joint Groupings

Channel Width (m)	Joint spacing (m)	Mean Time Lapse Between Events (hrs.)	N	Std. Dev.
0.61	0.03	0.34	43	0.82635
	0.06	0.83	24	1.29291
	Total	0.52	67	1.03560
1.17	0.03	-0.49	84	1.77151
	0.06	-0.35	24	1.56150
	Total	-0.46	108	1.72102
Total	0.03	-0.21	127	1.56592
	0.06	0.24	48	1.53868
	Total	-0.09	175	1.56698

Table C.25 Ranking of Width and Joint Spacing Groups by Time Lapse Between Events. Highest rank is 1

Rank	Channel Width (m)	Joint Spacing (m)	Mean Time Lapse Between Events (hrs.)
1	1.17	0.03	0.61
2	1.17	0.06	0.70
3	0.61	0.03	1.41
4	0.61	0.06	2.29

The greater difference by a factor of more than two is between channel width groupings. Interestingly, the narrower joint spacing in both channel width groupings resulted in lower time lapse between events although not as significantly as for channel width. The greater difference within the narrow width grouping may result from the lower mean discharge in Run B leading to higher time lapse between events. Similarly, the smaller difference between Run E and Runs D and G may result from more similar discharge regimes. Using the relationship between higher discharge and lower time lapse between events, the lower mean discharge in Run D compared to Run G may cause the slightly higher mean time lapse between events during Run D compared to Run G.

The dependency of lapse time on width, joint spacing, and mean discharge was further examined by a robust analysis of variance, where lapse is the dependent variable and width, joint spacing, and mean discharge are main effects (Table C.26).

Full Model:

Equation C.55

$$\ln(T_t) = \beta_0 + \beta_1 \ln(W) + \beta_2 J + \beta_3 \ln(Q)$$

Table C.26 Robust ANOVA for Full Model of Time Lapse Between Events

Coefficients:	Value	Std. Error	t value	p-value
Intercept	-2.4462	0.796	-3.0733	0.0025
$\ln(W)$	-0.6836	0.3165	-2.1597	0.0322
J	-3.822	7.7547	-0.4929	0.6227
$\ln(Q)$	-1.5532	0.4885	-3.1794	0.0018

Residual standard error:	1.3
Proportion of variation in response(s) explained by model:	0.08107

Terms Added Sequentially	df	Robust F Statistic	Pr(F)
Intercept	1		
$\ln(W)$	1	8.29867	0.0033295
J	1	0.452468	0.4930551
$\ln(Q)$	1	7.886509	0.0042133

Bias Test for Robust Models	Statistics	p-value
M-estimate	1.06	0.90062
LS-estimate	15.13	0.00445

Joint spacing was the least significant effect in the full model, with p-value greater than 0.10. Note that although the coefficient on joint spacing effect is negative, the opposite of the influence indicated earlier, the standard error is nearly twice the value of the coefficient, which indicates a possible positive value for the coefficient. A reduced model with only width and mean discharge was subsequently constructed (Table C.27). Both width and mean discharge are significant in the model, with p-values less than 0.05.

However, both models explain only 8% of the variation seen in the data. The high variation in the data is not sufficiently explained by the model for predicting time lapse with any confidence.

Reduced Model:

Equation C.56

$$\ln(T_i) = \beta_0 + \beta_1 \ln(W) + \beta_2 \ln(Q)$$

Table C.27 Robust ANOVA for Reduced Model of Time Lapse Between Events

Coefficients:	Value	Std. Error	t value	p-value
Intercept	-2.4353	0.8289	-2.9381	0.0038
$\ln(W)$	-0.6895	0.3303	-2.0871	0.0384
$\ln(Q)$	-1.4632	0.4787	-3.0569	0.0026

Residual standard error:	1.29
Proportion of variation in response(s) explained by model:	0.08048

Terms Added Sequentially	df	Robust F Statistic	Pr(F)
Intercept	1		
$\ln(W)$	1	8.29867	0.0033295
$\ln(Q)$	1	8.502548	0.0029644

Bias Test for Robust Models	Statistics	p-value
M-estimate	1.4	0.70511
LS-estimate	14.7	0.00205

Despite the large variation in the data and resulting low predictive power of the model, our analysis qualitatively consistently links channel width, joint spacing, and mean discharge to time lapse between events. The analysis of variance provides some additional quantitative support for the influence of channel width and mean discharge on time lapse between events where increases in both result in lowering of time lapse. However, the predictive power of our model is lower than desired.

Recall that time lapse between events can be measured in terms of energy expenditure as *CTSP* or *CUSP*. Both energy expenditure measurements involve the integration of discharge over the time lapse between events. A higher time lapse between events or a higher mean discharge between events may result in higher energy expenditures. The direct correlation seen in our results between mean discharge and mean time lapse suggests an interaction between the two factors. This may be expressed in *CTSP* and *CUSP* by the integration of discharge over the time lapse between events term. A lower discharge will result in greater time lapse between events and vice versa given the same width. In the reduced model for time lapse as function of channel width and mean discharge, the relationship is augmented by the coefficient on the discharge effects of -1.46, which means that in the model a 1% change in discharge results in a -1.44 % change in time lapse between events (Table C.27). Increases in width decrease time lapse between events and energy expenditure given the same discharge. The expression for *CUSP* has channel width in the denominator, indicating higher width results in lower *CUSP*, all else being equal, in a manner similar to the effects seen in our results. The coefficient on the channel width term for the reduced model of time lapse is -0.69, meaning a 1% change in channel width results in a -0.68% change in time lapse between events (Table C.27).

C.5 Probability of Event Magnitude Supplement

A similar approach will be taken with the magnitude data as was used for the event occurrence probability analysis. First, cumulative density plots of the data were examined and a suitable probability distribution chosen. Further analysis compared

means between runs with particular attention to groupings by joint spacing and channel width.

For the empirical data, the CDF expresses the probability of equal or lesser event magnitude by volume when an event occurs. The possible values of volume lie in the domain from near 0 to infinity. The lognormal distribution appeared to best fit the data from all runs (e.g., Figure C.7 and Figure C.8). The lognormal distribution fit to each dataset uses the mean and standard deviation of the natural logarithm transform of the dataset (S-Plus, 2005).

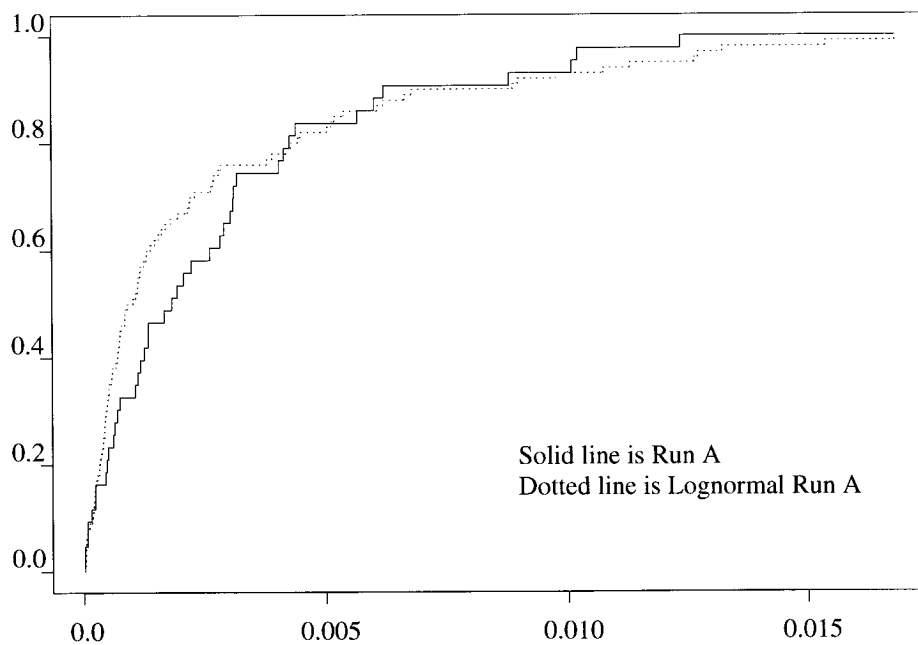


Figure C.7 Empirical Normal and Lognormal CDFs for Event Volume - Run A

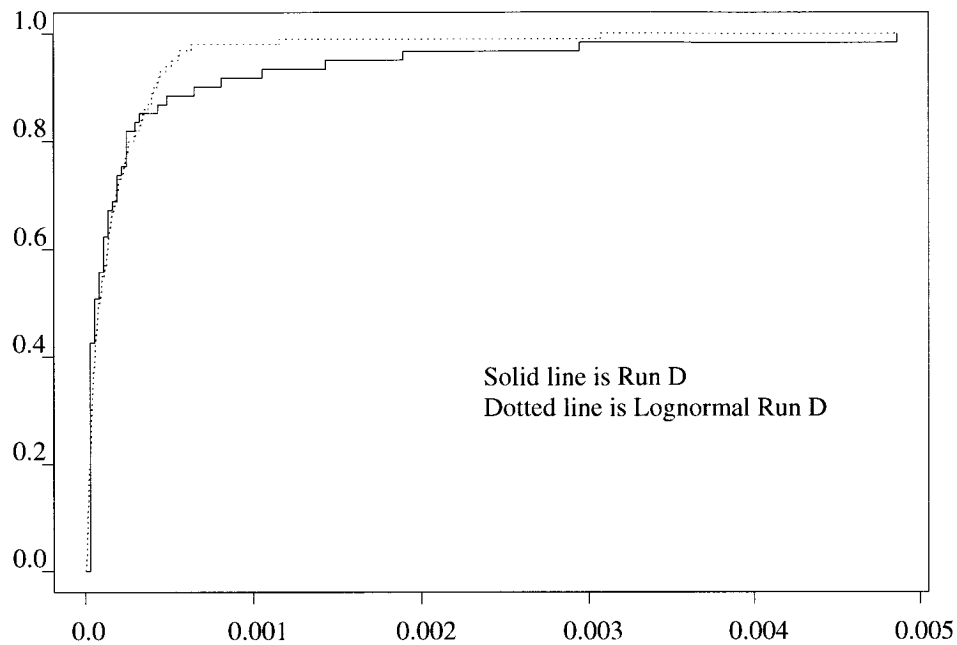


Figure C.8 Empirical Normal and Lognormal CDFs for Event Volume - Run D

The KS goodness of fit test was done on each fitted distribution to provide further support for fitting a lognormal distribution to the data (Table C.28) (S-Plus, 2005). The alternative hypothesis for the KS GOF is that at least one data point does not fit the distribution, so a high p-value indicates not to reject the null hypothesis that the fitted distribution describes the empirical dataset. The results of the KS GOF for all runs with the exception of Run D support the statement that the fitted distribution describes the empirical data.

Table C.28 KS GOF for Fitted CDF of Event Volume by Run

Run	KS Statistic	p-value
A	0.121	0.514
B	0.133	0.738
D	0.238	0.002
E	0.236	0.117
G	0.250	0.095

However, a visual comparison of the CDF of Run D and the fitted lognormal distribution supports the hypothesis that the fitted lognormal distribution describes the empirical CDF of Run D (Figure C.8).

A comparison of means between runs using the lognormal transform of the data was done to satisfy the assumption of a normal distribution in multiple comparison methods. A comparison of the means and standard deviations of the log-transform data for each run shows the means of Runs A and B appear to be nearly equal and greater than those of Runs D, E, and G (Table C.29 and Figure C.9).

Table C.29 Descriptive Statistics for Event Volume by Run

Run	Mean ln(Event Volume)	Std. Dev.	N	Event Volume (cm ³)
A	-6.63	1.507	43	1322
B	-5.53	1.512	24	3954
D	-9.30	1.381	61	92
E	-7.36	1.633	24	634
G	-9.30	1.449	23	91

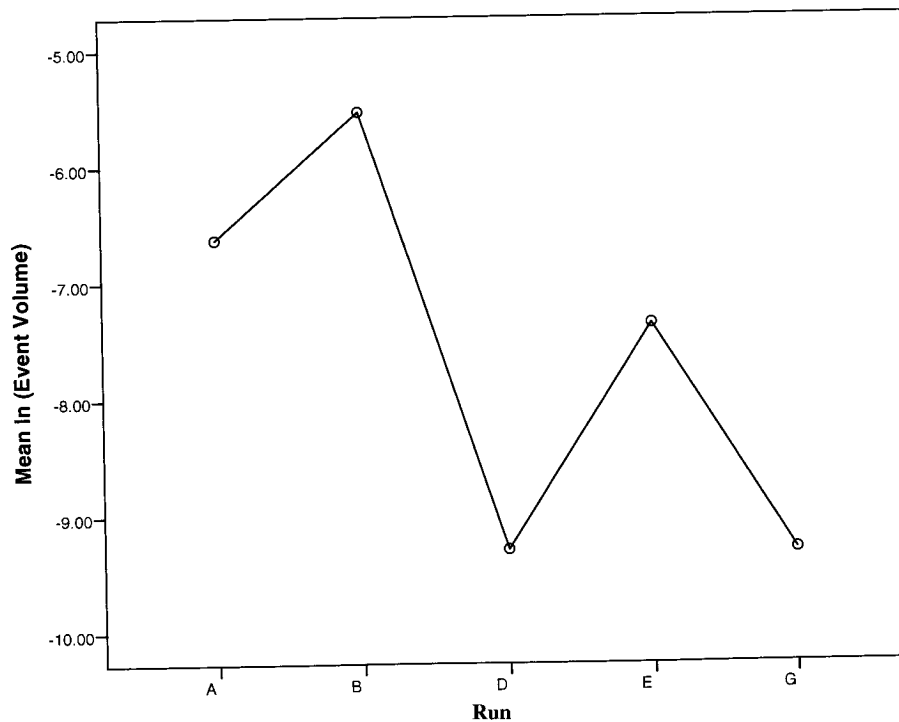


Figure C.9 Comparison of Mean ln(Event Volume) by Run

Levene's test for homogeneity of variances confirms that the equal variance assumption is valid despite different sample sizes (Table C.30). ANOVA and Welch robust test of equality of means indicate significant differences between runs (Table C.31 and Table C.32). Comparisons were also made between the empirical CDFs of each run graphically and using the KS GOF test with similar results (Table C.33). Multiple comparisons were conducted using Tukey and robust Dunnett's C because of unequal sample sizes (Table C.34). A comparison of the results between Tukey and Dunnett's C method show the same significance results, suggesting the lack of equal sample size was not a significant bias.

Table C.30 Levene's Test of Homogeneity of Variances for ln(Event Volume) by Run

Levene Statistic	df1	df2	Sig.
0.637	4	170	0.637

Table C.31 ANOVA for ln(Event Volume)

Source	Sum of Squares	df	Mean Square	F	Sig.
Between Groups	375.123	4	93.781	43.083	0.000
Within Groups	370.044	170	2.177		
Total	745.168	174			

Table C.32 Welch Robust Test of Equality of Means for ln(Event Volume) by Run

Welch Statistic	df1	df2	Sig.
42.589	4	65.805	0.000

Table C.33 KS GOF Comparison of ln (Event Volume) by Run

Comparison	KS Statistic	p-value
A-B	0.379	0.017
A-D	0.706	0.000
A-E	0.296	0.105
A-G	0.663	0.000
B-D	0.811	0.000
B-E	0.542	0.001
B-G	0.784	0.000
D-E	0.557	0.000
D-G	0.101	0.978
E-G	0.652	0.000

Table C.34 Multiple Comparisons by Run of ln(Event Volume) using Tukey and Dunnett's C

Method	(I) Run	(J) Run	Mean Difference (I-J)	Std. Error	Sig.	90% Confidence Interval	
						Upper Bound	Lower Bound
Tukey HSD	A	B	-1.09591(*)	0.37592	0.032	-2.0283	-0.1635
		D	2.66905(*)	0.29378	0.000	1.9404	3.3977
		E	0.73410	0.37592	0.294	-0.1983	1.6665
		G	2.67476(*)	0.38113	0.000	1.7295	3.6200
	B	A	1.09591(*)	0.37592	0.032	0.1635	2.0283
		D	3.76496(*)	0.35550	0.000	2.8832	4.6467
		E	1.83000(*)	0.42590	0.000	0.7737	2.8863
		G	3.77067(*)	0.43051	0.000	2.7029	4.8384
	D	A	-2.66905(*)	0.29378	0.000	-3.3977	-1.9404
		B	-3.76496(*)	0.35550	0.000	-4.6467	-2.8832
		E	-1.93495(*)	0.35550	0.000	-2.8167	-1.0532
		G	0.00571	0.36100	1.000	-0.8897	0.9011
	E	A	-0.73410	0.37592	0.294	-1.6665	0.1983
		B	-1.83000(*)	0.42590	0.000	-2.8863	-0.7737
		D	1.93495(*)	0.35550	0.000	1.0532	2.8167
		G	1.94066(*)	0.43051	0.000	0.8729	3.0084
	G	A	-2.67476(*)	0.38113	0.000	-3.6200	-1.7295
		B	-3.77067(*)	0.43051	0.000	-4.8384	-2.7029
		D	-0.00571	0.36100	1.000	-0.9011	0.8897
		E	-1.94066(*)	0.43051	0.000	-3.0084	-0.8729
Dunnett's C	A	B	-1.09591(*)	0.38486		-2.0932	-0.0986
		D	2.66905(*)	0.29003		1.9339	3.4042
		E	0.73410	0.40489		-0.3161	1.7843
		G	2.67476(*)	0.37970		1.6893	3.6602
	B	A	1.09591(*)	0.38486		0.0986	2.0932
		D	3.76496(*)	0.35575		2.8425	4.6874
		E	1.83000(*)	0.45428		0.6410	3.0190
		G	3.77067(*)	0.43199		2.6384	4.9029
	D	A	-2.66905(*)	0.29003		-3.4042	-1.9339
		B	-3.76496(*)	0.35575		-4.6874	-2.8425
		E	-1.93495(*)	0.37733		-2.9144	-0.9556
		G	0.00571	0.35016		-0.9039	0.9153
	E	A	-0.73410	0.40489		-1.7843	0.3161
		B	-1.83000(*)	0.45428		-3.0190	-0.6410
		D	1.93495(*)	0.37733		0.9556	2.9144
		G	1.94066(*)	0.44992		0.7616	3.1198
	G	A	-2.67476(*)	0.37970		-3.6602	-1.6893
		B	-3.77067(*)	0.43199		-4.9029	-2.6384
		D	-0.00571	0.35016		-0.9153	0.9039
		E	-1.94066(*)	0.44992		-3.1198	-0.7616

* The mean difference is significant at the 0.10 level.

The clear associations present in the previous analysis of event occurrence are not present but there are significant differences which deserve further inquiry. Differences between channel width groupings exist but there are also significant differences within groupings (e.g., between Runs A and B). Run D and Run G appear to have very similar distributions with estimated difference of only 0.01 from the multiple comparisons tests and p-value of 0.978 from the KS GOF test. This is expected because Run D and Run G have very similar setups (e.g., similar discharge, width, and joint spacing) but different run times. Non-significant differences from the multiple comparisons tests were between Run A and Run E where both joint spacing and flume width were different. This was a significant difference in the multiple comparisons tests from the KS GOF test, although not as significant as between Run D and Run G. All other combinations that were significantly different in the multiple comparisons results have either different joint spacing but the same channel width (Runs A and D; Runs A and G; Runs B and E) or the same joint spacing but different channel width (Runs A and B; Runs D and G; Runs E and G). Channel width and joint spacing correlate with event magnitude probabilities. The comparison of means by groupings shows differences between both channel width and joint spacing groupings (Table C.35).

Table C.35 Descriptive Statistics for Full Model of Event Volume

Channel Width (<i>W</i>)	Joint Spacing (<i>J</i>)	Mean ln(Event Volume)	Std. Dev.	N
0.61m	0.03m	-6.6289	1.50734	43
	0.06m	-5.5330	1.51219	24
	Total	-6.2363	1.58841	67
1.17m	0.03m	-9.2995	1.39145	84
	0.06m	-7.3630	1.63287	24
	Total	-8.8692	1.65203	108
Total	0.03m	-8.3953	1.90857	127
	0.06m	-6.4480	1.81076	48
	Total	-7.8612	2.06944	175

A linear regression of the dummy variables width, joint spacing, and their interaction term on the log-transform of event volume was done to quantitatively clarify the role of width and joint spacing in event magnitude. The analysis of variance table shows channel width and joint spacing with significant correlation to the log-transform of event volume with p-values of less than 0.0001 (Table C.36). Levene's test for homogeneity of error variances does not invalidate the assumption of equal variances between runs (Table C.37). No significant statistical interaction was detected between channel width and joint spacing (Figure C.10). The channel width term contributes the most with *partial eta squared* of 0.387 whereas the *partial eta squared* for joint spacing is 0.180. *Partial eta squared* gives the contribution of each factor or interaction, taken as if it were the only variable so that it is not masked by any more powerful variable independent of the number of factors. Overall the model has an R-squared value of 0.495 (~ 50%) and significant F value of 84.34.

Full Model of Event Volume:

Equation C.57

$$\ln(V) = \beta_0 + \beta_1 W + \beta_2 J$$

Table C.36 AOV for Full Model of Event Volume

Source	Type III Sum of Squares	df	Mean Square	F	Sig.	Partial Eta Squared
Corrected Model	369.160	2	184.580	84.434	0.000	0.495
Intercept	7116.273	1	7116.273	3255.246	0.000	0.950
W	237.069	1	237.069	108.444	0.000	0.387
J	82.538	1	82.538	37.756	0.000	0.180
Error	376.008	172	2.186			
Total	11559.856	175				
Corrected Total	745.168	174				

R Squared = 0.495 (Adjusted R Squared = 0.490)

Table C.37 Levene's Test of Equality of Error Variances for Full Model of Event Volume

F	df1	df2	Sig.
.850	3	171	0.468

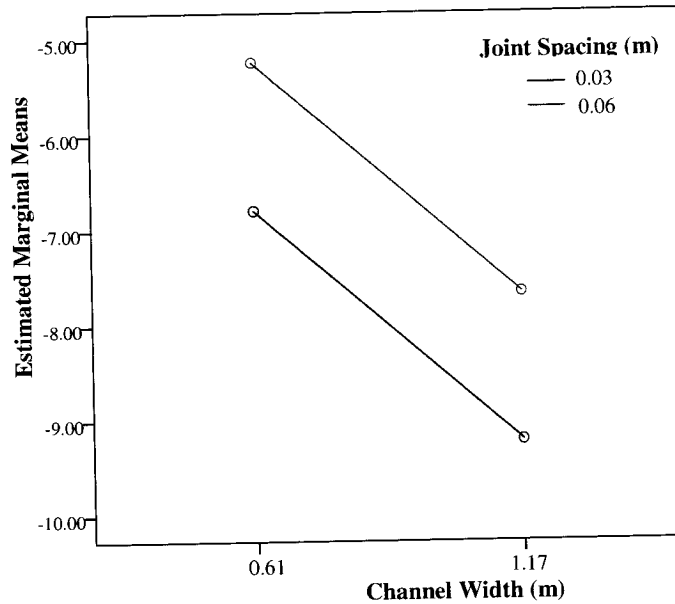


Figure C.10 Estimated Marginal Means of ln(Event Volume) by Channel Width and Joint Spacing

Event magnitude may also be expressed in terms of blocks eroded instead of the total volume of the blocks in the event. Runs were compared using log-transformed event block count data. Comparison of means by run shows similarities between Run A and B and between Run D and G (Table C.38 and Figure C.11). Levene's test for homogeneity of variances confirms that the equal variance assumption is valid despite different sample sizes (Table C.39). ANOVA and Welch robust test of equality of means indicate significant differences between runs (Table C.39 and Table C.40). Multiple comparisons were done using Tukey and Dunnett's C and show the mean event block

counts of Runs A and B to be statistically similar but different from Run D, E, and G, which are similar to each other (Table C.42).

Table C.38 Event Block Count by Run

Run	N	Mean ln(Event Block Count)	Std. Dev.	Block Count
A	43	3.8908	1.50734	49.0
B	24	3.6004	1.51219	36.6
E	61	1.2217	1.38132	3.4
D	24	1.7704	1.63287	5.9
G	23	1.216	1.44937	3.4
Total	175	2.2782	1.89379	9.8

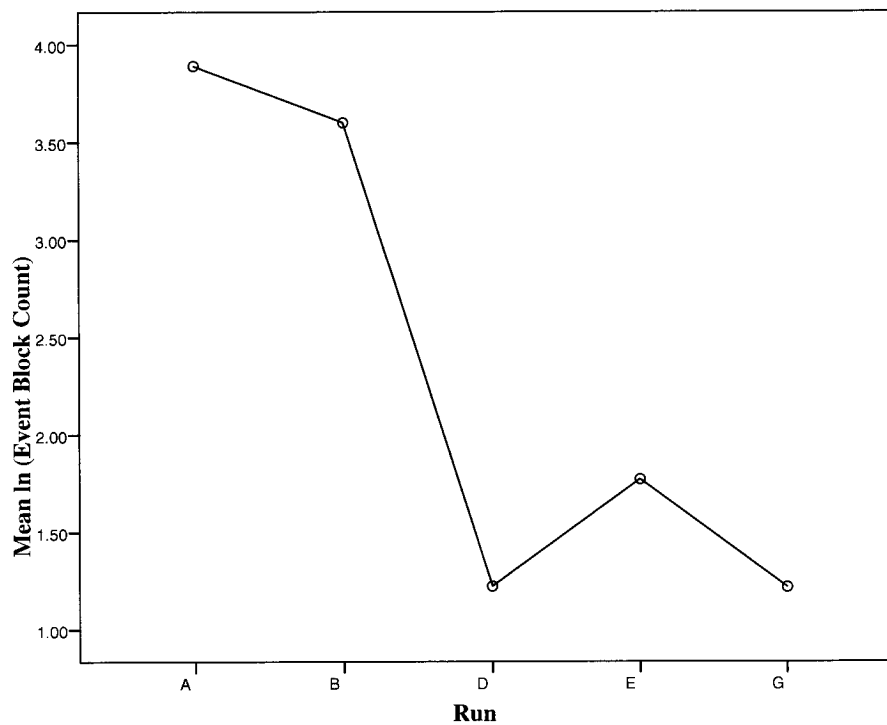


Figure C.11 Comparison of Mean ln(Event Block Count) by Run

Table C.39 Levene's Test of Homogeneity of Variances for ln(Event Block Count) by Run

Levene Statistic	df1	df2	Sig.
0.637	4	170	0.637

Table C.40 ANOVA for ln(Event Block Count) by Run

Source	Sum of Squares	df	Mean Square	F	Sig.
Between Groups	253.996	4	63.499	29.172	0.000
Within Groups	370.044	170	2.177		
Total	624.041	174			

Table C.41 Welch robust test of equality of means for ln(Event Block Count) by Run

Welch Statistic	df1	df2	Sig.
28.517	4	65.805	0.000

Table C.42 Multiple Comparisons by Run of ln(Event Block Count) using Tukey and Dunnett's C

Method	(I) Run	(J) Run	Mean Difference (I-J)	Std. Error	90% Confidence Interval	
					Lower Bound	Upper Bound
Tukey HSD	A	B	0.29038	0.37592	-0.6420	1.2227
		D	2.66905(*)	0.29378	1.9404	3.3977
		E	2.12039(*)	0.37592	1.1880	3.0528
		G	2.67476(*)	0.38113	1.7295	3.6200
	B	A	-0.29038	0.37592	-1.2227	0.6420
		D	2.37866(*)	0.35550	1.4970	3.2604
		E	1.83000(*)	0.42590	0.7737	2.8863
		G	2.38437(*)	0.43051	1.3166	3.4521
	D	A	-2.66905(*)	0.29378	-3.3977	-1.9404
		B	-2.37866(*)	0.35550	-3.2604	-1.4970
		E	-0.54866	0.35550	-1.4304	0.3331
		G	0.00571	0.36100	-0.8897	0.9011
	E	A	-2.12039(*)	0.37592	-3.0528	-1.1880
		B	-1.83000(*)	0.42590	-2.8863	-0.7737
		D	0.54866	0.35550	-0.3331	1.4304
		G	0.55437	0.43051	-0.5134	1.6221
	G	A	-2.67476(*)	0.38113	-3.6200	-1.7295
		B	-2.38437(*)	0.43051	-3.4521	-1.3166
		D	-0.00571	0.36100	-0.9011	0.8897
		E	-0.55437	0.43051	-1.6221	0.5134
Dunnett's C	A	B	0.29038	0.38486	-0.7069	1.2877
		D	2.66905(*)	0.29003	1.9339	3.4042
		E	2.12039(*)	0.40489	1.0702	3.1706
		G	2.67476(*)	0.37970	1.6893	3.6602
	B	A	-0.29038	0.38486	-1.2877	0.7069
		D	2.37866(*)	0.35575	1.4562	3.3011
		E	1.83000(*)	0.45428	0.6410	3.0190
		G	2.38437(*)	0.43199	1.2521	3.5166
	D	A	-2.66905(*)	0.29003	-3.4042	-1.9339
		B	-2.37866(*)	0.35575	-3.3011	-1.4562
		E	-0.54866	0.37733	-1.5281	0.4307
		G	0.00571	0.35016	-0.9039	0.9153
	E	A	-2.12039(*)	0.40489	-3.1706	-1.0702
		B	-1.83000(*)	0.45428	-3.0190	-0.6410
		D	0.54866	0.37733	-0.4307	1.5281
		G	0.55437	0.44992	-0.6247	1.7335
	G	A	-2.67476(*)	0.37970	-3.6602	-1.6893
		B	-2.38437(*)	0.43199	-3.5166	-1.2521
		D	-0.00571	0.35016	-0.9153	0.9039
		E	-0.55437	0.44992	-1.7335	0.6247

* The mean difference is significant at the 0.10 level.

Comparison of mean log-transformed event block count by groupings show differences between channel width groupings but no significant difference by joint spacing within channel width groups.

Table C.43 Descriptive Statistics for Full Model of Event Block Count

Channel Width (<i>W</i>)	Joint Spacing (<i>J</i>)	Mean ln(Event Block Count)	Std. Dev.	N
0.61m	0.03m	3.8908	1.50734	43
	0.06m	3.6004	1.51219	24
	Total	3.7867	1.50414	67
1.17m	0.03m	1.2202	1.39145	84
	0.06m	1.7704	1.63287	24
	Total	1.3424	1.45870	108
Total	0.03m	2.1244	1.90857	127
	0.06m	2.6854	1.81076	48
	Total	2.2782	1.89379	175

A model with width and joint spacing as factors for ln(Event Block Count) was constructed because width and joint spacing were significant factors in determining event volume. Levene's test for homogeneity of error variances does not invalidate the assumption of equal variances between runs (Table C.44). The analysis of variance shows channel width to be significantly correlated to the log-transform of event volume, but joint spacing is not significant (Table C.45). The comparison of marginal means suggests no interaction between channel width and joint spacing (Figure C.12).

Full Model of Event Block Count:

Equation C.58

$$\ln(BC) = \beta_0 + \beta_1 W + \beta_2 J$$

Table C.44 Levene's Test for Equality of Error Variances for ln (Event Block Count)

F	df1	df2	Sig.
0.850	3	171	0.468

Table C.45 AOV for Full Model of Event Block Count

Source	Type III Sum of Squares	df	Mean Square	F	Sig.	Partial Eta Squared
Corrected Model	248.032(a)	2	124.016	56.730	0.000	0.397
Intercept	921.445	1	921.445	421.503	0.000	0.710
W	237.069	1	237.069	108.444	0.000	0.387
J	0.987	1	0.987	0.451	0.503	0.003
Error	376.008	172	2.186			
Total	1532.364	175				
Corrected Total	624.041	174				

R Squared = 0.397 (Adjusted R Squared = 0.390)

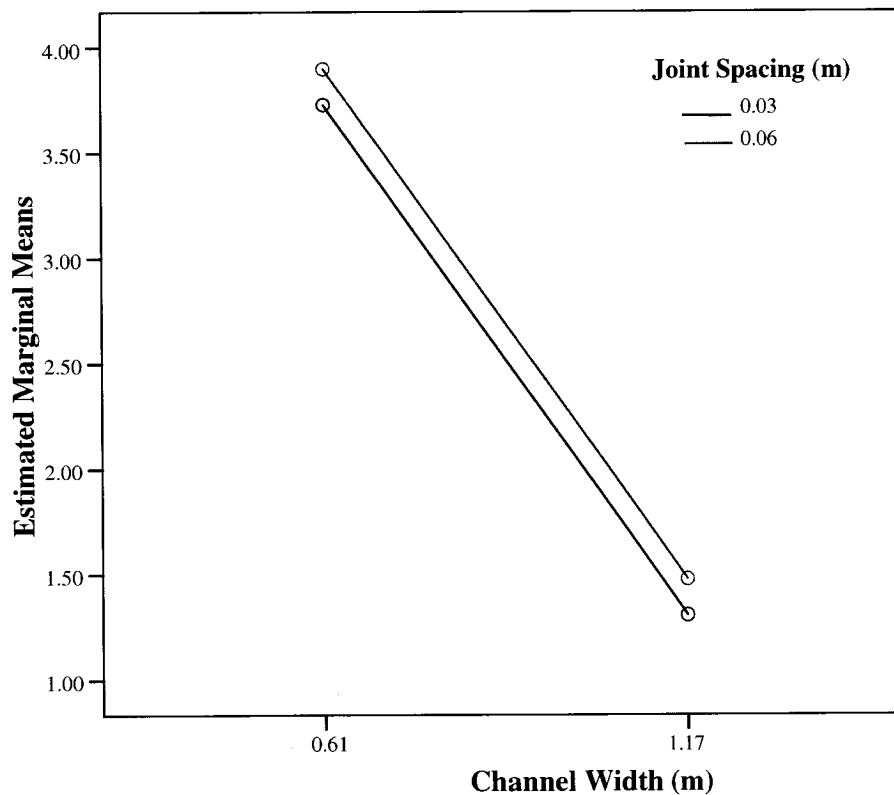


Figure C.12 Estimated Marginal Means for ln (Block Count) by Channel Width and Joint Spacing

Because width is much more significant than joint spacing in the full model of event block count, an AOV table for the reduced model with only channel width was constructed (Table C.46).

Reduced Model of Event Block Count:

Equation C.59

$$\ln(BC) = \beta_0 + \beta_1 W$$

Table C.46 AOV for Reduced Model of Event Block Count

Source	Type III Sum of Squares	df	Mean Square	F	Sig.	Partial Eta Squared
Corrected Model	247.046(a)	1	247.046	113.367	0.000	0.396
Intercept	1087.813	1	1087.813	499.189	0.000	0.743
W	247.046	1	247.046	113.367	0.000	0.396
Error	376.995	173	2.179			
Total	1532.364	175				
Corrected Total	624.041	174				

R Squared = 0.396 (Adjusted R Squared = 0.392)

Table C.47 Levene's Test for Equality of Error Variances for Reduced Model of Event Block Count

F	df1	df2	Sig.
0.109	1	173	0.742

Table C.48 Descriptive Statistics for Reduced Model of Event Block Count

Channel Width (W)	Mean ln(Event Block Count)	Std. Dev.	N
0.61m	3.7867	1.50414	67
1.17m	1.3424	1.45870	108
Total	2.2782	1.89379	175

The reduced model has an R-squared value of 0.396, almost the same as the previous model with 0.397. Levene's test for homogeneity of error variances supports the assumption of equal error variances (Table C.47). The difference in mean log-transformed event block count between channel width groupings is significant (Table C.48). Back-transforming the means yields mean event block count of approximately 44 blocks for the narrow channel width grouping and approximately 4 blocks for the wide channel width grouping. Channel width appears to have some significant correlation with event magnitudes although there is still much unexplained variability in the data.

C.6 Modeling Erosion Supplement

The purpose of this supplement is to provide expanded coverage and results for the previously presented material regarding statistical modeling of erosion. For this section, unlike previous sections of Appendix C, the main text contains much of the analysis and background and supplemental results are mostly provided here for the final model development expressing erosion over time.

A linear regression of width, joint spacing, $\ln(CUSP)$ per event) and interaction term between channel width and $\ln(CUSP)$ per event) on the log-transformed event volume was done and an AOV table constructed (Table C.49).

Final Model of Event Volume:

Equation 3.39

$$\ln(V) = \beta_0 + \beta_1 W + \beta_2 J + \beta_3 \ln(T_e) + \beta_4 \ln(T_e) W$$

Table C.49 AOV of Final Model of Event Volume

Coefficients:	Value	Std. Error	t value	p-value
Intercept	-0.472	4.707	-0.100	0.920
<i>W</i>	-9.230	4.211	-2.192	0.030
<i>J</i>	47.960	15.355	3.123	0.002
$\ln(T_e)$	-0.816	0.821	-0.994	0.322
<i>W</i> : $\ln(T_e)$ (Interaction Term)	0.777	0.740	1.051	0.295

**Proportion of variation in response(s)
explained by model:**

0.495

Terms Added Sequentially	Df	Robust F Statistic	Pr(F)
<i>W</i>	1	138.851	0.000
<i>J</i>	1	30.019	0.000
$\ln(T_e)$	1	0.537	0.455
<i>W</i> : $\ln(T_e)$ (Interaction Term)	1	4.058	0.040

Bias Test for Robust Models	Statistics	p-value
M-estimate	6.71	0.243
LS-estimate	4.87	0.433

The interaction term, despite having a p-value of 0.295, was retained because the term provided significance to the overall model with F statistic of 4 and p-value of 0.04. Also, the energy expenditure term was included in the model, so the previous correlation between width and energy expenditure suggests inclusion of an additional interaction term. The coefficient term for log-transformed *CTSP* is negative, which would mean longer periods of energy expenditure result in lower event volumes. However, the term is not very significant with a p-value of only 0.322. Overall, the model explained 49.5% of the variation seen in the event magnitude data. Over 50% of the variation in the event magnitude is left unexplained. A normal *QQ* plot of residuals shows some outliers and greater variation at the extremes of the data set (Figure C.13). Attempts to bring these elements into the model may yield a better explanation of the variation in event magnitude.

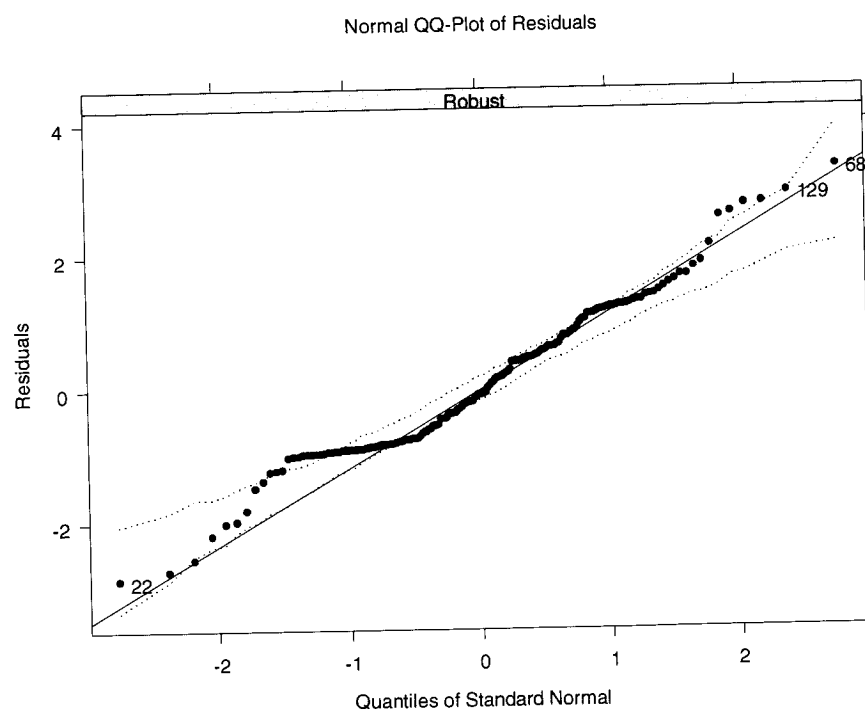


Figure C.13 Normal QQ Plot of Residuals of Final Model of Event Volume

A key block parameter was added to the previous model of event magnitude including width, joint spacing, and energy expenditure, and including an interactions term with energy expenditure. A robust statistical methodology was utilized as in previous models. Overall, the full model provided significantly more explanation of the variation in event magnitude at 66% compared to the previous model with explanatory value of 50% (Table C.50). The interaction term between key block classification and energy expenditure is fairly insignificant with p-value of 0.265 and term-added p-value of 0.279.

Full Revised Model of Event Volume:

Equation 3.40

$$\ln(V) = \beta_0 + \beta_1 W + \beta_2 J + \beta_3 M + \beta_4 \ln(T_e) + \beta_5 \ln(T_e) W + \beta_6 \ln(T_e) M$$

Table C.50 AOV for Full Revised Model of Event Volume

Coefficients:	Value	Std. Error	t value	p-value
Intercept	-2.299	1.935	-1.19	0.237
<i>W</i>	-7.185	1.711	-4.20	0.000
<i>J</i>	46.654	6.643	7.02	0.000
<i>M</i>	0.878	0.327	2.69	0.008
$\ln(T_e)$	-0.917	0.337	-2.72	0.007
<i>W</i> : $\ln(T_e)$ (Interaction Term)	0.810	0.303	2.67	0.008
<i>M</i> : $\ln(T_e)$ (Interaction Term)	0.069	0.062	1.12	0.265

**Proportion of variation in response(s)
explained by model:**

0.6617

Terms Added Sequentially	df	Robust F Statistic	Pr(F)
<i>W</i>	1	138.85	0.000
<i>J</i>	1	30.02	0.000
<i>M</i>	1	194.15	0.000
$\ln(T_e)$	1	1.09	0.288
<i>W</i> : $\ln(T_e)$ (Interaction Term)	1	6.77	0.008
<i>M</i> : $\ln(T_e)$ (Interaction Term)	1	1.13	0.279

Bias Test for Robust Models	Statistics	p-value
M-estimate	7.14	0.414
LS-estimate	11.58	0.115

A reduced model was analyzed without the inclusion of this interaction term with good results (Table C.51). The removal of the interaction term improved the significance of all the remaining terms with p-values less than 0.05. The reduced model also explains 69% of the variation in event magnitude, which is greater than the full model at 66% and much greater than the previous model with the energy expenditure term at 50%. The residuals are fairly normal and more contained than the previous model with the classification scheme (Figure C.14 to Figure C.16).

Reduced Revised Model of Event Volume:

Equation 3.41

$$\ln(V) = \beta_0 + \beta_1 W + \beta_2 J + \beta_3 M + \beta_4 \ln(T_e) + \beta_5 \ln(T_e) W$$

Table C.51 AOV for Reduced Revised Model of Event Volume

Coefficients:	Value	Std. Error	t value	p-value
Intercept	-3.427	1.607	-2.13	0.034
<i>W</i>	-5.922	1.430	-4.14	0.000
<i>J</i>	48.189	5.767	8.36	0.000
<i>M</i>	1.301	0.089	14.59	0.000
$\ln(T_e)$	-0.762	0.276	-2.76	0.006
<i>W</i> : $\ln(T_e)$ (Interaction Term)	0.622	0.251	2.48	0.014

**Proportion of variation in response(s)
explained by model:**

0.6879

Terms Added Sequentially	df	Robust F Statistic	Pr(F)
<i>W</i>	1	138.85	0.000
<i>J</i>	1	30.02	0.000
<i>M</i>	1	194.15	0.000
$\ln(T_e)$	1	1.09	0.288
<i>W</i> : $\ln(T_e)$ (Interaction Term)	1	6.77	0.008

Bias Test for Robust Models	Statistics	p-value
M-estimate	-1.51	1.000
LS-estimate	5.72	0.455

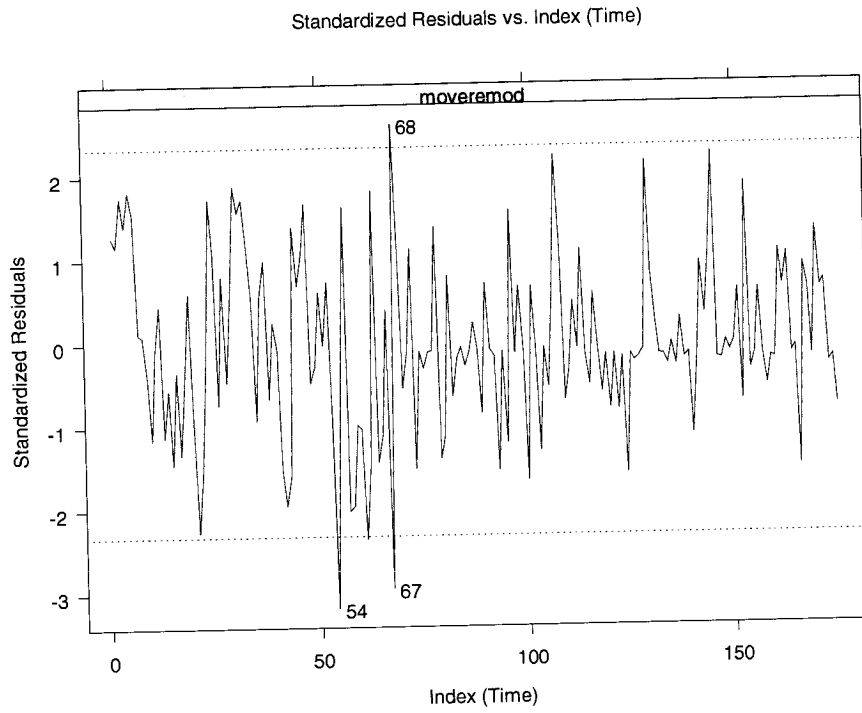


Figure C.14 Standardized Residuals for Reduced Revised Model of Event Volume

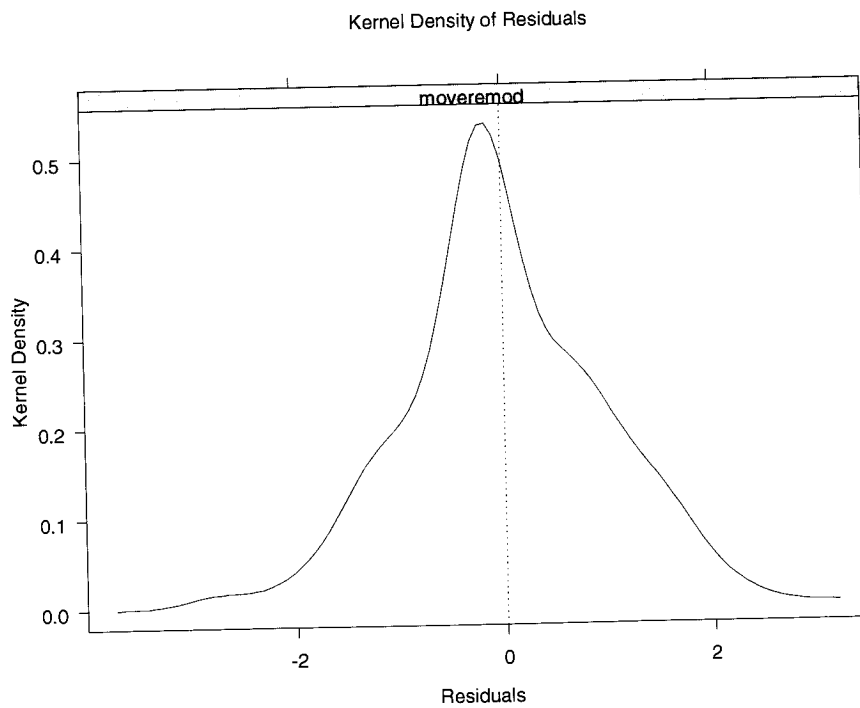


Figure C.15 Density Plot of Residual for Reduced Revised Model of Event Volume

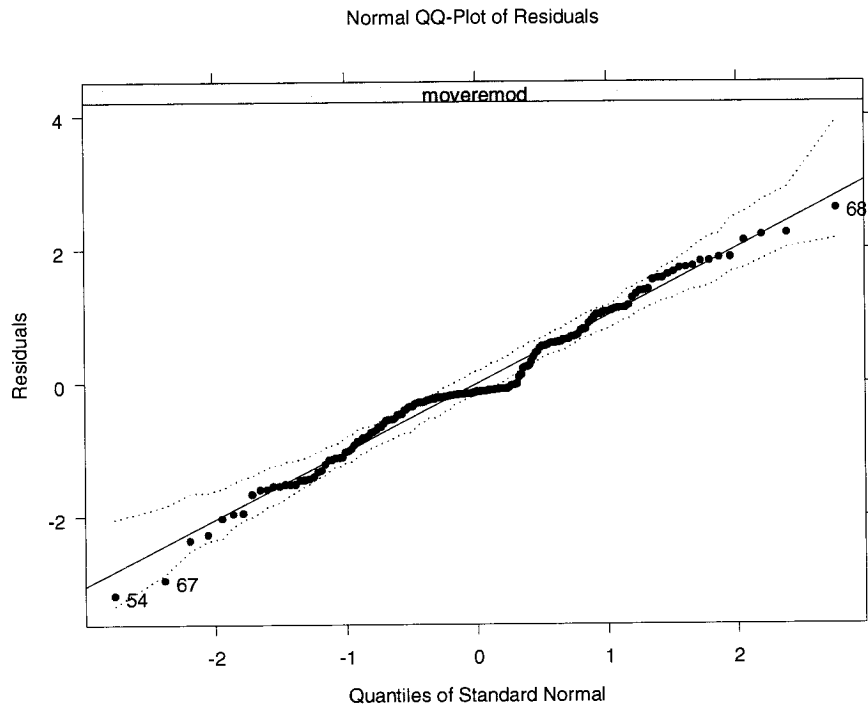


Figure C.16 Normal QQ Plot of Residuals for Reduced Revised Model of Event Volume

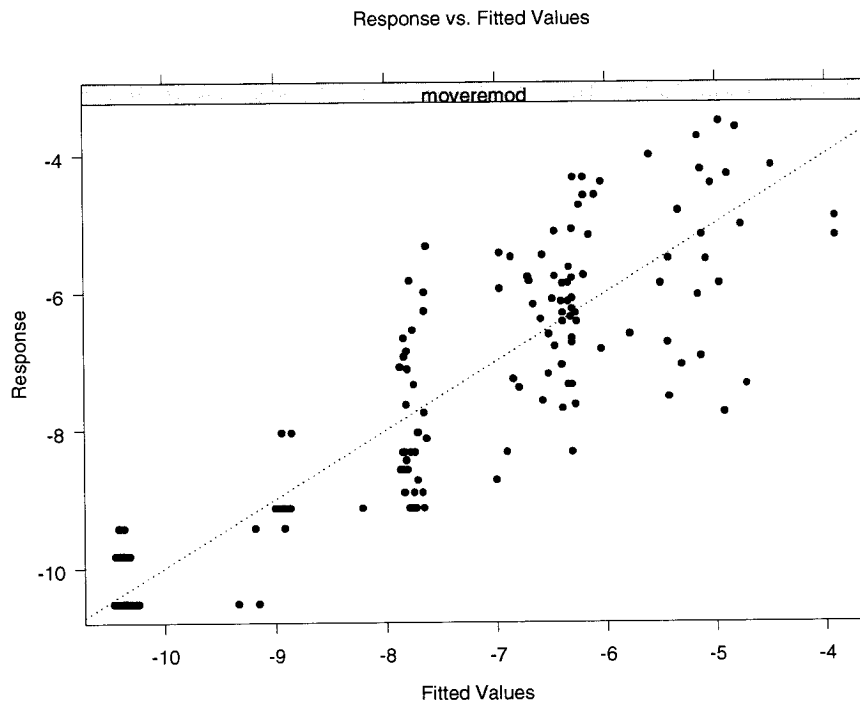


Figure C.17 Plot of Response versus Fitted Values for Reduced Revised Model of Event Volume

The comparison of event values versus the model values produces a fairly uniform variation around the model predictions, although much variation still exists (Figure C.17). This model of erosional efficiency allows inferences about the impact of width, joint spacing, key block classification, and energy expenditure on erosional efficiency:

Equation 3.45

$$\ln\left(\frac{V}{T_e}\right) = -3.427 + -5.992W + 48.189J + 1.301M + [-1.762 + 0.622W - 1] \ln(T_e)$$

or rewritten in exponential form:

Equation 3.46

$$\frac{V}{CTSP} = 0.325 e^{(-5.922W + 48.189J + 1.301M)} T_e^{(-1.762 + 0.622W)}$$

The change in width, joint spacing, or key block classification necessary for a unit change in the ln(erosional efficiency) for T_e of 5 kJ/m was determined using Equation 3.45 while holding other factors constant. Likewise, the change in energy expenditure necessary for a 1% increase in erosional efficiency assuming a width of 1 m was determined while holding other factors constant.

For W :

Equation C.60

$$\Delta \ln\left(\frac{V}{T_e}\right) = [\beta_1 + \beta_5 \ln(T_e)] \Delta W$$

$$1 = [-5.922 + 0.622 \ln(5)] \Delta W$$

$$\Delta W = -0.203 \text{ m} \sim -20 \text{ cm}$$

For J :

Equation C.61

$$\Delta \ln \left(\frac{V}{T_e} \right) = \beta_2 \Delta J$$

$$1 = 48.19 \Delta J$$

$$\Delta J = 0.0207 \text{ m} \sim 2 \text{ cm}$$

For M :

Equation C.62

$$\Delta \ln \left(\frac{V}{T_e} \right) = \beta_3$$

= 1.301 if Mass Event occurs otherwise it is equal to 0 for a Key Block Event

$\Delta (V/T_e)$ is by factor of 3.67 for mass events.

For T_e :

Equation C.63

$$\% \Delta \left(\frac{V}{T_e} \right) = [\% \Delta T_e]^{(-0.762 + 0.622 W)}$$

$$101 \% = [\% \Delta T_e]^{[-0.762 + 0.622 (1)]}$$

$$\% \Delta T_e = 93\% \text{ or } 7\% \text{ decrease in } T_e$$

The coefficients show that decreases in channel width and increases in joint spacing increase overall erosional efficiency. Events classified as mass block events are 3.7 times more efficient than those classified as key block events. As expected by simple inspection of the equations, a decrease in energy expenditure per event increases overall erosional efficiency. This appears to be influenced by width, such that greater widths require greater decreases in energy expenditure to be achieved for the same erosional efficiency.

Appendix D Orange River Joint Spacing Data

Table D.1 Summary of Joint Spacing Data from Sampling Sites - Orange River, South Africa

Sampling Site	Number of Individual Data Sets	Channel Type	Mean Joint Spacing (m)	Std. Dev. (m)	Max. (m)	Min. (m)	Total Joint Count
Kakamos I	1	S	0.42	0.832	10.12	0.01	366
Kakamos	3	S	0.39	0.707	10.12	0.01	744
Kakamos 2.Davido Vineyard	1	AS	0.26	0.283	1.80	0.01	185
Kakamos II	1	AS	0.19	0.180	1.05	0.01	184
Boeg I	1	AS	0.25	0.206	1.35	0.01	359
Boeg II	1	AS	0.25	0.196	1.35	0.01	248
Leapfrog	1	A	0.25	0.213	0.89	0.01	33
Augrabies	4	A	0.81	0.999	6.90	0.02	207
Augrabies 2	2	A	0.90	1.124	6.90	0.02	148
Dry Channel 1,2,3,4,5,6,7,8	9	A	0.94	1.118	8.70	0.05	288
Knob	1	A	0.37	0.336	1.93	0.01	52
Vaal II	8	A	1.41	3.236	30.95	0.03	266
Vaal III	8	AS	2.06	4.251	30.95	0.03	144